

High-precision measurements of heavy
p-process isotopes in early solar system materials

Inaugural-Dissertation

zur

Erlangung des Doktorgrades

der Mathematisch-Naturwissenschaftlichen Fakultät

der Universität zu Köln

vorgelegt von

Stefan Theodorus Maria Peters

aus Teteringen

Köln, 2014

Berichtstatter: Prof. Dr. Carsten Munker
(Gutachter)

Prof. Dr. Erik Scherer

Tag der mündlichen Prüfung: 11.04.2014

Solange du noch die Sterne fühlst als ein „Über-dir“,
fehlt dir noch der Blick des Erkennenden.

Friedrich Nietzsche
(Jenseits von Gut und Böse, Aph. 71)

CONTENTS

Abstract	3
Kurzzusammenfassung	6
1. Introduction	9
<i>1.1 Origin of the elements in the solar system</i>	10
<i>1.2 Isotopic composition of the elements in different solar system materials</i>	11
<i>1.3 The p-process of stellar nucleosynthesis</i>	13
<i>1.4 P-process isotopes and the supernova trigger hypothesis for solar system formation</i>	14
<i>1.5 The information provided by heavy p-process isotopes ^{174}Hf, ^{180}W and ^{190}Pt</i>	15
2. High-precision measurements of low-abundance isotopes ^{174}Hf, ^{180}W, ^{190}Pt using MC-ICP-MS with $10^{12}\Omega$ Faraday amplifiers	
2.1 INTRODUCTION	18
2.1.1 Previous determinations of natural abundances of ^{174}Hf , ^{180}W , ^{190}Pt	19
2.2.2 Relevance of high-precision ^{174}Hf , ^{180}W and ^{190}Pt data to geo- and cosmochemistry	20
2.2 ELEMENT PURIFICATION	21
2.2.1 Reagents and sample digestion	21
2.2.2 Ultra-pure separation of Hf from basaltic matrices and chondrites	22
2.2.3 Tungsten separation from silicate matrices for precise ^{180}W measurements	23
2.2.4 Platinum separation from metal matrices	26
2.3 MASS SPECTROMETRY	28
2.3.1 Apparatus, cup configurations and data processing	28
2.3.2 Effects of low beam intensities on measurement precisions	30
2.3.3 Precise and accurate isotope measurements of Hf	31
2.3.4 Isotope measurements of Pt	33
Standard-sample bracketing methods for monitoring neutron capture effects	35
Isobaric interferences and tailing effects of Ir	36
2.3.5 Isotope measurements of W	39
2.4 DATA FOR METEORITES AND TERRESTRIAL SAMPLES	40
2.4.1 Non-radiogenic Hf isotopic compositions of terrestrial basalts and chondrites	40
2.4.2 Platinum isotope composition of three iron meteorites	41
2.4.3 Tungsten isotope composition of terrestrial silicates and chondrites	42
2.4.4 Determination of isotope compositions	43
2.5. CONCLUSIONS	47

3. The distribution of p-process ^{174}Hf in early solar system materials	48
3.1 INTRODUCTION	49
3.2 SAMPLES AND METHODS	50
3.3 RESULTS	51
3.4 DISCUSSION	52
3.4.1 <i>Non-radiogenic heterogeneity in some chondrites and IAB silicate inclusion</i>	52
3.4.2 <i>Distribution of p-process ^{174}Hf on an asteroidal scale</i>	55
3.4.3 <i>Potential p-process deficit in CAIs</i>	57
3.4.4 <i>Implications for ^{176}Lu-^{176}Hf chronometry</i>	58
3.5 CONCLUSIONS	59
4. Alpha-decay of ^{184}Os revealed by radiogenic ^{180}W in iron meteorites: Half life determination and viability as geochronometer	60
4.1 INTRODUCTION	61
4.2 ANALYTICAL STRATEGY	62
4.3. RESULTS	65
4.3.1 <i>Combined ^{180}W and Os/W concentration measurements</i>	65
4.3.2 <i>Abundance of ^{180}W in chondrites and terrestrial silicates</i>	68
4.4 DISCUSSION	69
4.4.1 <i>Non-radiogenic effects on $\epsilon^{180}\text{W}$</i>	69
4.4.2 <i>Uniform distribution of ^{180}W in the solar nebula at 4.565 Ga</i>	72
4.4.3 <i>Chronological significance of ^{184}Os-^{180}W systematics in iron meteorites</i>	72
4.4.4 <i>^{180}W deficit in terrestrial silicates relative to chondrites</i>	73
4.5 OUTLOOK	75
4.5.1 <i>Viability of the ^{184}Os-^{180}W decay system as a geochronometer</i>	75
4.6 CONCLUSIONS	77
5. References	78
6. Acknowledgements	88
7. Erklaring	90
8. Lebenslauf	91

Abstract

This work investigates the abundances of rare, neutron poor isotopes of some heavy elements in meteorites. The elements in the solar system that are heavier than H and He were predominantly produced in stars. The Sun cannot have produced these elements during its lifetime as a small main sequence star, and their abundances must therefore have been inherited from interstellar matter that was produced by pre-existing massive stars. The elements lighter than iron were produced by nuclear fusion, whereas elements heavier than iron were produced predominantly by neutron capture reactions on pre-existing nuclei. This mechanism is referred to as the s-process when the produced nuclei decay before an additional neutron is captured, which is predominantly the case in asymptotic giant branch stars. When, in contrast, neutrons are captured before decay is possible, heavier nuclei may be formed (i.e., the r-process) and these conditions are achieved in core-collapse type supernovae. A group of rare, neutron-poor isotopes cannot have formed by s- or r-process nucleosynthesis and these are referred to as the p-process isotopes. The predominant mechanism by which p-process isotopes are produced includes photodisintegrations of pre-existing nuclei in core collapse type supernovae. However, this mechanism typically underproduces the solar system abundances of the light p-process isotopes, possibly implying decoupling between the nucleosynthetic sources of heavy and light p-process isotopes in the solar system.

The non-radiogenic, mass independent isotopic compositions of some heavy elements are variable between different types of early solar system materials, reflecting isotopic heterogeneities between different nucleosynthetic carrier phases in the nascent solar system. Whereas the distributions of the most abundant isotopes, typically consisting of s- and r-process nuclides, have been relatively well constrained in most types of early solar system materials, studies for heavy p-process isotopes have long been impossible because of analytical difficulties due to their low relative abundances (typically less than 1 %). These isotopes became of particular interest since the recent discovery of ^{180}W heterogeneities in iron meteorites, which were interpreted to predominantly reflect heterogeneity of heavy p-process components in the early solar system. In this dissertation, the systematics of heavy p-process isotopes in different solar system materials are examined. As examples, the abundances of heavy p-process ^{174}Hf , ^{180}W and to lesser extent ^{190}Pt in different types of early solar system materials are explored. Based on new data for ^{180}W in meteorites, an alternative

explanation for the ^{180}W heterogeneities is proposed, showing for the first time that measurable amounts of ^{180}W are produced by radioactive decay of ^{184}Os .

In **Chapter II**, analytical protocols for high-precision measurements of heavy p-process isotopes ^{174}Hf , ^{180}W and ^{190}Pt based using multicollector inductively-coupled plasma mass spectrometry (MC-ICP-MS) are presented. These protocols largely rely on the use of newly available Faraday amplifiers equipped with $10^{12}\Omega$ resistors that were used for collecting the isotopes of interest, as well as isotopes with which main isobaric interferences were monitored. It was found that measurement precisions strongly depend on signal intensity and become dramatically worse at < 50 mV on the low-abundance isotope of interest. At higher intensities, measurement precisions are typically ~ 1 parts per 10,000 or better, a ca. tenfold improvement compared to most earlier studies employing conventional $10^{11}\Omega$ resistors. As part of this work, absolute isotope abundances of ^{174}Hf (0.16106 ± 0.00006 %); ^{180}W (0.11910 ± 0.00009 %); and ^{190}Pt (0.01286 ± 0.00005 %) in standard reference materials were determined throughout approximately 10 analytical sessions for each target element, ranging over ~ 3 years. These are the most precise estimates of the terrestrial abundances of these isotopes available so far. For precisely determining ^{174}Hf , ^{180}W and ^{190}Pt in natural materials, ultra-clean separation schemes for Hf and W from silicate-rich matrices, and for Pt from iron meteorite matrices, have been developed. It is shown that iron meteorite samples from the IAB, IIAB and IIIAB groups, one sample each, have indistinguishable ^{190}Pt from terrestrial Pt. Data on ^{174}Hf and ^{180}W in natural materials are discussed in depth in Chapters III and IV, respectively.

Chapter III reports high-precision data for ^{174}Hf in different types of chondrites, eucrites, one silicate inclusion of a IAB type iron, and one calcium-aluminium rich inclusion (CAI) from the Allende CV3 chondrite. Some chondrites as well as the IAB silicate inclusion exhibit elevated mass-bias corrected $^{174}\text{Hf}/^{177}\text{Hf}$ that are correlated with $^{178}\text{Hf}/^{177}\text{Hf}$ and anti-correlated with $^{180}\text{Hf}/^{177}\text{Hf}$. This feature is interpreted to reflect the presence of small neutron capture effects ($< -43 \pm 14$ ppm on $^{180}\text{Hf}/^{177}\text{Hf}$) caused by exposure to cosmic rays. Chondrite and eucrite samples that appear to be unaffected by neutron capture reactions exhibit indistinguishable ^{174}Hf from the terrestrial composition. This indicates that the p-process contribution to ^{176}Hf ($\sim 3\%$ p-process; 97% s-process) in these materials is also indistinguishable from terrestrial Hf, and therefore the ^{176}Lu - ^{176}Hf chronometer in these materials was unaffected by a heterogeneous distribution of p-process Hf. In contrast, the CAI

sample yields mass-bias corrected $^{174}\text{Hf}/^{177}\text{Hf}$ and $^{180}\text{Hf}/^{177}\text{Hf}$ that are lower (200 ± 78 ppm) and higher (32 ± 9 ppm) than the terrestrial Hf compositions, respectively. Whereas the low value for $^{174}\text{Hf}/^{177}\text{Hf}$ may reflect a p-process deficit in the reservoir from which CAI formed, the elevated $^{180}\text{Hf}/^{177}\text{Hf}$ remains unexplained.

The observations that p-process ^{174}Hf and possibly ^{190}Pt do not show resolvable heterogeneities in bulk meteorites are difficult to reconcile with the previously proposed models that ^{180}W heterogeneities in iron meteorites are caused by a heterogeneous distribution of p-process W. In **Chapter IV**, combined ^{180}W and Os-W concentration data are presented that indicate that ^{180}W heterogeneities in iron meteorites are better explained by radiogenic ingrowth from the decay of the rare nuclide ^{184}Os . Alpha decay of ^{184}Os has been theoretically predicted, but was previously never observed in experiments. A combined ^{184}Os - ^{180}W isochron for iron meteorites and chondrites yields a decay constant value of $\lambda^{184}\text{Os}(\alpha)$ of $6.49 \pm 1.34 \times 10^{-14} \text{ a}^{-1}$ (half life $1.12 \pm 0.23 \times 10^{13}$ years), which is in good agreement with theoretical estimates. It is furthermore demonstrated that terrestrial silicate samples display a deficit in ^{180}W relative to chondrites by 1.16 ± 0.69 parts in 10,000, reflecting the expected long-term evolution of the silicate Earth with subchondritic Os/W since core formation occurred ~ 4.5 Ga ago.

Kurzzusammenfassung

In dieser Arbeit wird die Häufigkeit von seltenen, neutronenarmen Isotopen ausgewählter schwerer Elemente in Meteoriten untersucht. Alle Elemente in unserem Sonnensystem, die schwerer als H und He sind, wurden überwiegend in Sternen produziert. Die Sonne kann diese Elemente während ihrer Lebenszeit als kleinerer Hauptreihenstern nicht produziert haben und alle schweren Elemente in unserem Sonnensystem müssen daher aus interstellarer Materie stammen, die wiederum durch die Explosion massenreicher Sterne entstand. Die Entstehung aller Elemente leichter als Eisen kann gut durch Kernfusion erklärt werden. Der Mechanismus, durch den alle Elemente, die schwerer als Eisen sind, produziert wurden, beruht hingegen überwiegend auf Neutroneneinfang-Reaktionen in massenreichen Sternen. Wenn die neu produzierten Atomkerne zerfallen bevor zusätzliche Neutronen eingefangen werden können, wird dies als s- Prozess bezeichnet, was überwiegend in sogenannten AGB Sternen abläuft. Wenn im Gegensatz dazu Neutronen eingefangen werden, bevor radioaktiver Zerfall eintritt, können auch neutronenreichere Atomkerne gebildet werden. Dieser Vorgang wird als r-Prozess bezeichnet, für den die Synthesebedingungen in Kernkollaps-Supernovae erreicht werden. Eine Gruppe von seltenen, neutronenarmen Isotopen kann nicht durch s- oder r- Prozess Nukleosynthese gebildet worden sein. Diese werden als p-Prozess Isotope bezeichnet. Der vorherrschende Mechanismus, durch den die schweren p-Prozess Isotope hergestellt werden können, ist die sogenannte Photodesintegration von bereits vorhandenen Atomkernen in Kernkollaps-Supernovae. Dieser Mechanismus kann jedoch die relativ hohen solaren Häufigkeiten der leichten p-Kernen nicht reproduzieren. Diese Beobachtung impliziert dass schwere und leichte P-Prozess Isotope im Sonnensystem möglicherweise unterschiedliche Quellen haben.

Die Häufigkeiten von nicht-radiogenen Isotopen von manchen Elementen können in verschiedenen Meteoriten leicht variieren, was auf nukleosynthetische Heterogenitäten in verschiedenen Komponenten schließen lässt, die im frühen Sonnensystem gebildet wurden. Die Verteilungen von relativ häufigen Isotopen, die typischerweise durch den s- und r-Prozess während der Nukleosynthese gebildet wurden, sind in den meisten Meteoritenproben aus dem frühen Sonnensystem relativ gut charakterisiert. Untersuchungen der Häufigkeiten von schweren P-Prozess Isotopen sind aufgrund der niedrigen Häufigkeiten dieser Isotope lange unmöglich gewesen. Nach der Entdeckung von Heterogenitäten von p-Prozess ^{180}W in Eisenmeteoriten, die als nukleosynthetisch interpretiert wurden, ist das Interesse an genaueren

Messungen dieser Isotopen in letzter Zeit stark gestiegen. In dieser Dissertation werden die Häufigkeiten von p-Prozess ^{174}Hf und ^{190}Pt in unterschiedlichen Material-Arten aus dem frühen Sonnensystem untersucht. Aufgrund von neuen ^{180}W -Daten wird eine alternative Erklärung für die Heterogenitäten von ^{180}W vorgeschlagen und es wird zum ersten Mal gezeigt, dass messbare Mengen von ^{180}W durch radioaktiven Zerfall von ^{184}Os produziert geworden sind.

In **Kapitel II** werden analytische Protokolle für hochpräzise Messungen der p-Prozess Isotope ^{174}Hf , ^{180}W , und ^{190}Pt beschrieben, die auf der Messung mit Multikollektor ICP Massenspektrometrie basieren. Diese Protokolle beruhen auf der Verwendung von zwei mit $10^{12}\Omega$ Widerständen ausgestatteten Faraday Verstärkern für die Messung der entsprechenden p-Prozess Isotope, als auch für die Messung derjenigen Isotopen, die benutzt werden um isobare Interferenzen auf den jeweiligen p-Prozess Isotopen zu korrigieren. Es wurde festgestellt, dass die Reproduzierbarkeit stark von der Signalstärke abhängt und sich bei <50 mV auf den entsprechenden Isotopen dramatisch verschlechtert. Bei höheren Intensitäten ist die Reproduzierbarkeit in der Regel ± 100 ppm oder besser, was eine ca. zehnfach bessere Reproduzierbarkeit im Vergleich zu den meisten früheren Studien darstellt. Als Teil dieser Arbeit wurde die Isotopenhäufigkeit von ^{174}Hf ($0,16106 \pm 0,00006$ %), ^{180}W ($0,11910 \pm 0,00009$ %), und ^{190}Pt ($0,01286 \pm 0,00005$ %) in Referenzmaterialien bestimmt, jeweils als Mittel von ca. 10 Messtagen, verteilt über einen Zeitraum von ca. 3 Jahren. Diese Werte sind die bisher präzisesten Bestimmungen der terrestrischen Häufigkeiten dieser Isotope. Zur Messung von ^{174}Hf , ^{180}W und ^{190}Pt in natürlichen Gesteins- und Meteoritenproben wurden Methoden zur hochreinen Abtrennung von Hf und W aus silikatreichen Proben und von Pt aus Eisenmeteoriten entwickelt. Messungen von Eisenmeteoriten zeigen, dass in Meteoriten der IAB, IIAB und IIIAB Gruppen die Häufigkeiten an ^{190}Pt nicht von terrestrischem Pt zu unterscheiden ist. ^{174}Hf - und ^{180}W -Daten werden eingehend in der Tiefe in den Kapiteln III und IV diskutiert.

Kapitel III präsentiert hochpräzise Daten für das p-Prozess Isotop ^{174}Hf in verschiedenen Meteoritenproben. Der Probensatz umfasst verschiedene Arten von Chondriten, Eukriten, einem IAB Silikat-Einschluss und einem Calcium-Aluminium-reichen Einschluss (CAI) aus dem Allende CV3 Chondrit. Einige Chondrite sowie der IAB Silikat-Einschluss haben leicht erhöhte $^{174}\text{Hf}/^{177}\text{Hf}$ Verhältnisse, die mit $^{178}\text{Hf}/^{177}\text{Hf}$ positiv und mit $^{180}\text{Hf}/^{177}\text{Hf}$ negativ korrelieren, was auf Neutroneneinfang-Effekte durch Einwirkung

kosmischer Strahlung in diesen Proben deutet ($< -43 \pm 14$ ppm auf $^{180}\text{Hf}/^{177}\text{Hf}$). Proben von Chondriten und Eukriten, die nicht von Neutroneneinfang betroffen sind, weisen ^{174}Hf Häufigkeiten auf, die von der terrestrischem ^{174}Hf Häufigkeit nicht zu unterscheiden sind. Das nicht-radiogene oder initiale ^{176}Hf (~3% p-Prozess; ~97% s-Prozess) in diesen Meteoritenproben ist deswegen identisch mit der terrestrischen Häufigkeit an ^{176}Hf , und das ^{176}Lu - ^{176}Hf Zerfallssystem ist folglich in diesen Proben nicht durch eine möglicherweise heterogene Verteilung von p-Prozess ^{176}Hf beeinflusst worden. Im Gegensatz dazu ergibt die Messung der Allende CAI korrigierte $^{174}\text{Hf}/^{177}\text{Hf}$ und $^{180}\text{Hf}/^{177}\text{Hf}$ Werte, die niedriger (200 ± 78 ppm), bzw. höher (32 ± 9 ppm) sind als in terrestrischem Hf. Der niedrige Wert für $^{174}\text{Hf}/^{177}\text{Hf}$ könnte auf ein p-Prozess-Defizit im Reservoir deuten, aus dem CAIs gebildet wurden. Die Ursache für das erhöhte $^{180}\text{Hf}/^{177}\text{Hf}$ bleibt jedoch ungeklärt.

Die Schlussfolgerung, dass p-Prozess ^{174}Hf und möglicherweise ^{190}Pt keine auflösbaren Heterogenitäten in Meteoritenproben aus dem frühen Sonnensystem zeigen, ist nur schwierig in Einklang zu bringen mit einem vorher vorgeschlagenen Modell, nach dem die Heterogenitäten von ^{180}W in Eisenmeteoriten durch nukleosynthetische Heterogenitäten von p-Prozess Isotopen verursacht werden. In **Kapitel IV** werden kombinierte ^{180}W und Os-W Messungen vorgestellt, die zeigen, dass die ^{180}W Heterogenitäten in Eisenmeteoriten besser durch radioaktiven Zerfall des seltenen Nuklids ^{184}Os erklärt werden können. Alpha-Zerfall von ^{184}Os wurde aufgrund seiner nuklearen Struktur vorhergesagt, wurde aber bisher nie in Experimenten beobachtet. Eine kombinierte ^{184}Os - ^{180}W Isochrone für Eisenmeteoriten und Chondriten ergibt eine Zerfallskonstante $\lambda^{184}\text{Os}$ (α) von $6,49 \pm 1,34 \times 10^{-14} \text{ a}^{-1}$ (Halbwertszeit: $1,12 \pm 0,23 \times 10^{13}$ Jahre), in guter Übereinstimmung mit theoretischen Abschätzungen. Terrestrische Silikatproben zeigen ein Defizit in ^{180}W von $-1,16 \pm 0,69$ ϵ -Einheiten relativ zu Chondriten, was erwartungsgemäß auf eine langfristige ^{180}W Entwicklung der Silikat-Erde mit subchondritischen Os/W hinweist. Dies ist wiederum konsistent mit einer frühen Kernbildung vor ~4,5 Milliarden Jahren.

I. Introduction

1.1 Origin of the elements in the solar system

The Sun comprises more than 99.8 % of the mass of the solar system, and may therefore be considered an approximate compositional average of its chemical composition. The composition of the solar photosphere was measured by spectroscopy, and predominantly consists of the two lightest elements, i.e., H (74.9 %) and He (23.8 %), and additionally contains < 2% heavier elements (e.g., Lodders, 2003). Whereas in general, H and the largest amount of He in our solar system were directly produced by the Big Bang, the heavier elements are thought to have been produced by nucleosynthesis in precursor stars and here in particular by fusion and supernovae eruptions (e.g., Burbidge et al., 1957; Seeger et al., 1965; Clayton, 1968; Wallerstein et al., 1997). Helium, together with some C and N, is furthermore being produced in the Sun's core by a series of nuclear reactions that are facilitated by gravitational compression, but atoms that were formed this way were not transported towards the surface (e.g., Hansen et al., 2004 and references therein). Nevertheless, core temperatures of the Sun have probably been insufficient for the production of elements heavier than He, C and O. The heavy elements in the solar system therefore must have been inherited from the interstellar medium (e.g., Lodders, 2003).

The theory that elements heavier than H and He are produced in stars was first proposed by Hoyle (1946; 1954). The first empirical evidence was put forward by Merrill (1952) who showed that Tc was present in the outer envelopes of some S-type stars. As the longest-lived isotope of Tc has a half-life of $\sim 4 \times 10^6$ yr, it was concluded that Tc had been produced by these stars, and had evidently been transported to their surfaces. In 1957, Burbidge, Burbidge, Fowler, and Hoyle provided the first comprehensive review on stellar nucleosynthesis that became a cornerstone paper in nuclear astrophysics, which is generally referred to as B²FH. In this pioneering study it is shown that elements heavier than iron may be produced via three mechanisms, two of which are controlled by an interplay between neutron capture reactions and β -decay. In these two processes, heavier nuclei are formed by neutron capture from lighter nuclei. During the s-process, which is characterized by slow neutron capture rates, neutron capture reactions continue until an unstable nucleus is reached that β -decays to a nucleus with $Z+1$ (where Z stands for the atomic number). In contrast, when neutron capture rates are sufficiently high, a neutron may be captured by the unstable nucleus before it decays, resulting in the production of even heavier nuclei. This process may continue until a nucleus is formed that decays faster than that neutron capture can occur, and

is known as the r-process. In a plot of atomic number versus number of neutrons, the s-process follows a zigzag type pathway to which nuclei produced by the r-process plot on the right hand side (Fig. 1.1).

1.2. Isotopic composition of the elements in different solar system materials

Most elements show relatively homogeneous compositions in their non-radiogenic isotopes between different types of solar system materials, but some elements display isotope heterogeneities that are consistent with models for the selective enrichment or depletion of nuclides produced by a particular stellar nucleosynthetic process (e.g., Dauphas et al., 2004; Trinquier et al., 2007; Trinquier et al., 2009; Burkhardt et al., 2012). Such isotope anomalies are particularly pronounced in presolar grains in primitive meteorites (e.g., Zinner, 1998; 2003; Hoppe et al., 2000; Amari et al., 2001; Lodders and Amari, 2005). Evidently, these particular grains survived the physical conditions during solar system formation. The variations in nucleosynthetic components between different solar system materials may therefore reflect physical heterogeneities of carrier phases in the protosolar nebula. It has been argued that the evolution of these heterogeneities is time dependent, i.e., that nucleosynthetic material was injected into the solar system after the first solids (calcium-aluminium rich inclusions; CAIs) formed (e.g., Bizzarro et al., 2007; Brennecka et al., 2013). Some of the observed isotope patterns, however, are difficult to explain by the heterogeneity scenario and require the selective depletion of distinct nucleosynthetic carrier phases by thermal processing (e.g., Regelous et al., 2008; Trinquier et al., 2009).

After the first solar system materials had been formed, the isotope inventories of their elements may have further been modified by a series of nuclear reactions. These include 1) radioactive decay, which is a spontaneous process by which an unstable atom loses energy by emitting particles of ionizing radiation with a constant rate; and 2) reactions resulting from particle interactions such as, e.g., neutron capture. Possible modes of radioactive decay are the emission of ${}^4_2\text{He}$ nuclei (α -decay) or electrons (β^- decay); the conversion of a proton into a neutron by positron (β^+) decay or electron capture (E.C.); and spontaneous nuclear fission (splitting of a heavy nucleus into multiple lighter nuclei) for isotopes with $A > 230$, where A stands for the mass number. In a plot of atomic number versus number of neutrons, these decay modes can be recognized as distinct patterns, except for nuclear fission (Fig. 1.2). Nuclear reactions that are caused by particle interactions include the capturing of neutrons

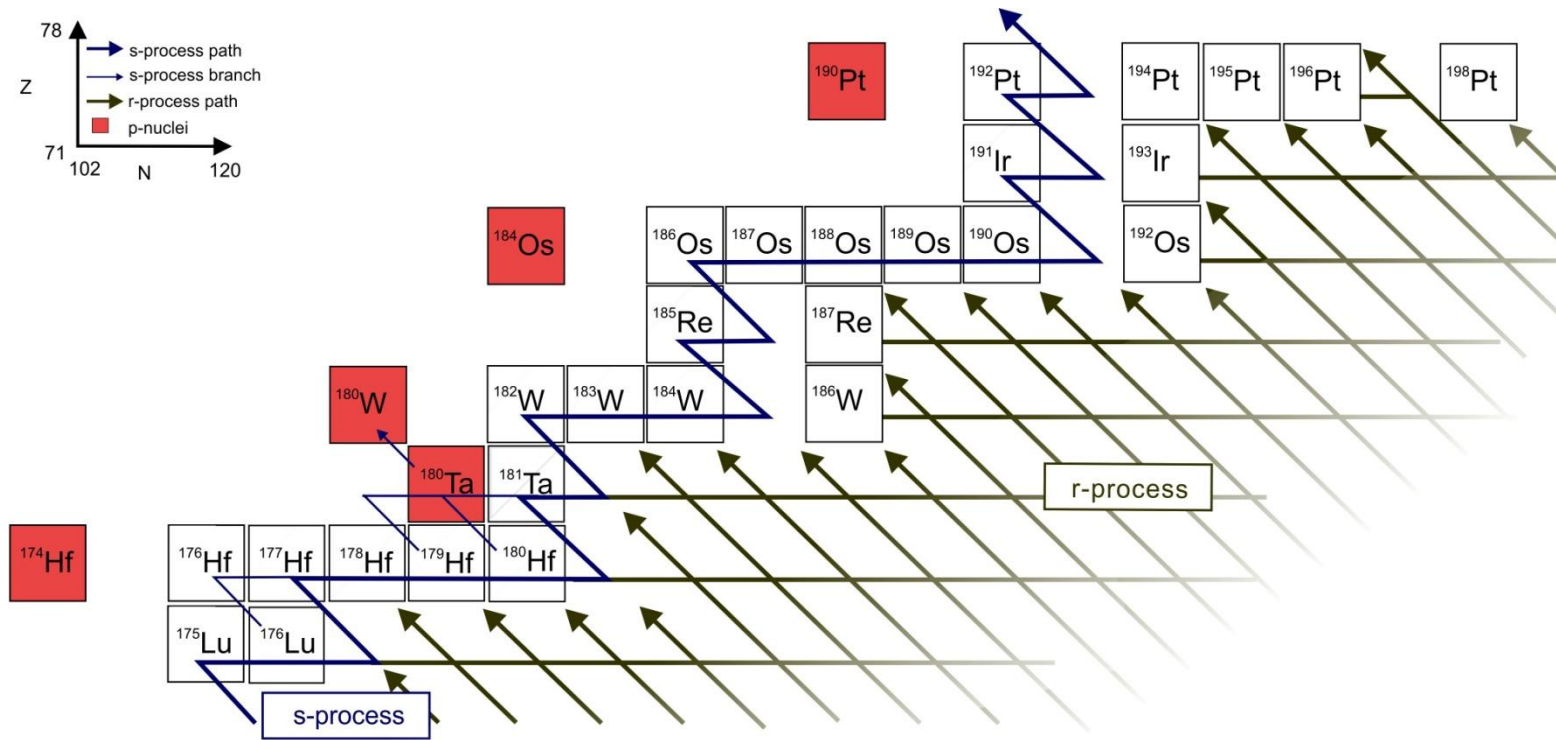


Fig. 1.1 Simplified nucleosynthetic pathways in the Hf-W-Pt mass region, showing the main s-process path (thick line) and branches (thin lines) in blue, whereas the r-process path is indicated in green. P-process nuclei plot on the neutron-poor side of the s-process path and therefore cannot be formed by neutron capture reactions. The branching of the s-process at ^{176}Lu is due to partial excitation to a short-lived nuclear isomer. Branching at ^{179}Hf and ^{180}Hf , also due to the excitation to short-lived nuclear isomers, has been proposed to explain the relatively high solar system abundance of ^{180}Ta (a nuclear isomeric state with half life $\geq 3 \times 10^{13}$ yr) with respect to the expected abundance from an exclusive origin by the p-process (e.g., Beer and Ward, 1981; Németh et al., 1992; Wisshak et al., 2001; Käppeler et al., 2004). Ground state ^{180}Ta , which rapidly decays to ^{180}W and ^{180}Hf with a half life of ~ 8 hours, would also be produced by this process, and therefore potentially provided a minor s-process contribution to ^{180}W .

that were produced by cosmic rays, and fission of some isotopes with $A < 230$ (cosmic ray spallation). When the nuclides that are produced by these processes are unstable, radioactive decay occurs until a stable nuclide is reached.

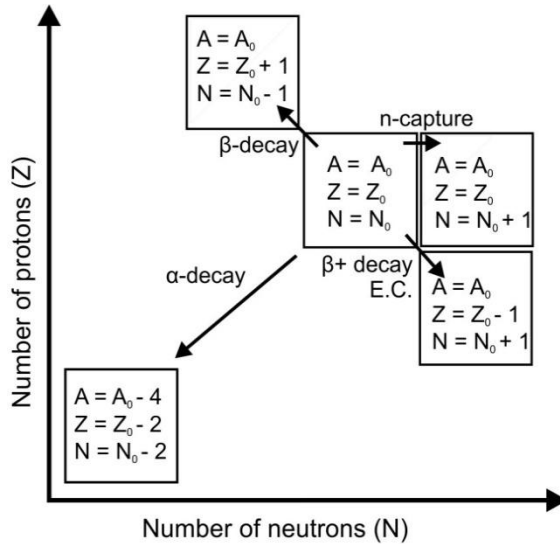


Fig. 1.2 Schematic representation of the effects of neutron capture and different modes of radioactive decay for a hypothetical nuclide with mass A_0 ; proton number Z_0 ; and number of neutrons N_0 .

Additionally, isotopes can be redistributed by roughly mass-dependent isotope fractionation processes. The most important of these processes (kinetic and equilibrium fractionation) are typically strongest for the lightest elements and are therefore not the focus of this dissertation, which deals with heavy elements only. Furthermore, if such effects were present in the samples that have been analysed, they would follow the same trend as the mass-dependent isotope fractionation effects during mass spectrometry, and are therefore corrected for during data reduction. It is important to note that mass-independent isotope fractionation effects, in contrast, would not be corrected for. However, such effects are generally small and were not observed during the course of this study.

1.3 The *p*-process of stellar nucleosynthesis

Some elements that are present in the solar system have isotopes that plot on the left-hand, neutron poor side isolated from the *s*-process path, and, hence, cannot have formed via neutron capture reactions. The components that constitute these isotopes are referred to as *p*-nuclides. The formation mechanism of *p*-nuclides was dubbed “the *p*-process” by B²FH and

was first ascribed to proton capture reactions. Subsequently, it became clear that proton capture reactions may play only a minor role in the production of these nuclides, and that probably more than one type of nuclear reaction at different astrophysical sites are required to account for the observed solar system abundances (e.g., Arnould & Goriely, 2003; Rauscher et al., 2013). In order to distinguish between different types of production mechanisms, recent literature in nuclear astrophysics suggests using the term “p-process” only for the production mechanism based on proton-capture reactions (Rauscher et al., 2013). In the meteorite community, however, there is generally less relevance for making this distinction, and the term “p-process” is therefore conventionally used as a collective term for the processes that produced the p-nuclides. Here, the term “p-process” is adopted in the latter manner.

The most successful mechanism in producing p-process isotopes with the relative solar system abundances is the γ -process, which includes the production via photodisintegrations of heavier s- and r-process nuclei in explosive O/Ne-shell burning during a core-collapse supernova. However, isotopes with masses $A < 124$ and $150 \leq A \leq 165$ are typically underproduced by this process (e.g., Rauscher et al., 2013 and references therein). The solar system abundances of isotopes with these particular masses may therefore reflect the enrichment by an additional nucleosynthetic source, therefore indicating a possible decoupling between the origins of p-process isotopes with different masses in the solar system. As p-process isotopes with $A \geq 165$ (hereafter: *heavy* p-process isotopes) are successfully produced by γ -process models, it may be assumed that these were indeed produced in core collapse type supernovae. In contrast, p-process isotopes with $A \leq 165$ (hereafter: *light* p-process isotopes), may have contributions from different nucleosynthetic sources. The rare heavy isotope ^{180}Ta forms an exception and probably yields a large s-process component in addition to a γ -process component (see Fig. 1.1).

1.4 P-process isotopes and the supernova trigger hypothesis for solar system formation

In order to explain the variable abundances of daughter products of some short-lived radionuclides in early solar system materials, Cameron and Truran (1978) suggested that the explosion of a nearby supernova triggered the collapse of the molecular cloud from which the solar system formed. Several short-lived radionuclides (e.g., ^{26}Al , ^{36}Cl , ^{41}Ca) have in the meanwhile been shown to possibly originate from irradiation of nebular material by accelerated H and He nuclei, whereas others (e.g., ^{60}Fe , ^{107}Pd , ^{129}I , ^{182}Hf) may have been

produced by steady state galactic nucleosynthesis (e.g., Russell et al., 2001; Leya and Wieler, 2003; Goswami et al., 2005; Gounelle et al., 2006; Gounelle and Meiboom, 2006), but the original hypothesis still holds. Independent of the argument from short-lived radionuclides, heterogeneities in Mo and Ba isotopes between early solar system materials have also been interpreted to reflect incomplete mixing between the molecular cloud and ejecta from nearby supernova sources (e.g., Yin et al., 2002; Andreasen and Sharma, 2007). As explained above, such heterogeneities may, however, also be caused by the selective thermal processing of isotope carrier phases. Collectively, there is still considerable uncertainty about whether a supernova injection provided a source of short-lived radionuclides in the solar system, and if so, whether this material was well mixed into existing solar system matter.

Notably, the abundances of heavy p-process isotopes in the solar system are relatively low for a given element, i.e., one to two orders of magnitude lower than the (combined) s- and r-process isotope abundances. If nearby heavy p-process isotope-enriched supernovae indeed contributed matter to the nascent solar system, it may therefore be expected that such injections would yield a relatively large excess in heavy p-process isotopes compared to the preexisting molecular cloud. Thus, if supernova nucleosynthetic matter was indeed not well mixed in the solar system, heavy p-process isotopes could provide a sensitive tracer for such heterogeneities. Several p-process isotopes in the *light* mass range were previously measured in extraterrestrial materials, including ^{84}Sr , $^{92,94}\text{Mo}$, $^{96,98}\text{Ru}$, ^{120}Te , $^{130,132}\text{Ba}$, and ^{144}Sm (e.g., Fehr et al., 2004; Andreasen and Sharma, 2006; Carlson et al., 2007; Burkhardt et al., 2011; Moynier et al., 2012). None of these show unambiguous evidence for p-process heterogeneity, except for possible ^{144}Sm heterogeneities. The work presented here is among the first to study p-process isotopes in the *heavy* mass range. Among the heavy p-process isotopes, only ^{184}Os and ^{180}W were previously reported in iron meteorites (Walker, 2012; Schulz et al., 2013). Whereas the abundance of ^{184}Os was undistinguishable from terrestrial Os, large excesses in ^{180}W were found.

1.5. The information provided by heavy p-process isotopes ^{174}Hf , ^{180}W and ^{190}Pt

This dissertation focuses on the abundances of heavy p-process isotopes ^{174}Hf , ^{180}W and ^{190}Pt in early solar system materials. The first part focuses on the analytical aspects for determining the abundances of these isotopes, which is challenging due to the low abundances. In this section, the first data for ^{190}Pt in iron meteorites are reported and

discussed. The second and third parts of the dissertation focus on the distributions of ^{174}Hf and ^{180}W in early solar system materials, respectively.

When interpreting the isotopic compositions of elements in the context of nucleosynthetic inventory, it is essential to assess the possibility that the isotopes of interest were furthermore affected by radioactive decay and particle interactions. All Hf, W and Pt isotope data are therefore critically assessed in terms of possible neutron capture effects caused by the exposure to cosmic rays. Furthermore, the possible role of α -decay of ^{184}Os in producing the ^{180}W excesses in iron meteorites is evaluated in a separate chapter, based on combined ^{180}W isotope and Os-W concentration data. This evaluation led to the discovery of the ^{184}Os - ^{180}W radioactive decay system, which is further explored as a possible tracer and chronometer in geo-cosmochemistry.

Chapter II

High-precision measurements of low-abundance isotopes ^{174}Hf , ^{180}W ,
 ^{190}Pt using multi-collector ICP-MS with $10^{12}\Omega$ Faraday amplifiers

2.1 INTRODUCTION

Throughout the past century, the improved precision of isotope measurements in natural rock samples has contributed a wealth of information on the geological processes that shaped the Earth and the solar system (e.g., Faure, 1977; Dickin, 2005; Sharp, 2006; Allègre, 2008). The most precise techniques available for isotope analyses of metals are thermal ionization mass spectrometry (TIMS) and multi-collector inductively coupled plasma mass spectrometry (MC-ICPMS) (see reviews by e.g., Albarède et al., 2004; Albarède & Beard, 2004; VanHaecke et al., 2009). Both methods routinely achieve precisions of several tens of ppm for isotopes with larger relative abundance using Faraday collectors, and challenging protocols even achieve precisions in the ppm range (for ^{142}Nd : Caro et al., 2006; for ^{182}W : Willbold et al., 2011; Touboul et al., 2012). For both Faraday detectors and ion counting systems, however, measurement precisions for isotopes with low abundances ($\leq 0.1\%$) have previously been restricted by counting statistics, typically not much better than $\pm 10,000$ ppm. In the case of Faraday collectors, this largely results from the Johnson noise that is generated by the high-ohmic feedback resistors that are used for current amplification (e.g., Wieser & Schwieters, 2005).

As the Johnson noise of these resistors scales with the resistor value as the square root only, signal-to-noise ratios are predicted to improve when recently developed $10^{12} \Omega$ resistors are used rather than the traditional $10^{11} \Omega$ ones. Indeed, it has been shown that the signal-to-noise ratio for $10^{12} \Omega$ current amplifiers is a factor of ~ 2 (Wieser & Schwieters, 2005) to $\sim 3-5$ (Koornneef et al., 2013) better than for amplifiers with $10^{11} \Omega$ resistors. Meanwhile, amplifiers with $10^{12} \Omega$ resistors were successfully employed for determining isotopic compositions in small sample amounts using MC-ICP-MS (e.g., Makishima & Nakamura, 2010, 2012; Schulz et al. 2013) and TIMS systems (Koornneef et al., 2013; Liu & Pearson, 2014). In contrast to most of these applications we explore here for the first time the versatility of these amplifiers in high-precision measurements of isotopes with extremely low relative abundances, namely ^{174}Hf , ^{180}W , and ^{190}Pt . These low abundance isotopes are of particular interest in cosmochemistry, as they were to a large extent produced by the p-process during stellar nucleosynthesis (e.g. Arnould and Goriely, 2003; Rauscher et al., 2013). Here we present analytical protocols including ultra-clean chemical separation procedures of the target elements that are necessary for obtaining accurate and precise data, and report long-term isotope compositions for the three isotopes that are significantly more precise than

previous estimates. Finally, the first high-precision data for ^{174}Hf and ^{190}Pt in terrestrial rock samples (^{174}Hf only) and meteorites are presented.

2.1.1 Previous determinations of natural abundances of ^{174}Hf , ^{180}W , ^{190}Pt

Previous studies in which the relative abundances of ^{174}Hf , ^{180}W and ^{190}Pt were determined mainly focused on the compositions of matrix-free, commercial standards. Most of these studies were performed with MC-ICP-MS, all of which employed conventional $10^{11}\Omega$ Faraday amplifiers. Hf-174 has been reported in the JMC 475 Hf standard solution with external precisions of 20-40 parts in ten thousand, based on TIMS (Patchett, 1983) and MC-ICP-MS measurements (Amelin, 2000; Chu et al. 2002). The same standard was measured by Thirlwall & Anczkiewicz, (2004) who reported internal precisions of < 2.5 parts in ten thousand and 2 times higher external precisions. These authors plotted their measured values for $^{174}\text{Hf}/^{177}\text{Hf}$ in the JMC 475 standard together with those for spiked rock samples for comparison (i.e., Fig. 8 of their paper), but without reporting the data for the latter. However, their internal precisions for ^{174}Hf in rock samples generally appear to be poorer than for the JMC 475, most likely due to the presence of matrix elements and isobaric ^{174}Yb . One study (Qin et al., 2011) that attempted to determine ^{174}Hf in leachates of carbonaceous chondrites did not report any data because the authors suspected an interfering species on ^{173}Yb , which was collected for monitoring the interference by ^{174}Yb .

In the 1990s, two pioneering studies were dedicated to determine the abundance of ^{180}W in natural materials. These studies reported ^{180}W abundances in purified standard materials at the level of 5-15 parts in ten thousand (Völkening et al., 1991a - TIMS measurements of an in house Na_2WO_4 standard; Lee & Halliday, 1995 - MC-ICP-MS measurements of NIST-3163 and H. Cross Company standard filament). More recently, by employing $10^{12}\Omega$ Faraday amplifiers on their MC-ICP-MS system, Schulz et al. (2013) reported the discovery of ^{180}W -heterogeneities in iron meteorites with measurement precisions of better than 1 parts in ten thousand. This spurred a search for the origin of these anomalies with new, but so far poorly documented high-precision protocols (Holst et al., 2011; Cook et al., 2013; Peters et al., 2014).

Platinum-190 was determined in purified Pt materials in four recent studies, using gas source mass spectrometry (Taylor et al., 1994); quadrupole ICP-MS (Wolff Briche et al., 2002); and MC-ICP-MS (Morgan et al., 2002; Creech et al., 2013). One older study used a

double focusing mass spectrometer with thermal ionization source (White et al., 1956) with an estimated uncertainty of 4%. Wolff Briche et al. (2002) and Creech et al. (2013) determined the isotopic composition of reference material IRMM-010, whereas others measured in-house standards only. Precisions of the four recent studies vary between 20 and 50 parts in ten thousand except for Creech et al. (2013) who report internal precisions for $^{190}\text{Pt}/^{194}\text{Pt}$ ratios of 1 parts in ten thousand on a Neptune Plus instrument, and double that on a Nu Plasma machine, using external mass bias normalization to the isotope composition of doped Pb. The reported ratios between these instruments varied, however, outside of the reported analytical uncertainties and the authors therefore estimated the $^{190}\text{Pt}/^{194}\text{Pt}$ ratio of IRMM-010 with an uncertainty level of ~ 100 parts per ten thousand. Notably, all values for the abundance of ^{190}Pt even reported by more recent studies vary outside of the reported analytical uncertainties, the studies of Morgan et al. (2002) and Creech et al. (2013) excluded. This shows that the terrestrial abundance of ^{190}Pt is in fact poorly constrained, or alternatively that true variations between reference materials exist or may have formed during sample preparation.

2.1.2 Relevance of high-precision ^{174}Hf , ^{180}W and ^{190}Pt data to geo- and cosmochemistry

Most heavy nuclides in the solar system were formed in a variety of stellar environments by an interplay between neutron capture reactions and β -decay (e.g., Burbidge et al., 1957; Clayton, 1968; Wallerstein et al., 1997). These so called s- and r-process nuclides make up the most abundant isotopes in the solar system. A minor group of proton-rich nuclides, including ^{174}Hf , ^{180}W and ^{190}Pt , however, cannot have formed by these nucleosynthetic processes. These nuclides make up a group of isotopes with typically low abundances, and their formation mechanism is referred to as the p-process (e.g., Arnould & Goriely, 2003). The abundances of s- and r-process isotopes in different solar system materials is relatively well constrained for most elements, but studies for p-process isotopes have long been hampered by analytical difficulties due to their low relative abundances. Yet, precise data on p-process isotopes for a given element may help to distinguish between s-process deficit and r-process excess in bulk meteorites and between meteorite components (e.g., Dauphas et al., 2004; Trinquier et al., 2007; Trinquier et al., 2009; Burkhardt et al., 2012). Furthermore, determining the p-process component in presolar carrier phases provides an important reference frame for theoretical nucleosynthetic models (e.g., Ávila et al., 2012; Akram et al., 2013; Rauscher et al., 2013).

2.2 ELEMENT PURIFICATION

Amongst others, the accurate determination of the abundances of ^{174}Hf , ^{180}W and ^{190}Pt is challenged by large isobaric interferences of more abundant (combined) s- and r-process isotopes (Table 2.1). Furthermore, the presence of sample matrix may affect the correction for instrumental mass bias more so than for isotopes with higher abundances, therefore resulting in apparently aberrant isotope ratios relative to the matrix-free standard solution. We therefore developed ultra-clean separation protocols for Hf, W and Pt, aimed at determining the low-abundance isotopes of these elements by MC-ICPMS. These protocols are mainly based on modifications of previously published separation schemes and are summarized below.

Table 2.1 Abundances of ^{174}Hf , ^{180}W , ^{190}Pt and elemental isobars

<i>Isotope of interest</i>	<i>Abundance^a</i>	<i>Elemental isobars</i>	<i>Abundance^a</i>	<i>Chondritic ratio^b</i>
^{174}Hf	0.0016(1)	^{174}Yb	0.32026(80)	Yb/Hf = 1.5
^{180}W	0.0012(1)	^{180}Hf	0.3520(16)	Hf/W = 1.2
		^{180}Ta	0.00012(2)	Ta/W = 0.2
^{190}Pt	0.00012(2)	^{190}Os	0.2626(2)	Os/Pt = 0.5

^aIUPAC recommended values for “representative isotopic compositions (mole fractions)” (Berglund & Wieser, 2009).

^bBased on the estimated concentrations by Palme & O’Neill (2003).

2.2.1 Reagents and sample digestion

Once-Teflon-distilled HNO_3 and double-Teflon-distilled HCl and HF were used throughout. Suprapur grade HClO_4 , H_2O_2 and citric acid were used. Ultra-pure water ($\sim 18 \text{ M}\Omega\text{-cm}$) for preparing acid mixtures was obtained from a Milli-QTM system. Only fresh double-distilled HF was used in order to minimize blanks for W, as the Teflon beakers in which the acid was stored may contain up to several ng of W (e.g., Kleine et al., 2004). For the same reason, all beakers that were used during sample preparation for W isotope analyses were pre-cleaned with 1 mM diethylene triamine pentaacetic acid (DTPA) dissolved in 1 M HCl , subsequent to regular cleaning in HNO_3 , aqua regia, HF , respectively.

SavillexTM Teflon beakers were used for sample digestions. Basaltic samples were digested in a $\sim 1:1$ mixture of 24N HF -14N HNO_3 at 120°C tabletop, whereas chondrite samples were digested in a $\sim 5:5:2$ mixture of 24N HF -14N HNO_3 -9.5N HClO_4 at 180°C tabletop. Iron meteorites (pure metal matrices) were digested in aqua regia at room temperature. After evaporation, samples were dried down three times in $\sim 14\text{N}$ HNO_3 with trace HF ($<0.05\text{N}$). A clear solution without fluoride precipitates was subsequently obtained

by re-dissolving the sample in 6N HCl-0.06N HF. The acid volumes that were used depend on the concentrations of the target elements in the samples and on the intensities at which the isotopes of interest may be measured at sufficient precisions, which is further discussed in paragraph 3.2. Typically, 0.5-1.5 g of chondrite sample, 0.1-0.3 g basalts, and 0.1 g of iron meteorite sample were digested.

For W, samples that had been digested in HClO₄ occasionally showed extremely low yields (<20%) after the first-stage anion chemistry, and yielded unacceptably high concentrations of matrix elements. This problem occurred erratically and possibly as the result of leftover trace HClO₄ from the digestion step, despite the samples being optically dry before loading. Equilibrated chondrites (metamorphic types 4-6) were therefore digested in HF-HNO₃ only, leaving a residue of pure graphite that was separated from the dissolved silicate and metal fractions by centrifuging. This is an acceptable digestion method for equilibrated chondrites, because they appear to be isotopically homogeneous, and graphite does not contain significant amounts of W. More care, however, must be taken with lower grade metamorphic chondrites that potentially yield isotopically anomalous presolar carrier phases. Some of these phases such as SiC grains are resistant to HF-HNO₃ digestion, and digestion without HClO₄ may therefore result in data that is not representative for the bulk sample.

2.2.2 Ultra-pure separation of Hf from basaltic matrices and chondrites

In order to obtain sufficiently clean Hf-cuts with respect to Yb, existing protocols (e.g., Münker et al., 2001; Weyer et al., 2002; Sprung et al., 2010) were optimized into a two-stage separation scheme (Table 2.2). In the first-stage chemistry, Hf is separated from the rock matrix using columns that are 6 mm in diameter filled with 1 mL EichromTM Ln-Spec resin (100-150µm, H⁺ form). Ln-Spec resin consists of an inert polymeric carrier that is coated with di(2-ethylhexyl)phosphoric acid (HDEHP) as the extractant. The resin was cleaned before loading with three times alternating ~10 resin volumes (rv) 2N HF (HFSE) and ~10 rv 6N HCl (matrix, HREE). Before equilibration of the resin in 3N HCl, a final cleaning step with ~5 rv 2N HF was used to remove HFSE from the HCl-blank, followed by 2×2 rv H₂O to rinse HF from the column. Most major and trace elements, including the light rare earth elements (LREE), are not retained by HDEHP in >1N HCl. In contrast, at these HCl molarities, the high field strength elements (HFSE; i.e., Ti, Zr, Nb, Hf, Ta) and at < 4N HCl also the heavy rare earth elements (HREE; i.e., Yb, Lu) are retained by the resin (e.g., Braun, 1975; Vin and

Khopkar, 1991; Münker, 2001). The sample is therefore best loaded in 5 rv 3N HCl. After an additional 10 rv 3N HCl are added, >99 % of the matrix, including significant amounts of HREE have been rinsed off the column. Subsequently, 20 rv of 6N HCl are added. By increasing the HCl molarity, the remaining Yb-Lu is rinsed off the column, whereas the HFSE are retained by the resin. Subsequent separation of Hf from Ti and Zr, both abundant elements in silicate samples, is necessary as their presence may affect instrumental mass bias behaviour of Hf (e.g., Münker et al. 2001). Titanium is efficiently eluted in a mixture of 0.09N Hcit (citric acid) - 0.45N HNO₃ - 1 wt% H₂O₂ as a yellow-orange peroxide complex, whereas all other HFSE are retained on the column as citrate complexes. The tolerance level to HF molarity is lower for Zr than for the other HFSE, making efficient separation of Hf from Zr possible by rinsing the latter off the column with 50 rv of 6N HCl - 0.06N HF. Hafnium (and some Ta, Nb) is subsequently eluted in 12 rv 2N HF. Note that previously published procedures to separate Hf from silicate matrices on Ln-Spec included ascorbic acid as an additive in the loading step with the aim to reduce all iron to Fe²⁺, because Fe³⁺ is weakly retained by the resin in 3N HCl (e.g., Weyer et al., 2000; Münker et al., 2001; Sprung et al., 2010). In our procedure, Fe³⁺ is removed during the second-stage clean-up and ascorbic acid was therefore not included in order to keeping acid blanks low.

The second-stage clean-up step is necessary to further purify Hf with respect to Yb, and employs columns that are 8 mm in diameter filled with 4 mL BioRad AG 1-X8 anion resin. Prior to loading, the resin was cleaned with ~4 rv DTPA; ~4 rv 3N HNO₃; ~8 rv 6N HNO₃-0.2N HF, respectively. On AG 1-X8 resin, HFSEs have high partition coefficients in HF, whereas most major elements show no adsorption (e.g., Faris, 1960; Kim et al., 1973). The Hf-cuts from the first-stage columns in 2 N HF can therefore directly be loaded on the anion resin columns without drying down and re-dissolving the sample in between. Any residual matrix elements including Yb and Fe³⁺ can be washed off the column with 2^{1/2} rv 0.5N HCl-0.5N HF. A clean Hf fraction can subsequently be eluted in 3^{3/4} rv 6N HCl-0.06N HF. Tantalum may also be eluted and optionally collected in an additional 3^{3/4} rv 6N HNO₃-0.2N HF-1% H₂O₂ for isotope analysis (e.g., Pfeifer et al., 2013).

Table 2.2 Hf-separation from silicate rocks for ^{174}Hf -measurements

<i>Step</i>	<i>Amount^a</i>	<i>Reagent</i>
Column I (1 mL EichromTM Ln-Spec; ϕ 6 mm)		
Equilibrate	5 rv	3N HCl
Load	5 rv	3N HCl
Rinse matrix	10 rv	3N HCl
Rinse HREE	10 + 5 +5 rv	6N HCl
Wash resin	2 x 2 rv	H ₂ O
Rinse Ti	Variable	0.09N HCit-0.4N HNO ₃ -1% H ₂ O ₂
Rinse Zr	5 x 10 rv	6N HCl-0.06N HF
Collect Hf (+Ta,Nb)	7 + 5 rv	2N HF
Column II (4 mL BioRad AG 1-X8; ϕ 8 mm)		
Equilibrate	2½ rv	2N HF
Load Hf-cut step I	3 rv	2N HF
Rinse	½ rv	2N HF
Rinse remaining matrix, Yb	2½ rv	0.5N HCl-0.5N HF
Collect Hf	3¾ rv	6N HCl-0.06N HF
(Collect Ta)	(3¾ rv)	(6N HNO ₃ -0.2N HF-1% H ₂ O ₂)

^aIndicated as number of resin volumes (rv)

2.2.3 Tungsten separation from silicate matrices for precise ^{180}W measurements

Sufficiently clean separation of W for ^{180}W measurements in iron meteorites (metal matrices) is achieved with the two-stage protocol described by Schulz et al. (2013) (modified after Kleine et al., 2004; Schulz et al., 2009). The first step of this previously published protocol included separation of W from the matrix, and the second step further purification with respect to Hf, and both steps were based on BioRad AG 1-X8 anion resin. Samples with silicate matrices have significantly higher Hf/W than iron meteorites, and we consequently noticed that the protocol by Schulz et al. (2013) insufficiently reduced Hf/W of silicate samples. Furthermore, samples with silicate matrices typically yield high abundances of Zr and Ti. These elements were observed to affect the mass bias behavior of W during mass spectrometry, typically resulting in worse precisions and occasionally inaccurate $\epsilon^{180}\text{W}$ through sample bracketing. Together, Hf, Ti and Zr must therefore be removed from the sample at high efficiency, but this is not sufficiently achieved using AG 1-X8 resin. We therefore present an alternative technique that is based on EichromTM TEVA resin. TEVA resin is comprised of an aliphatic quaternary amine sorbed on an inert polymeric substrate, and was originally developed to separate tetravalent actinides in radioactive waste (Horwitz et al., 1995). TEVA resin has been used routinely for the separation of Tc (e.g., Nevissi et al., 1994; Uchida and Tagami, 1997; Seki and Kondo, 2005; Paučová et al., 2012). These

procedures typically utilise the strong retention of Tc at all HCl molarities, whereas other elements can selectively be eluted. In most procedures, Tc is subsequently eluted at HNO₃ molarities higher than 2. Later, it was realized that Re could be separated from rock matrices based on TEVA resin in a way similar as Tc (e.g., Butterworth et al., 1995; Tagami and Uchida, 2000). Tungsten shares physiochemical properties with both Re and Tc, and TEVA resin was therefore considered an ideal candidate for developing a purification procedure. We therefore modified the first-stage chemistry by Schulz et al. (2013) and replaced the second-stage with an alternative clean-up procedure that was based on TEVA resin (Table 2.3).

Samples were loaded on \varnothing 8 mm columns filled with 4 mL BioRad AG 1-X8 anion resin in 1-1 $\frac{1}{4}$ rv 1N HCl-0.5N HF. Precipitation of Ca-Mg fluorides in the loading solution was observed to decrease yields for W, most likely due to co-precipitation of W in the interstitial liquid. This problem may largely be circumvented by washing the precipitate in 1 $\frac{1}{4}$ rv 0.5N HCl-0.5N HF and adding the wash solution to the column in a second loading step. This procedure increased the overall yields to typically ~80%. After the first and second loading steps, matrix elements can be further removed from the sample with 2 $\frac{1}{2}$ rv 0.5N HCl-0.5N HF whereas HFSE, W, Mo are retained on the column (Kleine et al., 2004 and references therein). Most of the HFSE, W and Mo are subsequently eluted in 6N HNO₃-0.2N HF, whereas Ta may subsequently be collected with a ~100 % yield in 2 $\frac{1}{2}$ r 6N HNO₃-0.2N HF-1 wt% H₂O₂ (e.g., Munker et al. 2001, Pfeifer et al., 2013).

After drying down and re-dissolving in 2 mL 6N HCl, the sample was loaded on \varnothing 6 mm columns with 0.5 mL TEVA resin. Prior to loading, the TEVA resin had been cleaned with three times alternating ~3 rv 3N HNO₃-0.2N HF and ~8 mL 3N HNO₃, respectively. Before equilibrating the resin with 6N HCl, ~1 rv H₂O was used to rinse remaining HNO₃ off the column. We found that among the HFSE, only W is retained by the resin in 6N HCl, whereas Hf, Ti and Zr immediately flush through (Fig. 2.1). After loading and rinsing with an additional 3 \times 1 rv 6N HCl, a clean W-fraction was eluted in 4 rv 3N HNO₃. The yield for this clean-up procedure was close to 100%.

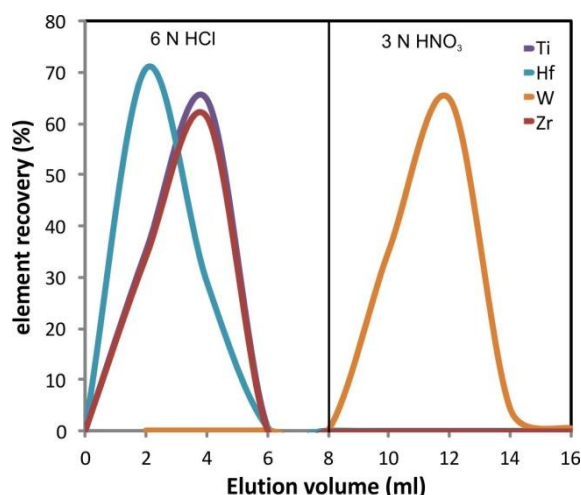


Fig. 2.1. Elution scheme for the HFSE on Eichroms™ TEVA resin, illustrating the second stage column chemistry for the purification of W for ^{180}W measurements. Curves are based on fractions of 2 mL.

Table 2.3 W-separation from silicate rocks for ^{180}W -measurements

Step	Amount ^a	Reagent
Column I (4 mL BioRad AG 1-X8; ø 8 mm)		
Equilibrate	2 × 1¼ rv	0.5N HCl-0.5N HF
Load ^a	1-1¼ rv	1N HCl-0.5N HF
Load ^b , rinse matrix	1¼ rv	0.5N HCl-0.5N HF
Rinse matrix	2 × 1¼ rv	0.5N HCl-0.5N HF
Collect W-Hf-Ti-Zr	3¾ rv	6N HNO ₃ -0.2N HF
Collect Ta (optional)	3¾ rv	6N HNO ₃ -0.2N HF-1% H ₂ O ₂
Column II (0.5 mL TEVA; ø 6 mm)		
Load W-Hf-Ti-Zr-cut	4 rv	6N HCl
Rinse Hf-Ti-Zr	4+4+4 rv	6N HCl
Collect W	16 rv	3N HNO ₃

^aIndicated as number of resin volumes (rv)

2.2.4 Platinum separation from metal matrices

Protocols for separating the platinum group elements (PGEs) from silicate matrices have, amongst others, been described by Rehkämper & Halliday (1997). These protocols are based on anion exchange and were successfully modified by Creech et al. (2014) with the purpose of obtaining sufficiently clean solutions for $^{198}\text{Pt}/^{194}\text{Pt}$ measurements by MC-ICPMS, using a double spike method (Creech et al., 2013). Although the protocols by Creech et al. (2014) included an elution scheme for an artificial iron meteorite matrix, no data for actual iron meteorites were reported. Our procedure for Pt-separation is similar to theirs, with the important differences that a larger resin volume was used, and that steps were added to

minimize Os/Pt and Ir/Pt (Table 2.4; Fig. 2.2). These procedures were necessary because ^{190}Pt and ^{192}Pt (~0.78 %) suffer from large isobaric interferences by $^{190,192}\text{Os}$ and tailing effects by $^{191,193}\text{Ir}$ during mass spectrometry. Furthermore, the presences of large amounts of Os and Ir in Pt-cuts affected the instrumental mass bias behavior of Pt, and long washout times were observed to reduce this effect.

Columns of 8 mm in diameter were prepared with 1.75 mL BioRad AG 1-X8 anion resin. The resin was cleaned with a sequence of 17 rv 0.8N HNO₃; 8 rv 11N HCl and 8 rv 13N HNO₃ and before equilibrating the resin with 0.5N HCl for loading, 23 rv 6N HCl was used to reconvert the resin to the chloride form (e.g., Rehkämper & Halliday, 1997). Samples were then loaded in 5-6 rv 0.5N HCl, such that Pt is retained on the column together with most of the PGEs, whereas other matrix elements flush through (Rehkämper & Halliday, 1997). The remaining matrix and some Ir(III), Ru, Rh and Pd is rinsed off the column with an additional 43 rv 0.5N HCl, and subsequently with 29 rv 1N HCl. In agreement with Creech et al. (2014) we subsequently eluted Ir in 29 rv 0.8N HNO₃, indicating that some iridium on the column occurs as Ir(IV), as Ir(IV) is retained by the resin in weak HCl, but not in HNO₃. Rhenium and some leftover Pd and Ir were eluted in 57 rv 11N HCl, before Pt was eluted and collected in 17 rv 13N HNO₃. After drying down the sample, 1 mL 9.5N HClO₄ was added to oxidize Os to OsO₄, which was then removed as a volatile compound by drying down the sample at 190°C. Furthermore, the dry-down step with HClO₄ results in the breakdown of large organic molecules that are potentially eluted from the anion resin, and may cause interferences during mass spectrometry. Organic interferences were occasionally observed for matrix-free Pt-solutions that were not dried down with HClO₄, and are a direct consequence of the high HNO₃ normality in the final elution step. The entire procedure was repeatedly tested by processing artificial iron meteorite matrices with admixed PGEs (~1 mg each), Fe, Ni, and Co (~100 mg each). The measured isotopic compositions of these experiments were indistinguishable from the matrix-free Alfa Aesar Pt-solution.

Table 2.4 Separation of Pt from metal matrices for ^{190}Pt - measurements

Step	Amount ^a	Reagent
Column I (1.75 mL BioRad AG 1-X8; ca ϕ 8 mm)		
Equilibrate	2×2 rv	0.5N HCl
Load	5-6 rv	0.5N HCl
Rinse matrix, Ru, Pd, Rh, Ir(III)	43 rv	0.5N HCl
Rinse Ru, Pd, Rh, Ir(III)	29 rv	1N HCl
Rinse matrix, Ir(IV)	29 rv	0.8N HNO ₃
Rinse transition metals, Re, Pd, Ir	57 rv	11N HCl
Collect Pt	17 rv	14N HNO ₃

^aIndicated as number of resin volumes (rv)

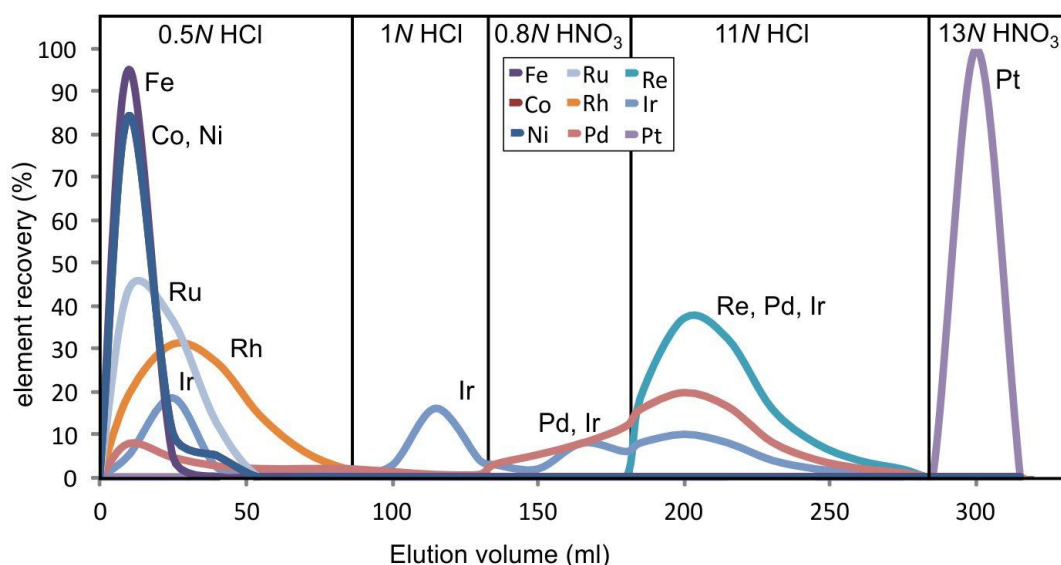


Fig. 2.2 Elution scheme for Pt separation from iron meteorites using BioRad AG 1-X8 anion resin.

2.3 MASS SPECTROMETRY

2.3.1 Apparatus, cup configurations and data processing

All MC-ICP-MS data were collected using the Thermo FinniganTM Neptune system at the Cologne-Bonn joint clean lab facility between October 2010 and January 2014. Samples and standards were introduced into the plasma using a CETAC Aridus IITM desolvating nebulizer system connected to a PFA nebulizer with sample uptake rates of typically $\sim 100 \mu\text{L min}^{-1}$. Oxide production levels were typically $< 0.1\%$. All measurements were performed with the combination of regular sampler cones and x-skimmer cones. Additionally, a sampler cone with large aperture (“Jet” cone) was tested in combination with an x-skimmer cone for Hf and W isotopic measurements. This setup allows a larger ion beam to enter the mass

spectrometer and requires the use of a high-vacuum interface pump, for which purpose an OnTool BoosterTM at 4500 r·min⁻¹ was used. In this setup, ca. 5 times higher beam intensities for Hf and W were achieved than in the regular setup. However, it was observed that only minute amounts of matrix had strong effects on the mass bias behavior of the target elements, making accurate sample bracketing with matrix-free solutions impossible. For Hf, these effects correlate with the relative Zr content in the sample (Fig. 2.3). Furthermore, mass scans revealed the presence of an interfering species on ¹⁷²Yb that was otherwise absent when regular sampler cones were used, resulting in an overcorrection for isobaric ¹⁷⁴Yb. The latter may relate to higher oxide-hydroxide production rates caused by poorer vacuum at the interface.

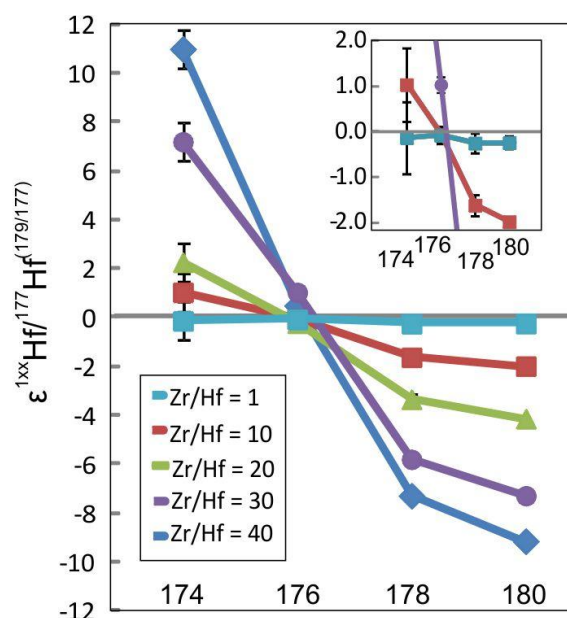


Fig. 2.3 $^{1xx}\text{Hf}/^{177}\text{Hf}$ in the Hf AMES metal standard with various amounts of admixed Zr, measured in the setup with Jet sampler cone and x-skimmer cone. $\epsilon^{1xx}\text{Hf}$ represents the deviation from the from the matrix-free solution in parts per 10,000 and increases with increasing Zr/Hf. This is interpreted to result from Zr affecting the instrumental mass bias behavior of Hf. The typical range in Zr/Hf after ion exchange chromatography was 1-10 and such effects can be significant at these levels, as illustrated by zoom window in inset. Normalization for instrumental mass bias is to $^{179}\text{Hf}/^{177}\text{Hf} = 0.7325$ using the exponential law.

All measurements were performed in low-resolution mode ($M/\Delta M \sim 1000$). The Neptune system at Bonn-Cologne is equipped with nine Faraday collectors that may be connected to eleven amplifiers: two with $10^{12}\Omega$ and nine with $10^{11}\Omega$ resistors. For each of the

target elements, one $10^{12}\Omega$ Faraday amplifiers was designated to the measurement of the low abundance isotope of interest, with the other being used for monitoring the isobaric interference (Table 2.5). The gain calibration factor for the $10^{12}\Omega$ amplifiers was determined with a stable reference current of 3.33333 V before each measurement sessions, i.e. a tenfold lower than the reference current for gain calibration of the $10^{11}\Omega$ amplifiers. Data were acquired for 60 cycles with 8.39 s integration time and a 2σ rejection was applied to each cycle, as well as to the total of 60 cycles. The magnet settling time (“idle time”) was set to 10 s. Baselines of 1000 s were taken prior to each measurement session. The typical abundance sensitivity of the instrument is ~ 2 ppm for mass 237/ ^{238}U .

Table 2.5 Collector set up^a

Target element	L4	L3	L2	L1	C	H1	H2	H3	H4
Hf	^{172}Yb ($10^{12}\Omega$)	^{174}Hf , ^{174}Yb ($10^{12}\Omega$)	^{175}Lu	^{176}Hf , ^{176}Lu	^{177}Hf	^{178}Hf	^{179}Hf	^{180}Hf , ^{180}W , ^{180}Ta	^{182}W
W	^{178}Hf ($10^{12}\Omega$)	^{180}W , ^{180}Hf ^{180}Ta ($10^{12}\Omega$)	^{181}Ta	^{182}W	^{183}W	^{184}W , ^{184}Os	^{186}W , ^{186}Os	^{188}Os	
Pt, all isotopes	^{188}Os ($10^{12}\Omega$)	^{190}Pt , ^{190}Os ($10^{12}\Omega$)	^{192}Pt , ^{192}Os	^{193}Ir	^{194}Pt	^{195}Pt	^{196}Pt , ^{196}Hg	^{198}Pt , ^{198}Hg	^{199}Hg
Pt, for high-precision $^{190}\text{Pt}/^{192}\text{Pt}$		^{188}Os ($10^{12}\Omega$)	^{190}Pt , ^{190}Os ($10^{12}\Omega$)	^{191}Ir	^{192}Pt , ^{192}Os			^{198}Pt , ^{198}Hg	^{199}Hg

^a $10^{12}\Omega$ amplifiers at indicated positions

2.3.2 Effects of low beam intensities on measurement precisions

Below a certain threshold level, measurement precisions for each low-abundance isotope of interest become rapidly worse with decreasing beam intensity (Fig. 2.4). Typically, beam intensities of ~ 50 mV for matrix-free solutions corresponded to measurement precisions of < 1 parts per 10,000, whereas intensities of > 100 mV resulted in precisions of < 0.5 parts per 10,000. At beam intensities < 50 mV, in-run precisions became increasingly worse following an apparent power law. The amount of sample that was processed for analysis was therefore aimed to reach at least > 50 mV on the isotope of interest. With the sensitivity of our instrument in the presented setup, this was ~ 30 ng Hf; ~ 40 ng W, and ~ 500 ng Pt. An additional artifact that was observed for very low beam intensities is that isotope ratios occasionally deviate from those measured at higher intensities outside the 2 S.E. in-run precisions. This effect may result from the different signal-to-noise ratios between the $10^{12}\Omega$

and $10^{11}\Omega$ amplifiers. In case when limited sample material is available, the intensities at which the samples and bracketing standards are measured therefore need to be matched closely (e.g., Elfers et al., 2013).

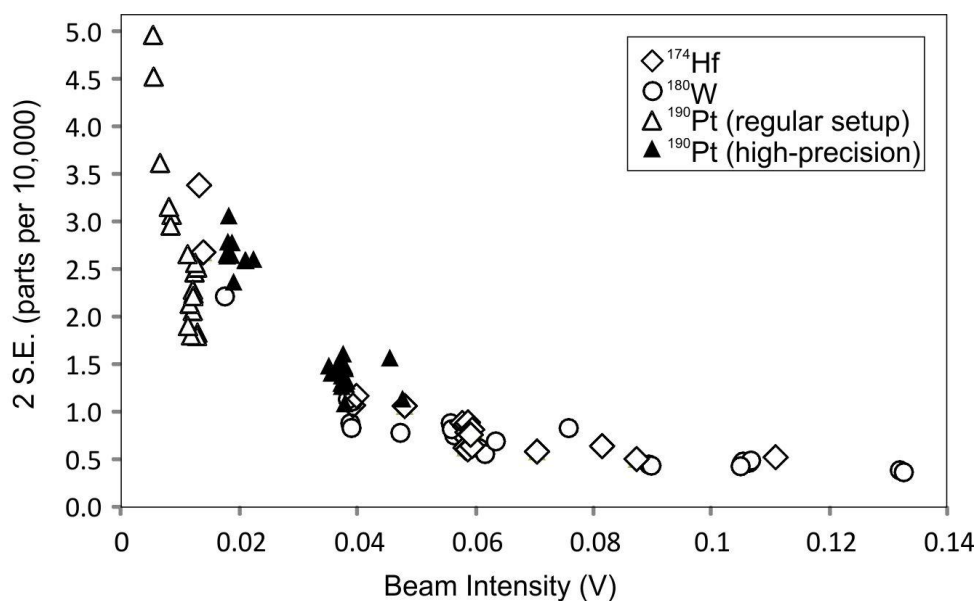


Fig. 2.4 2 S.E. in-run precisions for interference corrected, mass bias normalized isotope ratios $^{174}\text{Hf}/^{177}\text{Hf}$; $^{180}\text{W}/^{184}\text{W}$ and $^{190}\text{Pt}/^{192}\text{Pt}$, plotted against the beam intensity (V) at which the low-abundance isotope in the numerator is collected.

2.3.3 Precise and accurate isotope measurements of Hf

Hafnium has six observationally stable or long-lived isotopes, i.e., ^{174}Hf (~0.12%), ^{176}Hf (~5%), ^{177}Hf (~19%), ^{178}Hf (~27%) and ^{180}Hf (~35%). The abundance of ^{174}Hf was determined relative to the non-radiogenic isotopes in all possible combinations, i.e., $^{174}\text{Hf}/^{177}\text{Hf}$, $^{174}\text{Hf}/^{178}\text{Hf}$, $^{174}\text{Hf}/^{179}\text{Hf}$, $^{174}\text{Hf}/^{180}\text{Hf}$. These measure ratios were corrected for instrumental mass bias using $^{178}\text{Hf}/^{177}\text{Hf}$, $^{179}\text{Hf}/^{177}\text{Hf}$, $^{180}\text{Hf}/^{177}\text{Hf}$, $^{179}\text{Hf}/^{178}\text{Hf}$, $^{180}\text{Hf}/^{178}\text{Hf}$, respectively. Hafnium-176 may have variable radiogenic contributions from long-lived ^{176}Lu and therefore cannot be used for normalization. For mass bias correction, the exponential law and the recommended values by Blichert-Toft et al. (1997) were used. External uncertainties for all $^{174}\text{Hf}/^{1xx}\text{Hf}$ ratios are approximately ~1 parts in ten thousand for > 50 mV on ^{174}Hf , but are generally best for $^{174}\text{Hf}/^{177}\text{Hf}$. Internal uncertainties at this intensity are typically around 80 ppm but may be as low as 50 ppm for matrix-free solutions. For a given $^{174}\text{Hf}/^{1xx}\text{Hf}$ that is corrected for instrumental mass bias using different normalization ratios, the corrected values vary outside the internal reproducibility (Fig. 2.5). This variation increases with the mass

difference between ^{174}Hf and the isotope in the denominator, and reflects inadequate correction for instrumental mass bias using the exponential law. Thus, $^{174}\text{Hf}/^{177}\text{Hf}$ appears as the best approximation of a “true” isotope ratio. The instrumental mass bias is most accurately monitored by $^{179}\text{Hf}/^{177}\text{Hf}$, $^{180}\text{Hf}/^{177}\text{Hf}$, $^{180}\text{Hf}/^{178}\text{Hf}$, all of which have more than one atomic mass unit difference between numerator and denominator. Here, we adopt the $^{179}\text{Hf}/^{177}\text{Hf}$ ratio for mass bias correction, which is conventionally used for $^{176}\text{Hf}/^{177}\text{Hf}$ measurements.

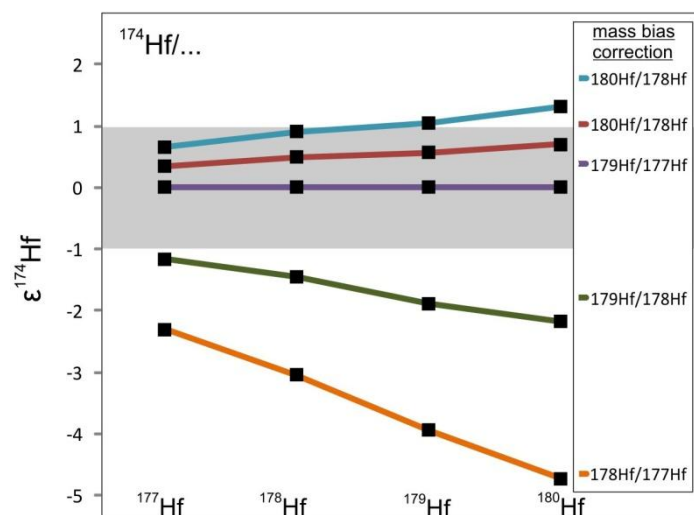


Fig. 2.5 Measured $^{174}\text{Hf}/^{17x}\text{Hf}$ for a typical run of the AMES Hf-metal standard, using the exponential law for mass bias correction. The indicated isotopes are those in the denominator. $\epsilon^{174}\text{Hf}$ represents the variability of the indicated $^{174}\text{Hf}/^{17x}\text{Hf}$ in parts per 10,000, normalized to $^{179}\text{Hf}/^{177}\text{Hf}$ for mass bias correction. The grey bar corresponds to an external reproducibility of 1 parts per ten thousand. Isotope ratios used for mass bias correction are from Blichert-Toft et al., (1997). Most accurate results are obtained for $^{174}\text{Hf}/^{177}\text{Hf}$ using $^{179}\text{Hf}/^{177}\text{Hf}$ for correction of the instrumental mass bias.

The level up to which the interference by isobaric ^{174}Yb can be corrected for was tested with Yb-doped Hf-standards. These tests indicated that the interference correction produces accurate results for solutions with $\text{Yb}/\text{Hf} < 2 \times 10^{-4}$. After our ion exchange chromatography protocol, samples with silicate matrices have Yb/Hf that lie well within this range (Fig. 2.6). Note that with the current setup of collectors, the minor isobaric interference by ^{180}Ta on ^{180}Hf is not monitored. Also, the minor isobaric interference by ^{180}W is not monitored accurately, because in some samples, ^{180}W and monitoring isotope ^{182}W may differ from the standard solution due to the decay of long-lived ^{184}Os (Peters et al., 2014) and short-lived ^{182}Hf , respectively. Before analyses, Ta concentrations were therefore always checked in

a minor aliquot of the sample. The signal on ^{181}Ta (99.99%) was typically < 10 mV after ion exchange chromatography, which is indistinguishable from the background of the mass spectrometer. Given the low abundance of ^{180}Ta ($\sim 0.012\%$) the interference on ^{180}Hf is consequently below detection limits. Differences in radiogenic $^{180,182}\text{W}$ are largest between chondrites and terrestrial samples, for which $^{180}\text{W}/^{182}\text{W}$ may vary in the range between 2-3 parts per 10,000 (e.g., Peters et al., 2014). After purification of the sample, W/Hf was typically $< 10^{-3}$ and at such level, the effects on the measured ^{180}Hf with respect to a W-free standard are maximum 0.02 parts per 10,000, i.e., within the limits of analytical uncertainty.

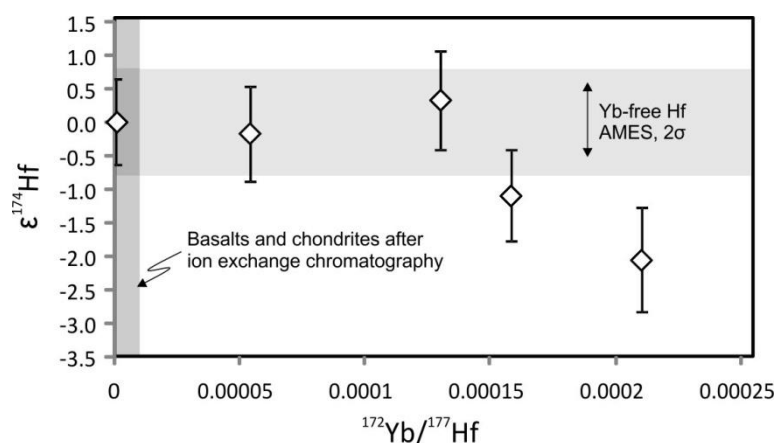


Fig. 2.6 ^{174}Yb -interference corrected $^{174}\text{Hf}/^{177}\text{Hf}$ in the AMES Hf-metal solution as a function of various amounts of doped Yb. The grey box represents the typical 2σ reproducibility of an Yb-free AMES Hf metal solution throughout a measurement session, i.e., $\pm 0.80 \epsilon^{174}\text{Hf}$ -units. The typical range in Yb/Hf for basaltic matrices and chondrites after anion exchange chromatography is well within the limits at which accurate correction for interference by ^{174}Yb is possible, i.e. Yb/Hf $\sim 2 \times 10^{-4}$.

2.3.4 Isotope measurements of Pt

Platinum has six isotopes that are stable or long-lived. The most abundant of these are ^{195}Pt ($\sim 34\%$), ^{194}Pt ($\sim 33\%$) and ^{196}Pt ($\sim 25\%$), followed by ^{198}Pt ($\sim 7\%$) and ^{192}Pt ($\sim 0.78\%$), with the ^{190}Pt being the least abundant by far ($\sim 0.014\%$). When all isotopes are collected, the maximum beam intensity at ^{190}Pt is governed by the level at which the amplifier of the collector for the most abundant isotope (^{195}Pt) becomes saturated. This is 50 V for the $10^{11}\Omega$ amplifiers of our detector system, corresponding to a maximum signal on ^{190}Pt of ~ 21 mV. However, as explained above, significantly better precisions are reached for beam intensities > 50 mV. Such intensities can be achieved on ^{190}Pt by collecting the three least abundant

isotopes only, i.e. ^{190}Pt , ^{192}Pt , and ^{198}Pt , such that the maximum intensity on ^{190}Pt is governed by the abundance of ^{198}Pt (~7 %) rather than ^{195}Pt (~34 %), and therefore the maximum ^{190}Pt signal increases to ~98 mV. Two sets of collector setups were therefore designed: one in which all Pt isotopes are collected simultaneously (hereafter: regular setup), and one in which only ^{190}Pt , ^{192}Pt , ^{198}Pt are collected (hereafter: high-precision setup). Samples were divided in aliquots and measured using each setup once, allowing obtaining high-precision data for all isotopes including ^{190}Pt .

For the setup in which all isotopes are collected, all possible normalization ratios for ^{190}Pt were tested. Reference ratios for instrumental mass bias were calculated from Creech et al. (2013). Only $^{190}\text{Pt}/^{192}\text{Pt}$ yielded consistent results with respect to different mass bias corrections and is therefore the most representative estimate approximating an absolute isotope ratio (Fig. 2.7). In this setup, internal precisions for $^{190}\text{Pt}/^{19x}\text{Pt}$ are typically between 2-3 parts per 10,000 when the interference correction is excluded and 3-5 parts per 10,000 after the interference correction. For the setup in which only ^{190}Pt , ^{192}Pt , ^{198}Pt are collected, internal and external precisions were typically ~1 part per 10,000.

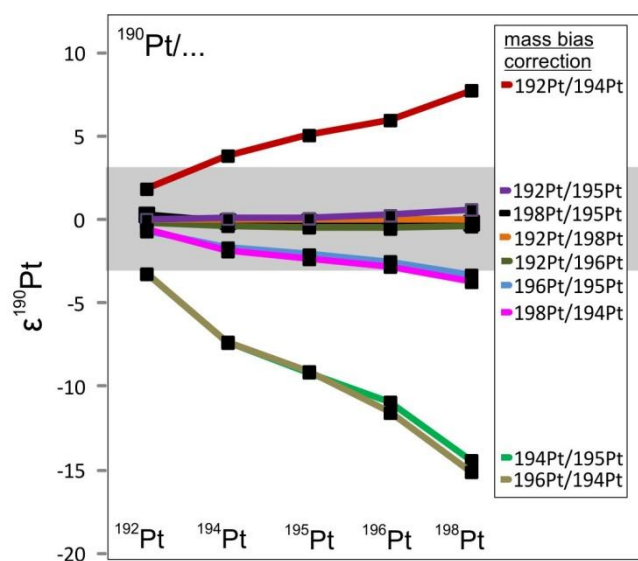


Fig. 2.7 Measured $^{190}\text{Pt}/^{19x}\text{Pt}$ for a typical run of the Alfa Aesar Pt-solution. The indicated isotopes are those in the denominator. $\epsilon^{190}\text{Pt}$ represents the variability of the indicated $^{190}\text{Pt}/^{19x}\text{Pt}$ in parts per 10,000 normalized to $^{192}\text{Pt}/^{198}\text{Pt}$ for the mass bias correction. For mass bias correction, the exponential law was used and isotope ratios were calculated from Creech et al. (2013). $^{190}\text{Pt}/^{192}\text{Pt}$ is the most consistent ratio with respect to different mass bias normalizations, and is therefore the most accurate isotope ratio. The differences between mass

bias corrected $^{190}\text{Pt}/^{192}\text{Pt}$ are within the limits of typical reproducibility for a single measurement, i.e. ~ 3 ϵ -units (grey field), when $^{192}\text{Pt}/^{198}\text{Pt}$ is used for the normalization.

Standard-sample bracketing methods for monitoring neutron capture effects

Before interpreting Pt isotope data of extraterrestrial samples in the context of the nucleosynthetic Pt inventory, it is essential to assess the possibility that the isotopic compositions of the samples were affected by secondary neutron capture reactions due to the exposure to cosmic rays. The measured ^{190}Pt can be affected directly by neutron capture on ^{190}Pt , and may additionally be affected by the burnout and production of the isotopes used for the correction of the instrumental mass bias. Efficient monitoring of neutron capture effects cannot be achieved with the isotopes that are collected in high-precision setup alone (^{190}Pt , ^{192}Pt , ^{198}Pt) and requires complementary information on ^{194}Pt , ^{195}Pt , and ^{196}Pt . We therefore developed an offline method to integrate the data that were collected in the high-precision setup with data from the regular setup for the same sample. Notably, the isotopic composition of ^{192}Pt may be affected by neutron capture on ^{191}Ir , following: $^{191}\text{Ir}(n,\gamma)^{192}\text{Ir}(\beta^-)^{192}\text{Pt}$. The ^{192}Pt abundance is consequently a function of Ir/Pt, and it is therefore more difficult to model neutron capture effects for ^{192}Pt than for e.g., ^{198}Pt , which can only be consumed by neutron capture (e.g., Kruijer et al., 2013; Wittig et al., 2013). The integration between the two setups is therefore illustrated for $^{190}\text{Pt}/^{198}\text{Pt}$ rather than for $^{190}\text{Pt}/^{192}\text{Pt}$, and is based on:

$$\left(^{190}\text{Pt}/^{198}\text{Pt} \right) = \left(M^{190}\text{Pt}/M^{198}\text{Pt} \right)^{\beta_3} \times \left\{ \frac{\left[\left(^{190}\text{Pt}/^{198}\text{Pt} \right)_{\text{meas,HP}} \left(M^{190}\text{Pt}/M^{198}\text{Pt} \right)^{\beta_1} \right]_{\text{mean}}}{\left(M^{190}\text{Pt}/M^{198}\text{Pt} \right)^{\beta_2}} \right\} \quad (1)$$

where $\left[\left(^{190}\text{Pt}/^{198}\text{Pt} \right)_{\text{meas,HP}} \left(M^{190}\text{Pt}/M^{198}\text{Pt} \right)^{\beta_1} \right]_{\text{mean}}$ represents the mean value for 60×8 s integrations of $^{190}\text{Pt}/^{198}\text{Pt}$ in the high-precision setup, corrected for instrumental mass bias using fractionation factor β_1 , defined as:

$$\beta_1 = \frac{\ln \left[\left(^{192}\text{Pt}/^{198}\text{Pt} \right)_{\text{ref}} / \left(^{192}\text{Pt}/^{198}\text{Pt} \right)_{\text{meas,HP}} \right]}{\ln \left(M^{192}\text{Pt}/M^{198}\text{Pt} \right)} \quad (2).$$

Thus, in eq. 1, the mass bias corrected $^{190}\text{Pt}/^{198}\text{Pt}$ from the high precision setup is first fractionated using fractionation factor β_2 that was determined for $^{192}\text{Pt}/^{198}\text{Pt}$ in the regular setup, i.e.,

$$\beta_2 = \frac{\ln \left[\left(^{192}\text{Pt}/^{198}\text{Pt} \right)_{\text{ref}} / \left(^{192}\text{Pt}/^{198}\text{Pt} \right)_{\text{meas,RS}} \right]}{\ln \left(M^{192}\text{Pt}/M^{198}\text{Pt} \right)} \quad (3).$$

The fractionated $^{190}\text{Pt}/^{198}\text{Pt}$ can subsequently be normalized to any fractionation factor β_3 from the regular setup, where

$$\beta_3 = \frac{\ln\left[\frac{(^{19x}\text{Pt}/^{19x}\text{Pt})_{\text{ref}}}{(^{19x}\text{Pt}/^{19x}\text{Pt})_{\text{meas,RS}}}\right]}{\ln(M^{19x}\text{Pt}/M^{19x}\text{Pt})} \quad (3).$$

In the above equations, $(^{19x}\text{Pt}/^{19x}\text{Pt})_{\text{ref}}$ represents the “true” (i.e., reference) value for the indicated isotope ratio, and $M^{19x}\text{Pt}$ represents the mass of the indicated isotope. Eq. 1 was applied to each 8 s integration cycle that was collected with the regular setup. Eq. 1 may furthermore be expanded by multiplying the right-hand side of the equation with the interference corrected, but not mass bias corrected, $^{19x}\text{Pt}/^{198}\text{Pt}$ from the regular setup, in order to obtain any high-precision $^{190}\text{Pt}/^{198}\text{Pt}$.

Importantly, this approach accounts for any potential isotopic heterogeneities in ^{192}Pt , because aliquots from the same sample are measured in regular and high-precision setup. Although this method accounts for instrumental drift related to potential changes in mass bias behavior of Pt, it cannot account for potential changes in baseline and background intensities. The maximum uncertainty on the calculated $^{190}\text{Pt}/^{198}\text{Pt}$ was therefore always estimated from the reproducibility of the Alfa Aesar Pt-standard solution in high-precision setup, i.e. normalized for instrumental mass bias to $^{192}\text{Pt}/^{198}\text{Pt}$, throughout the measurement session. Furthermore, the uncertainty in β_3 propagates towards the calculated $^{190}\text{Pt}/^{198}\text{Pt}$ and typically adds an additional 0.1-0.3 parts in 10,000 of uncertainty. Data on standard measurements that were used for bracketing a specific sample in high resolution setup, e.g., with Ir/Pt matched to the sample, were processed offline, and the recalculated data were again used for bracketing the specific sample.

Isobaric interferences and tailing effects of Ir

Platinum-190 and ^{192}Pt suffer from large isobaric interferences by ^{190}Os and ^{192}Os (abundances: ~26% and ~41%, respectively). The extent to which these interferences can accurately be corrected was tested by doping Pt-solutions with various amounts of Os. The maximum tolerance level of the interference correction in high-precision setup is at $\text{Os}/\text{Pt} < 3 \times 10^{-6}$ (Fig. 2.8). After the treatment with HClO_4 , all mixed Pt-Os solutions were well within this range, and in some cases Os corrections on ^{190}Pt and ^{192}Pt were only within the limits of analytical uncertainty. In such cases, corrections for Os-interferences can be ignored, as these increase analytical uncertainties due to detector-noise propagation. Iron meteorite matrices

showed a larger range in Os/Pt that possibly relates to different speciation of Os in the sample solutions, ranging up to the maximum tolerable level. In these cases and for the determination of the absolute $^{190}\text{Pt}/^{192}\text{Pt}$ in the Alfa Aesar Pt-solution, corrections were applied based on $^{190}\text{Os}/^{188}\text{Os} = 1.9828$ and $^{192}\text{Os}/^{188}\text{Os} = 3.0794$ (Völkening et al., 1991b). Additionally, the Alfa Aesar standard solution was treated with HClO_4 as well, after which Os contents in the standard Pt cuts were indistinguishable from the background of the mass spectrometer. Small isobaric interferences may furthermore be present as ^{196}Hg and ^{198}Hg on ^{196}Pt and ^{198}Pt . Mercury was present in small amounts in the sample gas with typically ~ 1 mV on ^{200}Hg . These interferences were therefore corrected based on $^{196}\text{Hg}/^{200}\text{Hg} = 0.00664$ and $^{198}\text{Hg}/^{200}\text{Hg} = 0.4316$ (Zadnik et al., 1989).

Some measurements of matrix-free Alfa Aesar Pt that had been processed over the columns yielded highly anomalous isotope ratios for some of the 8 s integration cycles, which correlate up to various degrees and show no correlation with Os/Pt, Hg/Pt, or Ir/Pt (Fig. 2.9A). These anomalous isotope ratios are interpreted to reflect multiple interfering species in the Pt mass array, possibly large organic molecules that were introduced with the sample even after treatment with HClO_4 . Memory effects related to these interferences appear to be absent. Although a 2σ rejection is applied before calculation of the mean isotope ratios for 60 integrations, these interferences may significantly bias the measurement (Fig. 2.9B). Each set of integrations was therefore always examined offline, and outliers were rejected in case of the obvious presence of interfering species. After this procedure, the calculated compositions of the processed and unprocessed Alfa Aesar Pt-solutions were identical.

The presence of Ir in samples may result in tailing of ^{191}Ir ($\sim 37\%$) and ^{193}Ir ($\sim 63\%$) on ^{190}Pt (^{191}Ir only) and ^{192}Pt (both isotopes). For example, for an abundance sensitivity of 2 ppm, measurements of solutions with Ir/Pt = 0.1 have predicted contributions of ^{191}Ir and ^{193}Ir on the low-mass sides to the Pt signals of ~ 550 ppm and ~ 15 ppm, respectively. One of these Ir isotopes was therefore continuously monitored during measurements: ^{191}Ir in high-precision setup and ^{193}Ir in regular setup. Indeed, Ir-doped Pt-solutions show a strong correlation of $^{190,192}\text{Pt}/^{19x}\text{Pt}$ (regular setup) and $^{190}\text{Pt}/^{192}\text{Pt}$ (high-precision setup) with Ir/Pt up to ~ 1 (Fig. 2.10). The correlation of this slope is variable between measurement sessions, and generally corresponds to an abundance sensitivity of 2-3 ppm. At Ir/Pt > 1 , ^{190}Pt , ^{192}Pt are elevated but the correlation with Ir/Pt becomes worse, as do in-run precisions. This probably reflects changes in mass bias behavior of Pt in the presence of larger amounts of Ir. After the ion

exchange chromatography protocol applied here, the Ir/Pt of iron meteorites were between 0.05-0.40. At such levels, Ir-induced changes in mass bias behavior of Pt were absent, and Ir tailing may therefore be dealt with by standard-sample bracketing using Pt-standards with admixed Ir. By matching Ir/Pt of the sample at the level of approximately ~10% or better, the estimated propagated uncertainty on any $^{190}\text{Pt}/^{19x}\text{Pt}$ is an additional < 0.1 parts in 10,000. For determination of the absolute $^{190}\text{Pt}/^{192}\text{Pt}$, background intensities on ^{191}Ir were sufficiently low for tailing effects to be absent (i.e. < 10 mV).

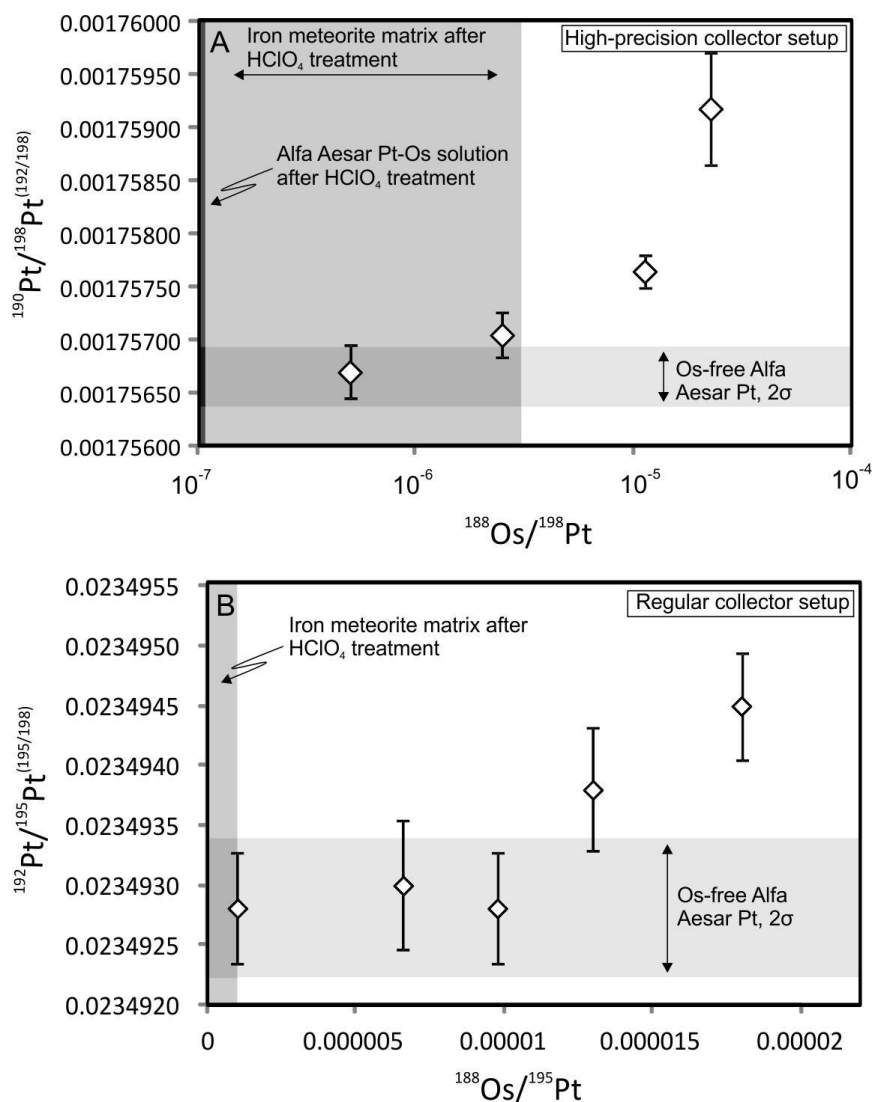


Fig. 2.8 A ^{190}Os -interference corrected $^{190}\text{Pt}/^{198}\text{Pt}$ in the Alfa Aesar Pt-solution standard with various amounts of admixed Os, determined with the high-precision collector configuration. In the example displayed, $\epsilon^{190}\text{Pt}$ is directly affected by isobaric ^{190}Os and indirectly by ^{192}Os through the mass bias correction to $^{192}\text{Pt}/^{198}\text{Pt}$. Both effects result in an apparent excess of $\epsilon^{190}\text{Pt}$. Note that the magnitude of the interference correction for any $^{192}\text{Pt}/^{19x}\text{Pt}$ is ~40 times

lower than for $^{190}\text{Pt}/^{19x}\text{Pt}$. Thus, after treatment with HClO_4 (typical range indicated with grey field) samples generally are sufficiently Os-free for determination of $\epsilon^{190}\text{Pt}$ in high-precision setup, as well as for determination of $\epsilon^{192}\text{Pt}$ with the regular collector setup, as illustrated in **B**.

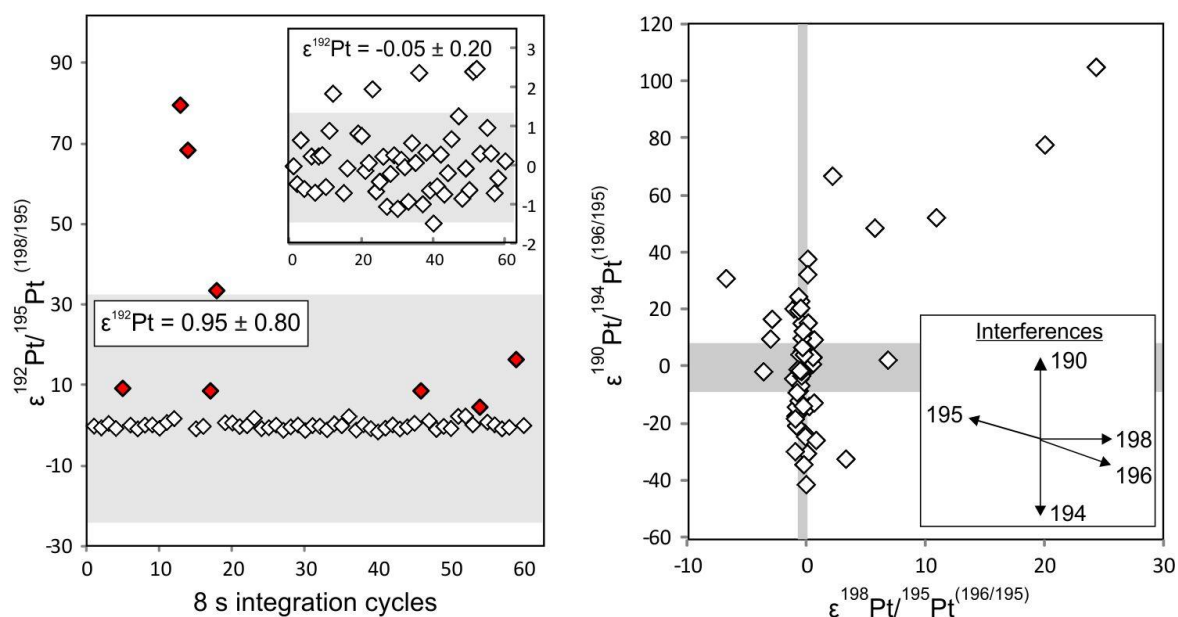


Fig. 2.9 Effects of interferences that were present in the Alfa Aesar Pt-solution after ion exchange chromatography on the reproducibility of measurements. **A)** Throughout a run of sixty cycles \times 8 s integrations, several cycles display implausibly high $^{192}\text{Pt}/^{195}\text{Pt}$ normalized for instrumental mass bias to $^{198}\text{Pt}/^{195}\text{Pt}$ (marked red). Although some of these “outliers” are excluded from the calculated mean by the 2σ rejection (grey box), others are within the limits of the calculated 2σ variation. The inset shows the same data after the marked ratios were rejected. Note that without rejection of the affected $^{192}\text{Pt}/^{195}\text{Pt}$ cycles the processed Alfa Aesar solution is analytically resolvable positive with respect to the unprocessed solution. **B)** There is no clear correlation between $^{190}\text{Pt}/^{196}\text{Pt}$ and $^{190}\text{Pt}/^{195}\text{Pt}$, both normalized to $^{196}\text{Pt}/^{195}\text{Pt}$ for instrumental mass bias, as would be expected in case of one interfering species only (inset). Each data point represents one 8s integration cycle. Boxes correspond to typical 2 S.E..

Isotope measurements of W

Tungsten has four observationally stable isotopes other than ^{180}W ($\sim 0.12\%$), i.e., ^{182}W ($\sim 27\%$), ^{183}W ($\sim 14\%$), ^{184}W ($\sim 31\%$) and ^{186}W ($\sim 28\%$). Among these, ^{182}W displays radiogenic heterogeneities in early solar system materials due to the decay of now-extinct ^{182}Hf and therefore cannot be used for normalization of ^{180}W . Furthermore, ^{183}W may suffer

from apparent mass independent fractionation effects during sample preparation or mass spectrometry (e.g., Shirai & Humayun, 2011) as well as interferences by organic species (e.g., Kleine et al., 2004) and is therefore not reliable for normalization. We therefore exclusively report the abundance of ^{180}W as the $^{180}\text{W}/^{184}\text{W}$ ratio, using $^{186}\text{W}/^{184}\text{W} = 0.92767$ for the mass bias correction. After TEVA based chromatography, samples with silicate matrices had $\text{Hf}/\text{W} = < 10^{-5}$ allowing accurate correction for isobaric ^{180}Hf (Schulz et al., 2013; Peters et al., 2014), using $^{180}\text{Hf}/^{178}\text{Hf} = 1.2860$. Small isobaric interferences by $^{184,186}\text{Os}$ were monitored by ^{188}Os using $^{184}\text{Os}/^{188}\text{Os} = 0.001356$ and $^{186}\text{Os}/^{188}\text{Os} = 0.11982$.

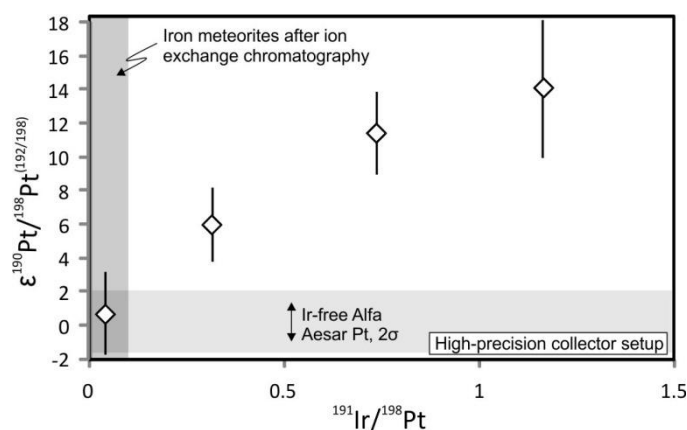


Fig. 2.10 Tailing effects of ^{191}Ir on the measured $\epsilon^{190}\text{Pt}$ in the Alfa Aesar Pt-solution with various amounts of admixed Ir. Although Ir/Pt of iron meteorites can be dramatically reduced by anion exchange chromatography, tailing effects of $\leq 3 \epsilon^{190}\text{Pt}$ -units may still occur and must be dealt with by sample bracketing with standards that have matched Ir/Pt to the sample at the level of $< 10\%$ or better. Note that tailing by ^{193}Ir and to lesser extent ^{191}Ir on ^{192}Pt is more than an order of magnitude less than tailing by ^{191}Ir on ^{190}Pt . $^{191}\text{Ir}/^{198}\text{Pt} = 1$ corresponds to a Ir/Pt of ~ 5 .

2.3. DATA FOR METEORITES AND TERRESTRIAL SAMPLES

2.3.1 Non-radiogenic Hf isotope compositions of terrestrial basalts and chondrites

The Hf isotope compositions of four terrestrial basalts and three chondrite samples are reported in Table 2.6 and are given as deviations from the Hf AMES metal standard in parts per 10,000. $\epsilon^{174}\text{Hf}$ in all samples are indistinguishable from Hf AMES metal. Furthermore, no significant variability in the major non-radiogenic isotopes is observed. This is in agreement with the conclusions by Sprung et al. (2010) that s- and r-process Hf is distributed homogeneously in the solar system on the planetesimal scale, and that Hf in chondrites was

unaffected by secondary neutron capture processes. For the first time, these data are now complemented with ^{174}Hf , suggesting that non-radiogenic hafnium is indeed distributed homogeneously in the solar system, although more data are needed to confirm this.

Table 2.6 Non-radiogenic Hf isotope compositions in terrestrial samples and chondrites^a

Sample	Type	$\epsilon^{174}\text{Hf}^{(179/177)}$	$\epsilon^{178}\text{Hf}^{(179/177)}$	$\epsilon^{180}\text{Hf}^{(179/177)}$	$\epsilon^{179}\text{Hf}^{(178/180)}$
<i>Terrestrial</i>					
BHVO-2	Oceanic island basalt	0.40 ± 1.02	0.15 ± 0.11	0.09 ± 0.22	0.25 ± 0.12
		0.80 ± 0.92	0.04 ± 0.09	0.06 ± 0.18	0.04 ± 0.10
		-0.12 ± 0.78	0.06 ± 0.07	0.16 ± 0.19	-0.11 ± 0.12
BCR-2	Continental flood basalt	-0.29 ± 0.54	0.11 ± 0.12	0.04 ± 0.19	-0.09 ± 0.12
		BB46A	Basalt (Leine Graben)	-0.46 ± 1.02	0.09 ± 0.11
3MU-13	Arc basalt (Sunda Arc)	-0.28 ± 0.96	-0.02 ± 0.13	0.18 ± 0.23	-0.04 ± 0.08
		-0.30 ± 0.78	0.10 ± 0.12	0.27 ± 0.19	-0.08 ± 0.10
<i>Chondrites</i>					
NWA 3118	CV3	0.02 ± 0.56	-0.03 ± 0.04	0.13 ± 0.15	-0.04 ± 0.09
NWA 515	L6	-0.02 ± 1.94	0.05 ± 0.19	0.14 ± 0.19	-0.07 ± 0.07
Pultusk	H5	0.53 ± 0.94	0.09 ± 0.13	-0.15 ± 0.22	0.23 ± 0.12

^a $\epsilon^{1xx}\text{Hf} = 10^4 \times [(\frac{^{1xx}\text{Hf}}{^{177}\text{Hf}})_{\text{sample}} / (\frac{^{1xx}\text{Hf}}{^{177}\text{Hf}})_{\text{AMES}} - 1]$ using $^{179}\text{Hf}/^{177}\text{Hf} = 0.7325$ for instrumental mass bias correction.

2.3.2 Platinum isotope composition of iron meteorites

The Pt isotope compositions of three iron meteorites were determined relative to the composition of the Alfa Aesar Pt-solution (Table 6). In order to test for nucleosynthetic heterogeneity, samples from different meteorite groups were analyzed, namely Odessa (IAB), Forsyth County (IIAB) and Cape York (IIIAB). Among these, Cape York and Forsyth County have cosmic ray exposure ages of < 100 Ma (Fisher and Schaeffer, 1960; Murty and Marti, 1986) and neutron capture effects are therefore expected to be minimal. Odessa has a higher exposure age of ~875 Ma (Voshage and Feldmann, 1979) and may therefore show significant neutron capture effects. In Table 2.7, in high-precision setup, $\epsilon^{190}\text{Pt}$ represents the $^{190}\text{Pt}/^{198}\text{Pt}$ ratio using $^{192}\text{Pt}/^{198}\text{Pt}$ to normalize for instrumental mass bias, whereas for regular setup measurements, $\epsilon^{19x}\text{Pt}$ represents the $^{190}\text{Pt}/^{195}\text{Pt}$ ratio that was normalized either to $^{198}\text{Pt}/^{195}\text{Pt}$ or to $^{196}\text{Pt}/^{195}\text{Pt}$. The reason for choosing these particular normalization ratios is the most straightforward representation of secondary neutron capture effects (e.g., Kruijer et al., 2013).

In high-precision setup, $^{190}\text{Pt}/^{198}\text{Pt}$ in Cape York and Forsyth County are indistinguishable from the Alfa Aesar solution, whereas Odessa shows a large negative $\epsilon^{190}\text{Pt}$. In contrast, when normalized to $^{198}\text{Pt}/^{185}\text{Pt}$ using eq. 1, all samples display $\epsilon^{190}\text{Pt}$ indistinguishable from the Alfa Aesar standard. The measured $\epsilon^{190}\text{Pt}$ in regular setup is within uncertainty from the calculated value, showing that eq. 1 indeed provides a valid approach.

Odessa furthermore shows positive anomalies in other Pt-isotopes that are consistent with secondary neutron capture effects (Fig. 2.11B,C). Cape York is indistinguishable from Alfa Aesar Pt in all isotopes, whereas Forsyth County shows resolvable negative and positive anomalies that may indicate a minor s-process deficit (Fig. 11A,B). In contrast, the isotope compositions of Odessa, Cape York and Forsyth County suggest a homogeneous distribution of p- and r-process Pt.

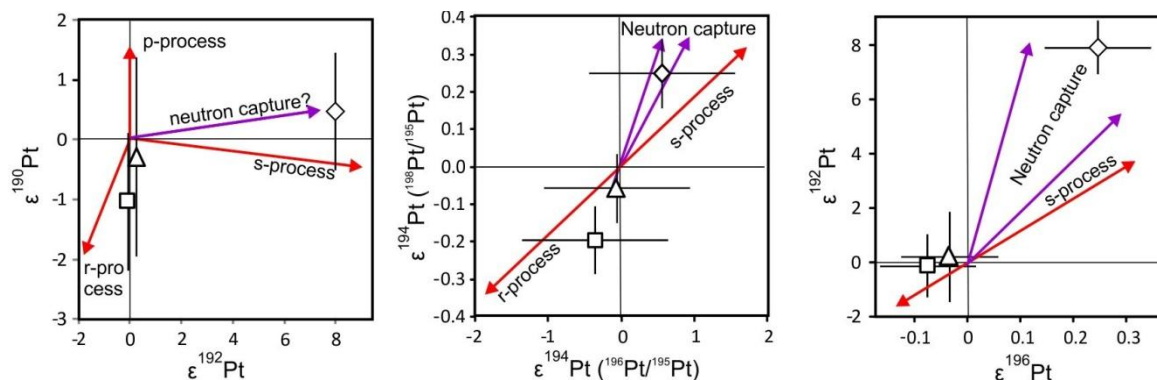


Fig. 2.11 Platinum isotope compositions of Cape York (triangle), Forsyth County (square) and Odessa (diamond). Red arrows indicate nucleosynthetic excesses as modeled from Arlandini et al. (1999), i.e. the arrow towards r-process corresponds to a s-process deficit and vice versa. The minor deficit of $\epsilon^{194}\text{Pt}$ in Forsyth County when normalized to $^{198}\text{Pt}/^{195}\text{Pt}$ for instrumental mass bias cannot be explained by r-process excess (A) or neutron capture effects (B). The anomalous composition of Odessa is well explained by neutron capture models (purple arrows correspond to Ir/Pt of 0.5-1 and are from Kruijer et al. 2013). No detailed model calculations for neutron capture effects in Odessa were made for $\epsilon^{190}\text{Pt}$. However, given the magnitude of the effects on $\epsilon^{194}\text{Pt}$ (i.e. < 0.32 ϵ -units), which are dominated by the production through $^{193}\text{Ir}(n,\gamma)^{194}\text{Ir}(\beta^-)^{194}\text{Pt}$, and the low resonance integral for ^{190}Pt compared to ^{193}Ir (~ 67 compared to 1350 barns; Mughabghab, 2003), it is safe to assume that such effects would be within the level of analytical uncertainty, i.e. < 1 $\epsilon^{190}\text{Pt}$ -unit.

2.3.3 Tungsten isotope composition of terrestrial silicates and chondrites

For precise data on ^{180}W in terrestrial silicates and chondrites as well as for the interpretation of these data we refer to Chapter 4.

Table 2.7 Pt isotope composition^a of iron meteorites

	<i>High-precision setup:</i>		<i>Low-precision setup:</i>		
	$\epsilon^{190}\text{Pt}/^{198}\text{Pt}^{(192/198)}$	$\epsilon^{190}\text{Pt}^{(198/195)}$	$\epsilon^{190}\text{Pt}^{(198/195)}$	$\epsilon^{192}\text{Pt}^{(198/195)}$	$\epsilon^{194}\text{Pt}^{(198/195)}$
	<u>Measured</u>	<u>Calculated^b</u>			
Odessa	-9.54 ± 0.93	0.73 ± 1.1	3.6 ± 5.7	7.77 ± 0.25	0.23 ± 0.06
			2.1 ± 5.7	8.15 ± 0.25	0.26 ± 0.06
Cape York	0.8 ± 1.6	1.0 ± 1.8	-1.9 ± 5.7	0.25 ± 0.25	-0.06 ± 0.06
	-1.7 ± 2.2	-1.5 ± 2.4			
	0.7 ± 1.3	0.8 ± 1.6			
Forsyth County	-0.9 ± 1.9	-1.2 ± 2.1	0.0 ± 5.7	-0.08 ± 0.21	-0.07 ± 0.06
	-0.8 ± 1.9	-1.1 ± 2.1			
Column tests ^c	-0.9 ± 1.3	-1.5 ± 1.8	2.0 ± 5.7	0.18 ± 0.25	-0.02 ± 0.06
	-1.2 ± 1.5	0.5 ± 1.8	-0.4 ± 5.7	-0.12 ± 0.25	-0.01 ± 0.06
	0.5 ± 1.3	0.9 ± 1.6	1.3 ± 5.7	0.04 ± 0.25	0.01 ± 0.06

Low-precision setup (continued):

	$\epsilon^{196}\text{Pt}^{(198/195)}$	$\epsilon^{192}\text{Pt}^{(196/195)}$	$\epsilon^{194}\text{Pt}^{(196/195)}$	$\epsilon^{198}\text{Pt}^{(196/195)}$
Odessa	0.23 ± 0.04	8.40 ± 0.25	0.55 ± 0.09	-0.80 ± 0.13
	0.26 ± 0.04	8.85 ± 0.25	0.55 ± 0.09	-0.78 ± 0.13
Cape York	-0.03 ± 0.04	0.04 ± 0.25	-0.07 ± 0.09	0.15 ± 0.13
Forsyth County	-0.07 ± 0.04	-0.36 ± 0.25	-0.20 ± 0.09	0.28 ± 0.13
Column tests ^c	-0.02 ± 0.04	0.12 ± 0.25	-0.02 ± 0.09	0.03 ± 0.13
	0.05 ± 0.04	-0.07 ± 0.25	0.02 ± 0.09	-0.10 ± 0.13
	0.00 ± 0.04	-0.01 ± 0.25	0.01 ± 0.09	0.04 ± 0.13

^aIn general, $\epsilon^{19x}\text{Pt} = 10^4 \times [({}^{19x}\text{Pt}/{}^{195}\text{Pt})_{\text{sample}} / ({}^{19x}\text{Pt}/{}^{195}\text{Pt})_{\text{ALFA AESAR}} - 1]$ except for the high-precision measurement (first column) in which $\epsilon^{190}\text{Pt} = 10^4 \times [({}^{190}\text{Pt}/{}^{198}\text{Pt})_{\text{sample}} / ({}^{190}\text{Pt}/{}^{198}\text{Pt})_{\text{ALFA AESAR}} - 1]$. Instrumental mass bias was corrected for based on ${}^{192}\text{Pt}/{}^{198}\text{Pt} = 0.10861$; ${}^{192}\text{Pt}/{}^{198}\text{Pt} = 0.10861$; and ${}^{196}\text{Pt}/{}^{194}\text{Pt} = 0.77086$, which cases are indicated in superscript.

^bCalculated from the measured high-precision $\epsilon^{190}\text{Pt}$ using the expanded version of eq. 1

^cData for the Alfa Aesar Pt-solution that was processed over the anion exchange resin together with admixed Fe, Ni, Co (100 mg each) and PGE (1 mg each).

2.3.4 Determination of isotope compositions

In an effort to determine the mean isotope ratios of matrix-free Hf-, W-, and Pt-element solutions, measurements performed throughout a period of approximately three years were compiled and are given together with the calculated relative abundances in Table 2.8, also showing the recommended values by IUPAC for comparison. The calculated average isotope ratios represent the weighted means over the mean values obtained in different measurement sessions, each in which the isotopic compositions of reference materials were determined throughout at least >10 runs of 60 × 8 s integrations. The uncertainty on these long-term isotope ratios are given as the 2σ variability between these different measurement

sessions, as is illustrated in Fig. 2.12. For the low-abundance isotopes of interest, a more detailed comparison with literature data is shown in Table 2.9.

Table 2.8 Representative isotopic compositions of Hf, W, and Pt measured on the Neptune MC-ICPMS at Cologne-Bonn

	^{174}Hf	^{176}Hf	^{177}Hf	^{178}Hf	^{179}Hf	^{180}Hf
$^{177}\text{Hf}^{\text{a}}$	0.0086608(26)	0.282152(4)		1.8869(2)	1.46724(6)	0.73247(2)
Mole fraction ^b (%)	0.16106(6)	5.2469(2)	18.596(1)	27.2850(3)	13.6212(2)	35.090(2)
IUPAC 2009 ^c :	0.16(1)	5.26(7)*	18.60(9)	27.28(7)	13.62(2)	35.08(16)
	^{180}W	^{182}W	^{183}W	^{184}W	^{186}W	
$^{184}\text{W}^{\text{d}}$	0.00383788(10)	0.86484(5)	0.46712(1)		0.9210(16)	
Mole fraction ^b (%)	0.11910(9)	26.554(15)	14.3513(11)	30.70(2)	28.30(4)	
IUPAC 2009:	0.12(1)	26.50(16)	14.31(4)	30.64(2)	28.43(19)	
	^{190}Pt	^{192}Pt	^{194}Pt	^{195}Pt	^{196}Pt	^{198}Pt
$^{192}\text{Pt}^{\text{d}}$	0.016174(45)		41.349(6)	42.30(15)	31.867(6)	9.2099(15)
Mole fraction	0.01286(5)	0.7953(10)	32.89(4)	33.76(4)	25.23(3)	7.326(9)
IUPAC 2009:	0.012(2)	0.782(24)	32.86(40)	33.78(24)	25.21(34)	7.356(130)

^aBerglund & Wieser (2011)

^bMole fractions of Hf and W isotopes depend on the radiogenic contributions to ^{176}Hf and ^{182}W , respectively, and are therefore only representative for AMES metal (Hf, W) and NIST 3163 (W).

^cNormalized for instrumental mass bias to $^{177}\text{Hf}/^{179}\text{Hf} = 0.7325$ except for ^{179}Hf , which was normalized to $^{180}\text{Hf}/^{178}\text{Hf} = 1.28584$

^dNormalized for instrumental mass bias to $^{186}\text{W}/^{184}\text{W} = 0.92767$ except for ^{180}W , which was normalized to $^{186}\text{W}/^{183}\text{W} = 1.9859$

^eNormalized for instrumental mass bias to $^{192}\text{Pt}/^{198}\text{Pt} = 0.10861$ except for ^{198}Pt , which was normalized to $^{196}\text{Pt}/^{194}\text{Pt} = 0.77086$ (Creech et al., 2013).

The isotopic composition of Hf was determined using the AMES Hf metal-standard between February 2011 and October 2013. The long-term value for $^{174}\text{Hf}/^{177}\text{Hf} = 0.0086608 \pm 26$ is in good agreement with previous data (Patchett, 1983; Amelin et al., 2000; Chu et al., 2002; Thirlwall & Anczkiewicz, 2004). Kawashima et al. (1993) reported a higher $^{174}\text{Hf}/^{177}\text{Hf}$ of 0.008748 ± 55 . However, this value was based on one measurement only. The calculated relative abundance of $^{174}\text{Hf} = 0.16106 \pm 0.00006$ % is within the uncertainty of all previous estimates, and is the most precise value reported so far. The isotopic composition of W was determined between May 2012 and November 2013 predominantly using the Münster AMES W-metal solution. To allow an enhanced possibility of interlaboratory comparison of our data, measurements were switched to the NIST 3163 W-solution in April 2013. It was previously shown that these standards were isotopically indistinguishable during a measurement session with multiple tens of runs for each standard (Peters et al., 2014). The weighted mean of $^{180}\text{W}/^{184}\text{W} = 0.0038788 \pm 6$, which is slightly lower than the value by Völkening et al. (1991a), i.e. $^{180}\text{W}/^{184}\text{W} = 0.003910 \pm 6$. The calculated abundance of $^{180}\text{W} = 0.11910 \pm 0.00009$ % overlaps with the IUPAC recommended value, but is slightly lower than the

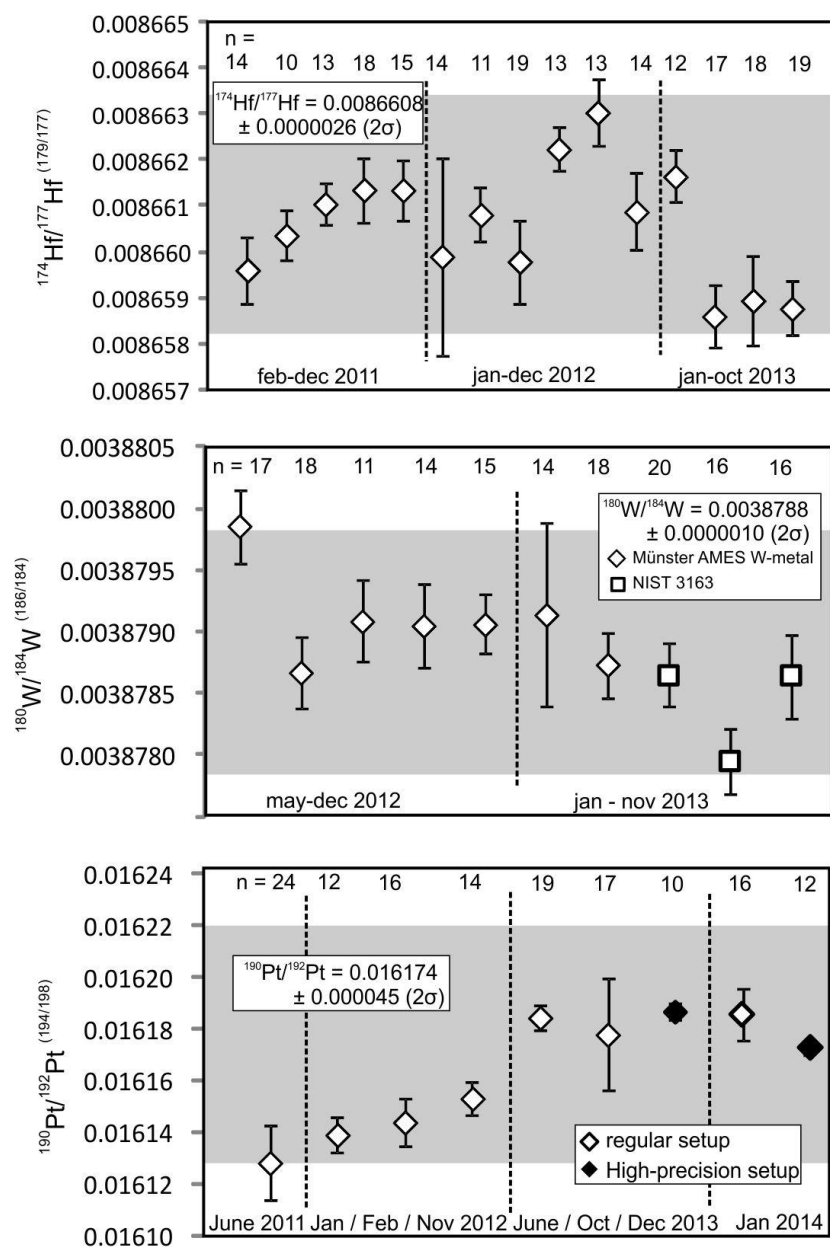


Fig. 2.12 Reproducibility for measurements of absolute abundances of low-abundance isotopes using $10^{12}\Omega$ Faraday current amplifiers on the Neptune MC-ICP-MS in Cologne-Bonn, for a period of 2-3 years. Error bars represent the 2σ variation of n runs acquired throughout one measurement session, whereas the grey boxes represent the 2σ variation between the different sessions.

Table 2.9 Compilation of measured isotope ratios^a and calculated relative abundances

<i>Isotope ratios</i>	<i>Abundance</i>	<i>Reference Material</i>	<i>Method (instrument)</i>	<i>Study</i>
Hafnium ¹⁷⁴ Hf				
n/a	0.0016(1)	n/a	n/a	IUPAC 2009 ^b
¹⁷⁴ Hf/ ¹⁷⁷ Hf ^(179/177)				
0.00871 ± 5	0.001620(9) ^x	JMC 475	TI-MS (n/a)	Patchett (1983)
0.008748 ± 55	0.00164(17)	n/a	N-TI-MS (VG Sector 54)	Kawashima et al. (1993)
0.008647 ± 20	0.001608(4) ^x	JMC 475	MC-ICP-MS (n/a)	Amelin et al. (2000)
0.008674 ± 32	0.001613(6) ^x	JMC 475	MC-ICP-MS (Isoprobe)	Chu et al. (2002)
0.008659 ± 5	0.0016102(11) ^x	JMC 475	MC-ICP-MS (Isoprobe)	Thirlwall & Anczkiewicz (2004)
0.0086608 ± 26	0.0016106(6)	AMES Hf-metal	MC-ICP-MS (Neptune)	This study
Tungsten ¹⁸⁰ W				
n/a	0.0012(1)	n/a	n/a	IUPAC 2009 ^b
	0.00126(6)		Nier-type mass spectrometer	White & Cameron (1948)
¹⁸⁰ W/ ¹⁸³ W ^(186/183)				
0.008336 ± 11	0.001193(1)	NIST-3163 + H. Cross W-filament	MC-ICP-MS (Fisons Instruments Plasma 54)	Lee & Halliday (1995)
¹⁸⁰ W/ ¹⁸⁴ W ^(183/184)				
0.003910 ± 6	0.001198(2)	n/a	N-TI-MS (Finnigan MAT 261)	Völkening et al. (1991a)
¹⁸⁰ W/ ¹⁸⁴ W ^(186/184)				
0.0038788 ± 10	0.0011910(9)	NIST3163 + AMES W-metal	MC-ICP-MS (Neptune)	This study
Platinum ¹⁹⁰ Pt				
n/a	0.00012(1)	n/a	n/a	IUPAC 2009 ^b
¹⁹⁰ Pt/ ¹⁹⁵ Pt ^(194/195)				
0.0003821 ± 10	0.0001292(2)	H. Cross Pt ribbon	MC-ICP-MS (VG Elemental Plasma 54)	Morgan et al. (2002)
¹⁹⁰ Pt/ ¹⁹⁵ Pt ^(n/a)				
0.000347 ± 17	0.0001172(58)	IRMM-010	Quadrupole ICP-MS (VG Plasmaquad 2+)	Wolff Briche et al. (2002)
¹⁹⁰ Pt/ ¹⁹⁴ Pt ^c				
0.00039330(39)	0.0001289(6)	IRMM-010	MC-ICP-MS (Neptune + Nu Plasma)	Creech et al. (2013)
¹⁹⁰ Pt/ ¹⁹² Pt ^(192/198)				
0.016174 ± 0.00047	0.0001286(5)	Alfa Aesar Pt-solution	MC-ICP-MS (Neptune)	This Study

^xWhen applicable, isotopes used for mass bias normalization are given in superscript.^bBerglund & Wieser (2011)^cBased on external mass bias normalization to the Pb isotope standard SRM981.

previous estimates by White & Cameron (1948), Völkening et al. (1991a) and Lee & Halliday (1995). However, also these previous estimates exhibit variability outside the reported levels of analytical uncertainty. The isotopic composition of Pt was determined between June 2011 and January 2014 in the Alfa Aesar Pt-solution in regular setup (all isotopes) and high-precision setup ($^{190}\text{Pt}/^{192}\text{Pt}$ only), for which $^{190}\text{Pt}/^{192}\text{Pt} = 0.016174 \pm 45$. No previous studies reported this isotope ratio. The calculated abundance of $^{190}\text{Pt} = 0.01286 \pm 5 \%$ and is in good agreement with the estimate by Creech et al. (2013), and is the most precise estimate reported so far.

2.4 CONCLUSIONS

This study demonstrates that low abundance isotopes ^{174}Hf , ^{180}W and ^{190}Pt can be measured at precisions of better than 1 parts per ten thousand using $10^{12} \Omega$ Faraday current amplifiers in MC-ICP-MS. This is a ca. tenfold improvement compared to most previous data. Because of isobaric interferences and matrix effects, ultra-clean element separations were developed to measure these isotopes in natural samples. Appropriate protocols for Hf and W from silicate matrices, and Pt from metal matrices are reported here. Representative isotope ratios of matrix-free element solutions are reported, as well as the first data for ^{174}Hf and ^{190}Pt in terrestrial silicates and chondrites (Hf), and iron meteorites (Pt). In these materials, ^{174}Hf and ^{190}Pt are indistinguishable from the terrestrial value. This tentatively suggests that Earth, ordinary chondrites and CV3 chondrites, and Earth, IAB, IIAB and IIIAB irons, formed from a uniform reservoir with respect to ^{174}Hf and ^{190}Pt , respectively.

Chapter III

The distribution of p-process ^{174}Hf in early solar system materials

3.1 INTRODUCTION

Mass-independent, non-radiogenic, i.e. “nucleosynthetic” isotope anomalies found in meteorites have been interpreted to reflect incomplete mixing between the molecular cloud from which the solar system formed and ejecta from nearby supernovae sources (e.g., Yin et al., 2002; Andreasen and Sharma, 2007). Nonetheless, such heterogeneities may also result from the selective processing of presolar dust and therefore do not provide conclusive evidence for a nearby supernova explosion (e.g., Regelous et al., 2008; Trinquier et al., 2009). The abundances of nucleosynthetic p-process isotopes in the solar system are typically low, i.e. one to two orders of magnitude lower than the (combined) s- and r-process isotopes for a given element, reflecting the relatively unusual formation conditions during core collapse supernovae. Thus, if nearby supernovae sources indeed contributed matter to the nascent solar system, it may be expected that such an injection would yield a relatively large p-process excess with respect to the existing molecular cloud. If supernova ejecta was indeed not well mixed in the solar system, p-process isotopes could therefore provide a sensitive tracer for such heterogeneities, more so than (combined) s- and r-process isotopes. Yet, because of analytical difficulties with the low abundances, p-process isotope abundances in extraterrestrial materials have been poorly investigated. Here, we present the first study on the nucleosynthetic inventory of p-process ^{174}Hf in a variety of extraterrestrial materials. Following the pioneering studies on ^{180}W (Schulz et al., 2013) and ^{184}Os (Walker, 2012), this work is among the first to investigate the distributions of p-process isotopes in the heavy mass range that may have a nucleosynthetic origin that is decoupled from the lighter p-process isotopes (e.g., Rauscher et al., 2013 and references therein).

The distribution of p-process Hf is of special interest, because ^{176}Hf , which has a ~3 % p-process contribution (Klay et al., 1991), is also produced by radioactive decay of long-lived ^{176}Lu . The long-lived ^{176}Lu - ^{176}Hf decay system is a potentially robust system for dating early solar system processes, but ^{176}Lu - ^{176}Hf ages for some chondrite, eucrite and angrite samples are too old with respect to the well calibrated U-Pb method (e.g., Patchett & Tatsumoto, 1980; Blichert-Toft and Albarède, 1997; Bizzarro et al., 2003; Bizzarro et al., 2012; Bast and Scherer, 2012; 2013, Righter et al., 2013; Bizzarro and Connelly, 2013). It has been suggested that this discrepancy may be explained by photoexcitation of ^{176}Lu to its isomeric state $^{176\text{m}}\text{Lu}$, which rapidly decays to ^{176}Hf in ($t_{1/2} \sim 3.7$ h) (Albarède et al., 2006; Thrane et al., 2010). Alternatively, some of the apparently older for chondrite samples were explained by

various degrees of thermal metamorphism (Bouvier et al., 2008; Martin et al., 2013). However, both explanations cannot account for mineral-separate isochrons for angrite (Bizzarro et al., 2012; Bast et al., 2013) and eucrite samples (Righter et al., 2013) that also yield ages apparently older than the solar system. As a result, the solar system initial $^{176}\text{Hf}/^{177}\text{Hf}$, as well as the decay constant for ^{176}Lu -decay in extraterrestrial samples, remains under debate.

Notably, a heterogeneous distribution of ^{176}Hf in the solar system at the time at which the chondrite and achondrite parent bodies formed could have potentially influenced the ^{176}Lu - ^{176}Hf chronometer by 1) juxtaposing a mixing curve on the isochron relation between different chondrites and eucrites; and 2) affecting the inferred initial $^{176}\text{Hf}/^{177}\text{Hf}$ from mineral separate isochrons for igneous rocks from different parent bodies, e.g. Earth and chondrites. It was previously shown that s-process Hf, which constitutes 97% of ^{176}Hf , was distributed homogeneously in the solar system (Sprung et al., 2010). Here, we complement these data with the first measurements of p-process Hf, which constitutes 3% of ^{176}Hf , in extraterrestrial materials.

3.2 SAMPLES AND METHODS

The sample suite that was analyzed covers chondrites from the ordinary H and L classes, one enstatite chondrite, and two CV3 chondrites. Mostly equilibrated chondrites (metamorphic types 4-6) were chosen for analyses in order to minimize the possibility of potential residual presolar grains, the incomplete digestion of which would obscure the measured isotopic compositions. In addition to chondrites, three different eucrites were analysed, as well as one CAI from the CV3 chondrite Allende (Becker, 2013), and one silicate inclusion from the Campo del Cielo IAB iron meteorite. Chondrite samples were cut with a rock saw and carefully crushed in an agate mortar. Typically 0.5-1.0 g of chondrite powder were digested in a 24N HF-14N HNO₃-9.5N HClO₄ mixture (~5:5:2) at 180°C tabletop, and terrestrial and extraterrestrial basalts (typically 0.1-0.3 g) were digested in a ~1:1 mixture of 24N HF-14N HNO₃. The silicate inclusion of Campo del Cielo contained high amounts of dark material that remained after table top digestion, possibly graphite, and the sample was therefore digested in Parr bombs in a 1:1 HF-HNO₃ mixture and left for three days, after which virtually all material was digested. Hafnium was then separated from the rock matrix using Ln-Spec based column chromatography, and was further purified with respect to Yb

using anion exchange resin (Chapter 2). Five samples of terrestrial basalts were repeatedly processed as a monitor for analytical artifacts that may be caused by, e.g., imperfect separation from the matrix.

All analyses were performed using the Thermo Finnigan Neptune MC-ICP-MS at the universities of Cologne-Bonn in the setup described in Chapter 2 in detail. In summary, measurement precisions of < 70 ppm on ^{174}Hf can be achieved by using $10^{12}\Omega$ Faraday amplifiers for the collection of ^{174}Hf and ^{172}Yb (monitor for the large isobaric interference by ^{174}Yb), provided that a signal with > 50 mV on ^{174}Hf is achieved. It is important to note that in this setup, the minor isobaric interference by ^{180}Ta ($^{180}\text{Ta}/^{181}\text{Ta} \sim 10^{-4}$) on ^{180}Hf was not monitored. Tantalum concentrations in samples were therefore always checked prior to analyses and were typically indistinguishable from the back ground of the mass spectrometer, i.e., < 10 mV for ^{181}Ta . Data are reported as the deviation from AMES Hf-metal in parts per million i.e. $\mu^{1xx}\text{Hf} = 10^6 \times [(^{1xx}\text{Hf}/^{177}\text{Hf})_{\text{sample}} / (^{1xx}\text{Hf}/^{177}\text{Hf})_{\text{AMES}} - 1]$ using $^{177}\text{Hf}/^{179}\text{Hf} = 0.7325$ and the exponential law to correct for instrumental mass bias.

3.3 RESULTS

Most chondrites show indistinguishable $\mu^{174}\text{Hf}$ from the AMES Hf-metal solution, as do the three eucrite samples, and the terrestrial basalts that were measured to verify to analytical procedure (Table 3.1; Fig. 3.1A). The EL chondrite Pillistfer and H3-4 chondrite Tulia(a) show slightly elevated $\mu^{174}\text{Hf}$ of 130 ± 89 and 65 ± 56 ppm, respectively. These samples are furthermore characterized by slightly elevated $\mu^{178}\text{Hf}$ and low $\mu^{180}\text{Hf}$, a feature which was furthermore found in Sierra Colorada (L5) and Wagon Mound (L6) (Fig. 3.1B-C). For the latter, this finding was reproduced for a replicate digestion. The silicate inclusion of the Campo del Cielo IAB iron meteorite displays an elevated $\mu^{174}\text{Hf}$ of 128 ± 92 as well as positive $\mu^{178}\text{Hf}$ and negative $\mu^{180}\text{Hf}$ similar to some chondrites. The CAI sample yields a negative $\mu^{174}\text{Hf}$ of 200 ppm, whereas $\mu^{178}\text{Hf}$ is indistinguishable from AMES Hf-metal, and $\mu^{180}\text{Hf}$ is positive with 32 ± 9 ppm.

3.4 DISCUSSION

3.4.1 Non-radiogenic heterogeneity in some chondrites and IAB silicate inclusion

Some chondrites (i.e., Pillistfer, Sierra Colorado, Tulia(a), Wagon Mound) yield aberrant isotope compositions with respect to the terrestrial value as defined by AMES Hf-

metal. The observation that most other chondrites, in contrast, exhibit terrestrial compositions within analytical uncertainty indicates that nucleosynthetic heterogeneity in the solar system is unlikely to be the cause for this variability. Moreover, three out of the four chondrite samples that show anomalous isotopic compositions are among the highest metamorphic grades (types 5-6). The potential of residual presolar grains after sample digestion causing these anomalies is therefore low.

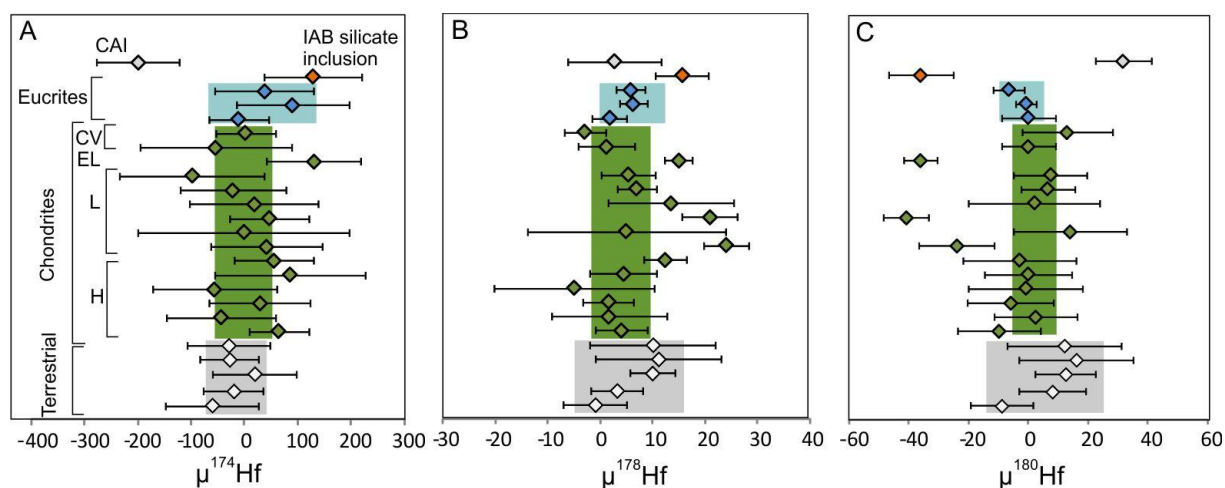


Fig. 3.1 Non-radiogenic Hf isotopic compositions of extraterrestrial and terrestrial samples, relative to the AMES Hf-metal in parts per million. Error bars represent either 2σ external reproducibility throughout a measurement sessions or 2 S.E. in-run variability, whichever is larger. Boxes correspond to 2σ deviations from the population means. The weighted mean for chondrites does not include samples with positive $\mu^{178}\text{Hf}$ if negatively correlated with $\mu^{180}\text{Hf}$, which will be explained in the next section to be indicative for secondary neutron capture effects.

A better explanation may therefore be that the Hf isotopic compositions in these samples were affected by secondary neutron capture reactions due to the exposure to galactic cosmic rays. Sprung et al. (2010) previously concluded that such effects are negligible in chondrites, but this conclusion was based on analytical precisions for $\mu^{178}\text{Hf}$ and $\mu^{180}\text{Hf}$ of typically around 10-20 ppm and 30-40 ppm, respectively. We achieved slightly better measurement precisions due to the need for having > 50 mV signal intensities on ^{174}Hf , therefore consuming up to twice as much Hf compared to their analyses (60-120 ng compared to 40-60 ng, respectively). Furthermore, in our dataset, $\mu^{178}\text{Hf}$ and $\mu^{180}\text{Hf}$ are complemented by the first precise $\mu^{174}\text{Hf}$, providing an additional constraint to assess the possible presence of secondary neutron

Table 3.1 Non-radiogenic Hf isotopic compositions in meteorites and terrestrial rocks^a

	Type	$\mu^{174}\text{Hf}$	$\mu^{178}\text{Hf}$	$\mu^{180}\text{Hf}$
Chondrites				
Tulia(a)	H3-4	65 ± 56	4 ± 5	-10 ± 14
NWA 4009	H5-6	-44 ± 102	2 ± 11	2 ± 14
Pullusk	H5	53 ± 94	9 ± 13	-15 ± 22
Pultusk replicate		60 ± 100	7 ± 5	1 ± 19
<i>Weighted Mean</i>		28 ± 69	2 ± 5	-6 ± 11
NWA 926	H4	-56 ± 115	-5 ± 15	-1 ± 19
Yelland Dry Lake	H4	85 ± 141	4 ± 6	0 ± 15
NWA 4296	H4	54 ± 74	12 ± 4	-3 ± 19
Sierra Colorada	L5	44 ± 104	24 ± 4	-24 ± 13
NWA 515	L6	-2 ± 198	5 ± 19	14 ± 19
Wagon Mound	L6	102 ± 74	26 ± 6	-43 ± 14
Wagon Mound replicate		79 ± 67	22 ± 12	-40 ± 9
<i>Weighted Mean</i>		46 ± 50	21 ± 5	-41 ± 8
NWA 904	L5	18 ± 56	14 ± 12	2 ± 22
Gilgoin	L6	-21 ± 99	7 ± 6	6 ± 9
NWA 4292	L6	-99 ± 136	5 ± 5	7 ± 12
Pillistfer	EL6	130 ± 89	15 ± 4	-36 ± 6
Vigarano	CV3	-54 ± 143	1 ± 5	0 ± 9
NWA 3118	CV3	2 ± 56	-3 ± 4	13 ± 15
Achondrites				
Millbillillie	Eucrite	-11 ± 57	2 ± 3	0 ± 9
NWA 4405	Eucrite	66 ± 105	6 ± 4	-11 ± 11
NWA 4405 replicate		127 ± 104	7 ± 4	-3 ± 5
NWA 4405 replicate		63 ± 142	7 ± 5	4 ± 5
<i>Weighted Mean</i>		90 ± 66	6 ± 3	-1 ± 3
Stannern	Eucrite	-31 ± 93	0 ± 4	-16 ± 9
Stannern replicate		8 ± 56	10 ± 9	0 ± 9
Stannern replicate		53 ± 41	10 ± 4	-3 ± 9
<i>Weighted Mean</i>		30 ± 31	6 ± 3	-7 ± 5
Campo del Cielo (silicate inclusion El Taco)	IAB iron	128 ± 92	16 ± 5	-36 ± 11
Allende CAI	CAI	-200 ± 78	3 ± 8	32 ± 9
Terrestrial				
BHVO-2	Basalt (Hawaii)	-7 ± 79	19 ± 9	21 ± 22
BHVO-2 replicate		40 ± 102	15 ± 11	9 ± 22
BHVO-2 replicate		80 ± 92	4 ± 9	6 ± 18
BHVO-2 replicate		-12 ± 78	6 ± 7	16 ± 19
<i>Weighted Mean</i>		19 ± 43	10 ± 4	12 ± 10
BCR-2	Basalt (Columbia River)	-29 ± 54	11 ± 12	4 ± 19
BB46A	Basalt (Leine Graben)	-6 ± 56	4 ± 8	12 ± 22
BB46A replicate		-68 ± 92	0 ± 9	-5 ± 22
BB46A replicate		-28 ± 96	2 ± 13	18 ± 23
BB46A replicate		-46 ± 102	9 ± 11	9 ± 22
<i>Weighted Mean</i>		-21 ± 39	3 ± 5	8 ± 11
I12MU	Basalt (Muriah, Sunda Arc)	-61 ± 88	-1 ± 6	-9 ± 11
3MU-13	Basalt (Muriah, Sunda Arc)	-30 ± 78	10 ± 12	27 ± 19

^aReported as the deviation from AMES-Hf in parts metal per million, i.e. $\mu^{1xx}\text{Hf} = 10^6 \times [(^{1xx}\text{Hf}/^{177}\text{Hf})_{\text{sample}} / (^{1xx}\text{Hf}/^{177}\text{Hf})_{\text{AMES}} - 1]$ using $^{177}\text{Hf}/^{179}\text{Hf} = 0.7325$ to correct for instrumental mass bias.

capture effects, because $\mu^{174}\text{Hf}$ is expected to be stronger affected than $\mu^{178}\text{Hf}$ and $\mu^{180}\text{Hf}$. For those chondrites with anomalous isotopic compositions, as well as in

the silicate inclusion of the IAB iron meteorite El Taco, $\mu^{180}\text{Hf}$ negatively correlates with $\mu^{174}\text{Hf}$ as well as with $\mu^{178}\text{Hf}$, and a minor positive correlation is seen between $\mu^{174}\text{Hf}$ and $\mu^{178}\text{Hf}$. The slopes of these correlations agree well with the expected values for neutron capture effects on Hf isotopes (Fig. 3.2). The predominant types of neutron capture reactions would namely result in burnout of ^{177}Hf , ^{178}Hf , and in the production of ^{178}Hf , ^{179}Hf , where the production of ^{178}Hf exceeds the burnout. As a result, with increasing neutron capture effects, $\mu^{174}\text{Hf}$ is expected to increase with decreasing $\mu^{180}\text{Hf}$ due to the normalisation directly to ^{177}Hf and indirectly to $^{177}\text{Hf}/^{179}\text{Hf}$ for the instrumental mass bias. $\mu^{178}\text{Hf}$ is expected to positively correlate with these effects. Thus, it seems plausible that small neutron capture effects that were unresolved by Sprung et al. (2010) (maximum -40 ppm on $\mu^{180}\text{Hf}$) are in fact present in some chondrites.

The most probable neutron capture reactions that may contribute to these effects are, at epithermal energy levels, $^{177}\text{Hf}(n,\gamma)^{178}\text{Hf}$ and $^{178}\text{Hf}(n,\gamma)^{179}\text{Hf}$ with resonance integrals of ~ 7173 barn and 1910 barn, respectively (Mughabghab, 2003). Hafnium-174 is shielded from the production by neutron capture by stable ^{174}Yb and has a small capture cross section in the epithermal range (RI ~ 436 barn). However, apparent positive $\mu^{174}\text{Hf}$ may result from the normalization to ^{177}Hf and the correction for instrumental mass bias to $^{177}\text{Hf}/^{179}\text{Hf}$. Similarly, burn-out of ^{180}Hf by neutron capture is relatively improbable (RI ~ 35), as is its production by neutron capture on ^{179}Hf (RI ~ 630); and $\mu^{180}\text{Hf}$ is therefore predominantly affected by the normalization. At thermal energies, the reaction $^{176}\text{Lu}(n,\gamma)^{177}\text{Lu}(\beta^-)^{177}\text{Hf}$ with $\sigma_{\text{th}300\text{K}} \sim 3640$ barn may furthermore affect to the isotopic composition of Hf, but overall the expected effects are predominantly governed by epithermal neutrons (Sprung et al., 2010).

The reason that samples of only some chondrites were affected by neutron capture, whereas others remained largely unaffected, thus relates to the relative doses of epithermal neutrons that these samples received. The latter depends on the duration of exposure to cosmic rays, the size and chemical composition of the target, and the depth of the sample within the target (e.g., Leya, 1997; Kollár et al., 2006). The fact that the composition of target material plays a role is probably illustrated by the neutron capture effects recorded by the IAB silicate inclusion, which was embedded in Fe-rich metal. Iron is a highly inefficient neutron

moderator and absorbs neutrons in the epithermal range before they become thermal, therefore resulting in higher epithermal/thermal neutron spectra in Fe-rich target materials, by which neutron capture reactions on Hf isotopes become more probable (e.g., Kollár et al., 2006; Sprung et al., 2010). Iron contents in chondrites are, in contrast, significantly lower, and may therefore play a lesser role in moderating the neutron energy spectra. This is illustrated by the observation that several H-chondrites show no resolvable neutron capture effects, whereas some L-chondrites and the EL chondrite Pillistfer, which by definition have lower Fe-contents, show the largest neutron capture effects observed in this study. Thus, for chondrites, potential neutron capture effects are therefore probably predominantly determined by the duration of exposure to cosmic rays as well as the depth of the sample in the parent body.

Importantly, secondary neutron capture effects were found here in high-grade metamorphic chondrites (types 5-6). These chondrite types are generally thought to represent the inner parts of the asteroidal parent bodies (e.g., Trieloff et al., 2003), where they must have been largely shielded from irradiation by cosmic rays. Irradiation of these samples therefore must have predominantly occurred after asteroidal break-up, and fluences of epithermal neutrons during this time were apparently sufficient to induce neutron capture effects, despite the relatively short cosmic ray exposure ages for most chondrites (Leya and Masarik, 2009 and references therein).

3.4.2 Distribution of p-process ^{174}Hf on an asteroidal scale

When samples that appear to be affected by secondary neutron capture reactions are excluded from the dataset, the Hf isotopic composition in each chondrite and eucrite sample is indistinguishable from the terrestrial value. The weighted mean for $\mu^{174}\text{Hf}$ in terrestrial samples is -14 ± 57 ppm, and the grand weighted mean for extraterrestrial samples that are unaffected by neutron capture is -9 ± 110 ppm. Thus, there is no resolvable difference between the terrestrial and extraterrestrial abundances of p-process ^{174}Hf . The grand weighted mean for $\mu^{174}\text{Hf}$ in chondrites, eucrites and terrestrial silicates is -7 ± 100 ppm and at this level, p-process ^{174}Hf may therefore be considered uniformly distributed between these materials. Thus, if a supernova source would have injected p-process ^{174}Hf into the nascent solar system, this material must have become homogenized by the time that the chondrite and eucrite parent bodies formed. Alternatively, the amount of ^{174}Hf injected could have been

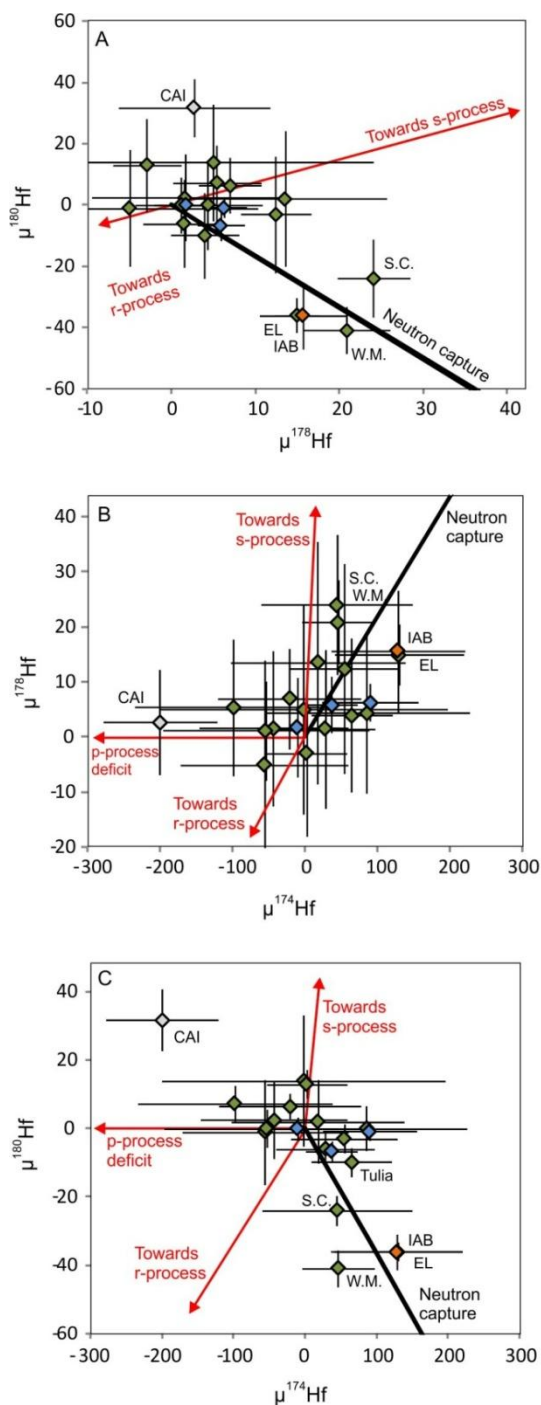


Fig. 3.2 Non-radiogenic Hf isotope compositions in extraterrestrial samples. Chondrites with elevated $\mu^{178}\text{Hf}$ and $\mu^{174}\text{Hf}$ generally yield a deficit in $\mu^{180}\text{Hf}$, in good agreement with the model for secondary neutron capture by Sprung et al., 2010 (Sprung, personal communication). Heterogeneities in Hf isotope compositions between chondrites are therefore interpreted to reflect variable fluences of epithermal neutrons. In CAI, the low $\mu^{174}\text{Hf}$ may indicate a p-process deficit, whereas the elevated $\mu^{180}\text{Hf}$ remains of unknown origin. Black lines correspond to the effects that are expected from neutron fluences with

epithermal/thermal ratios of 1 to 8. Modeling of nucleosynthetic effects was based on s-process yields by Wisshak et al. (2006). IAB = silicate inclusion from El Taco (Campo del Cielo); EL = Pillistfer; W.M. = Wagon Mound; S.C. = Sierra Colorada. Color coding is as in Fig. 3.1.

negligible compared to the amount of ^{174}Hf contributed by older interstellar material. Both conclusions are in agreement with recent studies on heavy p-process isotopes ^{184}Os , ^{180}W and ^{190}Pt that appear to be uniformly distributed between the iron meteorite parent bodies at levels of < 2700 ppm, <100 ppm, and <100 ppm, respectively (Walker, 2012; Peters et al., Chapters 2-3).

3.4.3 Potential p-process deficit in CAIs

In the CAI from Allende, $\mu^{174}\text{Hf}$ and $\mu^{180}\text{Hf}$ show negative and positive anomalies, respectively. This is opposite to what is expected from neutron capture effects, which would result in positive and negative anomalies, respectively. Furthermore, these anomalies cannot be matched by mixing chondritic Hf with pure s-, r- or p-process derived Hf (Fig. 3.2; s-process yields from Wisshak et al., 2006). However, a combined p- and r-process deficit may account for the negative $\mu^{174}\text{Hf}$ as well as for the positive $\mu^{180}\text{Hf}$, and would be in agreement with models for combined p- and r-process nucleosynthesis in supernovae. However, this scenario would also result in a pronounced effect in $\mu^{178}\text{Hf}$, which is not the case. We therefore suggest that either 1) the variability in $\mu^{174}\text{Hf}$ and $\mu^{180}\text{Hf}$ is coupled and is caused by a yet unidentified process; or 2) the negative $\mu^{174}\text{Hf}$ signature is explained by a p-process deficit, whereas the positive $\mu^{180}\text{Hf}$ is caused by a second, yet unidentified, decoupled process.

Independent of the cause for the positive $\mu^{180}\text{Hf}$ in the Allende CAI, it is worth considering whether the negative $\mu^{174}\text{Hf}$ is indeed likely to represent a p-process deficit. CAIs were previously reported to yield a p-process deficit in ^{144}Sm but show chondritic abundances of p-process isotopes $^{92,94}\text{Mo}$, $^{96,98}\text{Ru}$, and $^{130,132}\text{Ba}$ (Chen et al., 2010; Brennecka et al., 2013; Bouvier and Boyet, 2013), and possibly excess ^{84}Sr (Paton et al., 2012). The apparent excess in ^{84}Sr was, however, alternatively explained by an excess in r-process Sr (e.g., Moynier et al., 2012). This interpretation agrees well with the r-process excesses found in other elements with isotopes $A < 140$, i.e. Zr, Mo, Ru and Ba (Brennecka et al., 2013 and references therein). In the latter study, it was furthermore noticed that Nd and Sm, i.e., elements with isotopes $A >$

¹⁴⁰ rather display r-process deficits in CAIs. This observation was interpreted as the result of multiple nucleosynthetic sources having contributed to the r-process inventory of the solar system, furthermore requiring the existence of a reservoir with r-process synthesized material that remained untapped by CAIs. Given the great difficulty to produce the abundances of p-process isotopes in the solar system by a single mechanism, it is plausible that a similar decoupling exists for p-nuclides. A deficit in p-process ¹⁷⁴Hf found here in CAIs is therefore not in disagreement with the absences of p-process isotope anomalies in elements in a much lighter mass range, i.e. ^{92,94}Mo, ^{96,98}Ru, ^{130,132}Ba, and possibly ⁸⁴Sr. these light p-process isotopes may have at least partially originated from a different source. In contrast, the negative p-process anomalies observed for ¹⁴⁴Sm in CAIs may indicate production of ¹⁴⁴Sm by the same nucleosynthetic mechanism as ¹⁷⁴Hf. Altogether, the r-process reservoir that was apparently not tapped by CAIs, as inferred by Brennecke et al. (2013), may furthermore have provided additional heavy p-process isotopes such as ¹⁴⁴Sm and ¹⁷⁴Hf. This model is in good agreement with the view that light and heavy p-process production mechanisms may be decoupled and that p- and r-process nucleosynthesis both take place in supernovae.

3.4.4 Implications for ¹⁷⁶Lu-¹⁷⁶Hf chronometry

The observation that secondary neutron capture reactions have modified the non-radiogenic Hf isotopic compositions in some chondrites implies that for these samples, ¹⁷⁶Hf/¹⁷⁷Hf may be affected as well. This effect would however be < 35 ppm according to the model by Sprung et al. (2010) and therefore cannot explain the difference in the inferred decay constant for ¹⁷⁶Lu in meteorites and terrestrial rocks.

After samples with secondary neutron capture effects were excluded from our dataset, the weighted means for $\mu^{174}\text{Hf}$ in terrestrial samples (-14 ± 57 ppm) and extraterrestrial samples (-9 ± 110 ppm) are indistinguishable. As the estimated p-process contribution to ¹⁷⁶Hf is approximately 3%, it may be concluded that the maximum possible effects on the initial ¹⁷⁶Hf/¹⁷⁷Hf caused by heterogeneity in p-process Hf are ~3% of the combined uncertainty of these values, i.e. ~5 ppm. No indications were found here for heterogeneity in s-process Hf, in agreement with Sprung et al. (2010). Together, this provides conclusive evidence that the ¹⁷⁶Lu-¹⁷⁶Hf chronometer in early solar system materials is unaffected by nucleosynthetic heterogeneities in the Hf isotope compositions of meteorites.

3.5 CONCLUSIONS

We report the first high-precision data for p-process ^{174}Hf in extraterrestrial samples. Positive $\mu^{174}\text{Hf}$ in some chondrites and in a silicate inclusion of the El Taco IAB iron show co-variations with $\mu^{178}\text{Hf}$ and $\mu^{180}\text{Hf}$, respectively, indicating that Hf isotope abundances in these samples were modified by secondary neutron capture reactions. A negative $\mu^{174}\text{Hf}$ of ~200 ppm in a CAI from CV3 chondrite Allende may indicate a p-process isotope deficit in the CAI forming region. This ^{174}Hf deficit would imply a decoupling between the sources of heavy and light p-process isotopes in the solar system, which is in agreement with nucleosynthetic model considerations. However, such a scenario cannot account for the positive $\mu^{180}\text{Hf}$ found for the Allende CAI, which therefore remains unexplained. After neutron capture effects have been considered, the isotopic composition of Hf is uniform between different chondrite groups, eucrites, silicate inclusions IAB irons, and Earth. The absence of significant p- and s-process isotope anomalies in chondrites, eucrites and IAB inclusions suggests that the ^{176}Lu - ^{176}Hf systematics in these materials were unaffected by nucleosynthetic heterogeneities for Hf. The discovery of small neutron capture effects in some chondrites implies that $^{176}\text{Hf}/^{177}\text{Hf}$ in these samples could have become slightly (< 35 ppm) elevated due to cosmic ray exposure.

Chapter IV

Alpha-decay of ^{184}Os revealed by radiogenic ^{180}W in meteorites:
Half life determination and viability as geochronometer

4.1 INTRODUCTION

Tungsten-180 is a proton-rich nuclide that is among the rarest nuclides in the solar system. This nuclide was mostly produced by the p-process during nucleosynthesis (e.g., Arnould and Goriely, 2003). Precise measurements of ^{180}W in natural materials have long been difficult due to the low relative abundance ($\sim 0.12\%$), but recent advances in multi-collector ICP mass spectrometry (MC-ICPMS) have achieved precisions of better than 1 parts in 10,000, a ca. 10 fold improvement compared to earlier data (Schulz et al., 2013). In the latter study it was discovered that the abundance of ^{180}W in some iron meteorites is different than in terrestrial materials and varies between iron meteorite classes. One explanation for this observation included a heterogeneous distribution of p-process components in the early solar system. However, this interpretation can account for the following observations only with great difficulty: First, a variability of ^{180}W was reported between individual IVB group iron meteorites (Cook et al., 2013). Second, the ^{180}W values reported for the Cape York meteorite between different studies (Holst et al., 2011; Schulz et al., 2013) vary outside the reported analytical uncertainties. Secondary neutron capture on ^{180}W due to cosmic ray exposure may explain some of this variability. For Cape York, however, secondary neutron capture effects are known to be minimal for ^{182}W (< 10 ppm; Kruijer et al., 2012). Consequently, neutron capture effects on ^{180}W , which has a similar neutron capture cross section (Kang et al., 2007) should be negligible. Based on new data, we show here that ^{180}W heterogeneities in iron meteorites and chondrites rather may reflect in situ radiogenic ingrowth caused by α -decay of the rare nuclide ^{184}Os .

Osmium-184, also a rare proton-rich nuclide, has been proposed to decay by alpha emission (Sperlein and Wolke, 1976; Kolesnikov and Svarovsky, 2001; Medeiros et al., 2006; Gangopadhyay 2009), but decay was not observed during alpha-particle counting experiments, which therefore could only constrain a minimum half life of $> 5.6 \times 10^{13}$ years (Sperlein and Wolke, 1976). Additional decay by neutrinoless double-electron capture with a half life of $> 10^{14}$ years was also suggested, however this decay mode has presently not been observed for any nuclide, including ^{184}Os (Belli et al., 2013). Based on the experimentally established minimum value for the half-life for α -decay, the radiogenic contribution to ^{180}W in iron meteorites has previously been considered to be negligible, i.e. below measurement error (Schulz et al., 2013). However, theoretical estimates for the half life range as low as 5×10^9 years (Sperlein and Wolke, 1976) and at such levels the radiogenic production would indeed be significant. We therefore re-assessed the origin of ^{180}W heterogeneities in iron meteorites

for the first time by combining ^{180}W isotope and Os-W concentration measurements and also report the first ^{180}W data for silicate samples.

4.2 ANALYTICAL STRATEGY

Eleven specimens from six different iron meteorite classes were selected to cover virtually the whole known range of Os/W ratios observed in meteorites (e.g., Scott, 1978; Smoliar et al., 1996; Ryan et al., 1990; Petaev and Jacobsen, 2004; McCoy et al., 2011). Because secondary neutron capture effects on ^{180}W due to cosmic ray exposure could potentially obscure radiogenic ingrowth, mostly specimens with low exposure ages (≤ 100 Myrs) were selected. Importantly, the parent asteroids of iron meteorites are known to have accreted within few million years of one another, approximately 4.565 Ga ago (e.g., Kleine et al., 2005; Scherstén et al., 2006; Kruijer et al., 2012). This period is negligible compared to the expected half life for α -decay of ^{184}Os . A calibrated isotopic tracer enriched in ^{190}Os was added prior to digestion of these iron meteorites and the chondrite Pultusk in 2 ml HCl and 6 ml HNO_3 using an Anton Paar high-pressure asher. Osmium was subsequently separated by solvent extraction and further purified by microdistillation, after which the Os fractions were measured on Faraday cups by N-TIMS at Berlin (Fisher-Gödde et al., 2010). The yield for co-extraction of W in CCl_4 was tested for one ordinary chondrite (NWA 4009) and one iron meteorite (Muonionalusta, type IVA) by isotope dilution, each in two replicate experiments (Table 4.1). In all of these experiments, negligible amounts of W ($< 0.05\%$) were lost during the solvent extraction step.

The remaining sample after solvent extraction was again completely dissolved and divided in two aliquots. A tracer enriched in ^{183}W that was calibrated against $>99.9\%$ pure W metal was added to the smaller aliquot from which W was separated by anion exchange chromatography. The isotope composition of the spiked W fraction was measured using the Neptune MC-ICPMS at Cologne-Bonn. The aliquot containing unspiked W was used for isotope abundance measurements using the Neptune MC-ICPMS at Cologne-Bonn that is equipped with two $10^{12}\ \Omega$ Faraday amplifiers that were used for masses 180 (W, Hf, Ta) and 178 (Hf interference monitor). All samples were run with signal intensities between 40 and 80 mV on ^{180}W for 60 cycles with 8 seconds integration time. Standard solutions that were used for sample bracketing were prepared to match intensities at the level of $< 30\%$. Samples were

sufficiently clean with respect to Hf (typical Hf/W < 10⁻⁵) for accurately correcting interference by isobaric ¹⁸⁰Hf (Schulz et al., 2013). Procedural blanks were ~300 pg W. Samples were bracketed with a solution of Münster AMES W metal, which is isotopically indistinguishable from the NIST W solution standard (SRM 3163) (Fig. 4.1), and is hereafter reported as $\epsilon^{180}\text{W} = 10^4 \times [(\text{}^{180}\text{W}/\text{}^{184}\text{W})_{\text{SAMPLE}}/(\text{}^{180}\text{W}/\text{}^{184}\text{W})_{\text{AMES}} - 1]$. The reason for normalisation to ¹⁸⁴W rather than ¹⁸³W is that the latter isotope may potentially be affected by mass independent isotope fractionation effects (Shirai and Humayun, 2011) and organic interferences may also be present on ¹⁸³W (e.g., Kleine et al. 2004). Measured ¹⁸⁰W/¹⁸⁴W ratios were normalised to correct for instrumental mass bias effects to a ¹⁸⁶W/¹⁸⁴W of 0.92767 using the exponential law. Calculated $\epsilon^{180}\text{W}$ values are identical within analytical precision when using ¹⁸⁶W/¹⁸³W and ¹⁸⁴W/¹⁸³W for mass bias corrections, but generally yield better in-run precisions if normalized to ¹⁸⁶W/¹⁸⁴W. Isobaric interferences of Os were corrected for based on the measured, i.e., spiked, isotope ratios, but were generally low (Os/W ~10⁻⁶). The external reproducibility (2 σ) for ¹⁸⁰W/¹⁸⁴W of a 50 ppb AMES metal solution was typically better than 65 ppm. ¹⁸⁴Os/¹⁸⁴W ratios were calculated from element concentrations, assuming uniform abundances of ¹⁸⁴Os and ¹⁸⁴W in iron meteorites, which is known to a sufficiently precise level (< 2700 ppm (Walker, 2012) and ~10 ppm (Qin et al., 2008), respectively).

Table 4.1 Co-extraction of W in CCl₄ (%) during Os separation.

<i>NWA 4009 (H Chondrite)</i>		<i>Replicate</i>
$C_{\text{W}}^{\text{Sample}}$ (ng g ⁻¹)	145	
W in aliquot (ng) ^a	18	20
W in CCl ₄ (ng) ^b	0.0065	0.0052
Co-extracted W (%)	< 0.036	< 0.027
<i>Muonionalusta (IVA iron)</i>		<i>Replicate</i>
$C_{\text{W}}^{\text{Sample}}$ (ng g ⁻¹)	3451	
W in aliquot (ng) ^a	123	153
W in CCl ₄ (ng) ^b	0.033	0.031
Co-extracted W (%)	< 0.027	< 0.020

^aCalculated from W concentrations and from aliquot weights.

^bMeasured quantities are corrected for the lower limit of the procedural blank (5 pg).

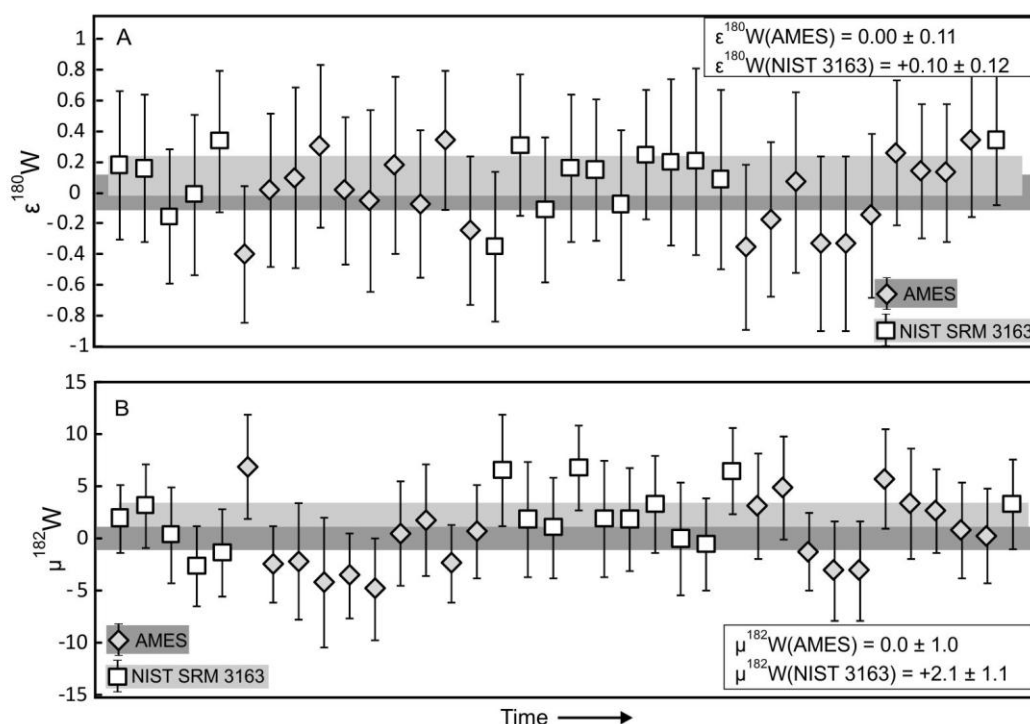


Fig. 4.1 Comparison of the isotopic compositions between the AMES W-metal and the NIST SRM 3163 W-solution reference materials, measured during one analytical session, and expressed relative to the average composition of AMES metal. The abundances of ^{180}W and ^{182}W are shown normalised to ^{184}W and were corrected for instrumental mass bias effects to a $^{186}\text{W}/^{184}\text{W}$ of 0.92767 using the exponential law. (A) The weighted means for $\epsilon^{180}\text{W}$ are 0.00 ± 0.11 for AMES and 0.10 ± 0.12 for NIST SRM 3163, respectively (95% confidence limits, indicated). The external reproducibility (2σ) of $\epsilon^{180}\text{W}$ is 0.48 ϵ -units for AMES metal, and 0.39 ϵ -units for NIST SRM 3163. (B) The weighted means for $\mu^{182}\text{W}$ (i.e., the deviation from the AMES metal standard in parts per 10^6) are 0.0 ± 1.0 for AMES and 2.1 ± 1.1 for NIST SRM 3163, respectively (95% confidence limits). The external reproducibility for $\mu^{182}\text{W}$ is 3.4 and 2.8 μ -units for AMES and NIST SRM 3163, respectively.

In order to verify the radiogenic contribution to ^{180}W for other solar system materials than iron meteorites, ^{180}W was also analysed in four ordinary chondrites, and three terrestrial basalts. Only equilibrated chondrites (H/L4-6) were selected to minimize the possibility of incomplete digestion of isotopically anomalous presolar grains. Only chondrites with low weathering grades were selected, because sulfides and metal that are most susceptible to terrestrial weathering are also major carriers of Os. The Os/W ratio was only measured for the H chondrite Pultusk and is considered representative for the other samples, because refractory

siderophile elements are known to show limited fractionation within chondrite classes (e.g., Wasson and Kallemeyn, 1988). An additional separation step based on Eichrom TEVA resin was included for these silicate-rich samples to efficiently separate Hf (isobaric interference on ^{180}W), Ti, and Zr, which were observed to affect the instrumental mass bias behavior of W. In this clean-up step, samples are loaded in 2 ml 6N HCl on columns that are 5 mm in diameter and have 0.5 ml TEVA resin. Virtually all Hf, Ti, Zr is subsequently rinsed from the column with an additional 3 steps in 2 ml 6N HCl. A close to 100% yield for W is then eluted in 3N HNO_3 . Sample cuts that were prepared according to this procedure were found to be sufficiently clean for analysis (basaltic matrix: $\text{Hf}/\text{W} < 10^{-5}$; $\text{Ti}/\text{W} < 10^{-1}$, $\text{Zr}/\text{W} < 10^{-3}$) (see Schulz et al., 2013). Prior to loading, the resin was repeatedly cleaned with a mixture of 3M $\text{HNO}_3/0.2\text{M HF}$ and subsequently rinsed with H_2O and equilibrated with 6N HCl.

4.3 RESULTS

4.3.1 Combined ^{180}W and Os-W concentration measurements

The relative abundance of ^{180}W in our iron meteorite samples is variable and correlates significantly with Os/W ratios (MSWD = 1.4) (Fig. 4.2A, Table 3.2). We therefore propose that this correlation represents an isochron for the iron meteorite parent bodies. This isochron is the first empirical evidence for α -decay of ^{184}Os . No inverse correlation is observed between $\epsilon^{180}\text{W}$ and W concentration, indicating that the correlation between $\epsilon^{180}\text{W}$ and Os/W ratio cannot be explained by mixing of two compositionally distinct reservoirs with respect to W isotopic compositions (Fig. 4.2B). The slope of the isochron $m = 0.000298 \pm 0.000061$ corresponds to a decay constant of $\lambda^{184}\text{Os}(\alpha) = 6.53 \pm 1.36 \times 10^{-14} \text{ a}^{-1}$. The calculated half life of $1.11 \pm 0.23 \times 10^{13} \text{ yr}$ is only slightly shorter than the minimum estimate from alpha particle counting, and is in relative good agreement with theoretical considerations (Table 4.3). The weighted mean for $\epsilon^{180}\text{W}$ in ordinary chondrites may be plotted against the Os/W ratio of chondrite Pultusk in Fig. 4.2A. In this case, $\epsilon^{180}\text{W}$ in ordinary chondrites overlaps the 4.565 Ga isochron for the iron meteorite parent bodies and slightly improves the precision of the slope (MSWD = 1.3). The reservoir from which the ordinary chondrite parent bodies formed has per definition uniform chondritic Os/W and formed as early condensates approximately 4.568 Ga ago (e.g., Amelin et al., 2002), very similar to the accretion ages of the iron meteorite parent bodies. The slope of the combined isochron for iron meteorites and the chondrite reservoir $m = 0.000296 \pm 0.000061$ therefore gives our preferred value of $\lambda^{184}\text{Os}(\alpha)$

$= 6.49 \pm 1.34 \times 10^{-14} \text{ a}^{-1}$. This value corresponds to a half life of $1.12 \pm 0.23 \times 10^{13}$ years. The lower intercept of the isochron yields the initial abundance of ^{180}W in the solar system (BSSI) that can be expressed as $\epsilon^{180}\text{W}_{\text{BSSI}} (\text{AMES}) = -0.80 \pm 0.41$ relative to AMES metal or, alternatively, as $\epsilon^{180}\text{W}_{\text{BSSI}} (\text{OC}) = -1.67 \pm 0.79$ relative to the composition of ordinary chondrite.

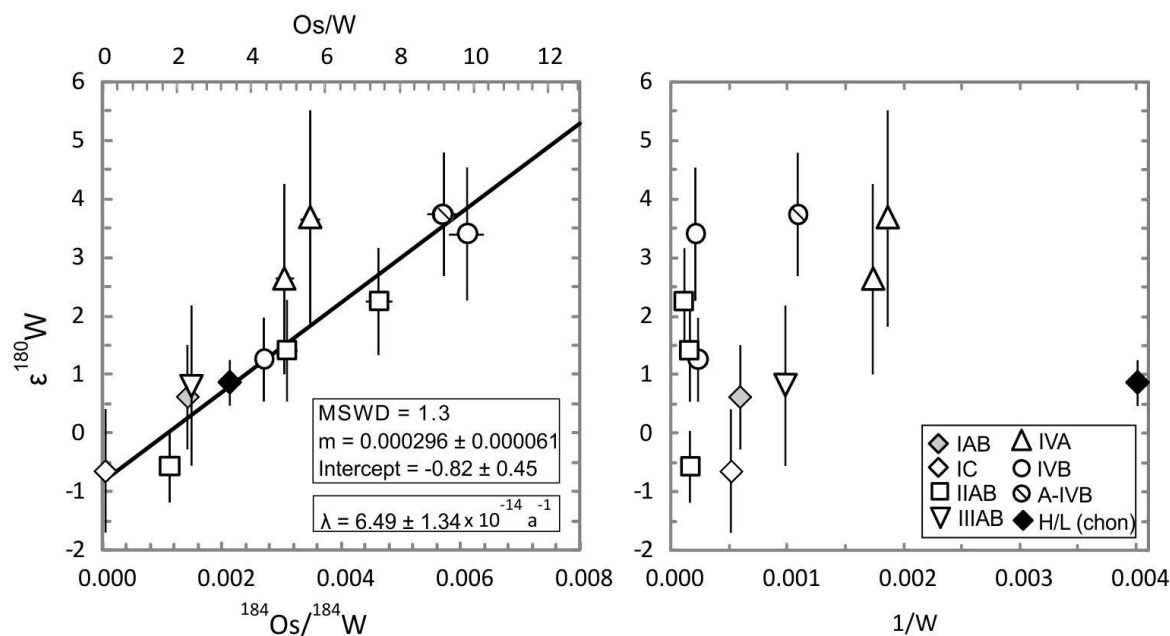


Fig. 4.2 Tests for a radiogenic origin of ^{180}W heterogeneities in meteorites. (A) $\epsilon^{180}\text{W}$ plotted against $^{184}\text{Os}/^{184}\text{W}$ ratios for 11 iron meteorites from different meteorite classes, and the weighted mean for $\epsilon^{180}\text{W}$ in ordinary chondrites plotted against the $^{184}\text{Os}/^{184}\text{W}$ ratio of the ordinary chondrite Pultusk. $\epsilon^{180}\text{W}$ values represent $^{180}\text{W}/^{184}\text{W}$ ratios of samples relative to the average composition of AMES metal throughout the different measuring sessions with $^{180}\text{W}/^{184}\text{W}_{\text{AMES}} = 0.0038780 \pm 0.0000002$ (2σ). $^{184}\text{Os}/^{184}\text{W}$ ratios were calculated from Os-W concentrations using a relative abundance of $^{184}\text{Os} = 0.0197 \pm 0.0005\%$ (Völkening et al., 1991), the atomic weight of W and abundance of ^{184}W were corrected for radiogenic ^{182}W deficits and ^{180}W excesses. Errors on $\epsilon^{180}\text{W}$ correspond to 2σ r.s.d.. Estimated errors on the $^{184}\text{Os}/^{184}\text{W}$ ratios are 4.5% and are generally smaller than symbol sizes. Regression shows a York-type model 1 fit (Ludwig, 2008). (B) No inverse correlation is observed between $\epsilon^{180}\text{W}$ and W concentration.

Table 4.2 Tungsten isotopic compositions and Os-W concentrations for iron meteorites, chondrites and terrestrial basalts.

	Type	Os ^a (ppb)	W ^b (ppb)	$\epsilon^{180}\text{W}^c$	$\epsilon^{182}\text{W}^c$	$^{184}\text{Os}/^{184}\text{W}^d$	$^{180}\text{W}/^{184}\text{W}^e$
Iron meteorites							
Bendego	IC	106	1981	-0.64 ± 1.05	-3.84 ± 0.10	0.00003	0.00387775(41)
Campo del Cielo (El Taco)	IAB	3855	1695	$+0.63 \pm 0.88$	-3.03 ± 0.12	0.00141	0.00387824(34)
Forsyth County	IIAB	31417	6341	$+1.42 \pm 0.86$	-3.47 ± 0.08	0.00308	0.00387855(33)
Holland's Store	IIAB	11307	6383	-0.56 ± 0.60	-3.43 ± 0.07	0.00110	0.00387778(23)
Negrillos	IIAB	64725	8712	$+2.25 \pm 0.91$	-3.58 ± 0.09	0.00462	0.00387887(35)
Cape York	IIIAB	2397	1016	$+0.83 \pm 1.36$	-3.42 ± 0.10	0.00147	0.00387832(53)
Gibeon	IVA	2836	579	$+2.65 \pm 1.62$	-3.45 ± 0.14	0.00304	0.00387903(63)
La Grange	IVA	2997	537	$+3.68 \pm 1.84$	-3.38 ± 0.13	0.00347	0.00387943(71)
Cape of Good Hope	IVB	47431	4841	$+3.41 \pm 1.14$	-3.39 ± 0.09	0.00609	0.00387932(44)
Weaver Mountains	IVB	18484	4274	$+1.27 \pm 0.71$	-3.23 ± 0.08	0.00269	0.00387849(28)
Chinga	IVB-an	8469	923	$+3.74 \pm 1.05$	-3.04 ± 0.09	0.00570	0.00387945(41)
Chondrites							
Pultusk	H5	857	249	$+1.36 \pm 1.14$	-2.22 ± 0.09	0.00214	0.00387853(53)
NWA 4009	H5-6			$+0.79 \pm 0.63$	-2.28 ± 0.11		0.00387831(31)
Tulia (a)	H3-4			$+1.02 \pm 1.00$	-2.29 ± 0.12		0.00387840(40)
Sierra Colorada	L5			$+0.74 \pm 0.61$	-1.10 ± 0.12		0.00387829(29)
<i>Weighted Mean</i>				$+0.87 \pm 0.38$			<i>0.00387834(15)</i>
Terrestrial							
BG-49	Basalt			-0.30 ± 0.44			0.00387788(17)
LP-7	Basalt			-0.15 ± 1.05			0.00387794(47)
I13MU3	Basalt			$+0.16 \pm 0.87$			0.00387806(34)

^aPrecisions of Os concentrations are at the 1% level or better (2 sm), based on non-stoichiometry of ammonium hexachlorosmate standards used for spike calibration (Morgan et al. 1995).

^bPrecisions of W concentrations are better than 1% (2 σ r.s.d.)

^c $\epsilon^{18x}\text{W} = 10^4 \times [({}^{18x}\text{W}/{}^{184}\text{W})_{\text{SAMPLE}} / ({}^{18x}\text{W}/{}^{184}\text{W})_{\text{AMES}} - 1]$. Errors correspond to 2 σ r.s.d..

^dCalculated from the relative abundances of $^{184}\text{Os} = 0.0197 \pm 0.0005\%$ (Völkering et al., 1991) and $^{184}\text{W} = 30.64 \pm 0.03\%$ and the atomic weights, corrected for radiogenic ^{182}W deficits and ^{180}W excesses. Estimated precisions are better than 4.5% and largely depend on the uncertainty at which the abundance of ^{184}Os is known.

^eCalculated from the measured $\epsilon^{180}\text{W}$ using the average composition of AMES metal throughout the different measuring sessions with $^{180}\text{W}/^{184}\text{W}_{\text{AMES}} = 0.0038780 \pm 0.0000002$ (2 σ).

Table 4.3 Estimates on the half life for α -decay of ^{184}Os

$T_{1/2} \text{ } ^{184}\text{Os}(\alpha)$ (yr)	Approach	Reference
$5 \times 10^9 - 4 \times 10^{14}$	Gamow-Condon-Gurney theory (theoretical)	Sperlein and Wolke, 1976
$> 5.6 \times 10^{13}$	Alpha particle counting: decay not observed (experimental)	Sperlein and Wolke, 1976
$10^{12} - 10^{13}$	Extrapolated from ^{190}Pt alpha decay (semi-empirical)	Kolesnikov and Svarovsky, 2001
2.6×10^{13}	Extrapolated from 336 alpha-emitters (semi-empirical)	Medeiros et al., 2006
1.3×10^{13}	Microscopic super asymmetric fission model (theoretical)	Gangopadhyay, 2009
$1.12 \pm 0.23 \times 10^{13}$	Combined 4.565 Ga isochron for iron meteorites and chondrite reservoir (empirical)	This study

4.3.2 Abundance of ^{180}W in chondrites and terrestrial silicates

The terrestrial basalts that were analysed overlap with the composition of Münster AMES metal solution (Table 4.2). They show a deficit of ^{180}W of on average 1.16 ± 0.69 ϵ -units with respect to the composition of chondrites, which have slightly elevated $\epsilon^{180}\text{W}$ with respect to AMES metal (Fig. 4.3). No resolvable variability of $\epsilon^{180}\text{W}$ between different basalts, nor between different chondrites, was found.

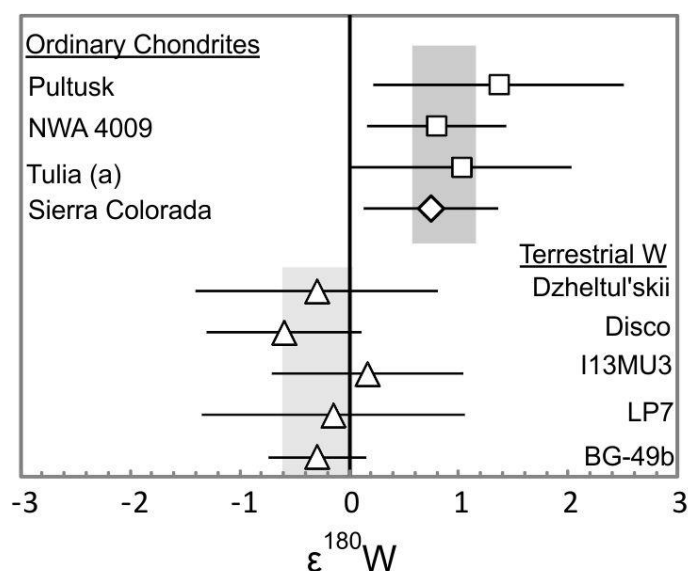


Fig. 4.3 $\epsilon^{180}\text{W}$ of H and L chondrites (squares and diamond, respectively) compared to terrestrial rocks (triangles), relative to AMES metal (vertical line). Error bars correspond to 2σ measurement uncertainties. Boxes represent the 2σ variation of the weighted means expressed as the square root of the sum of the inverse square of measurement errors (Leo,

1992). I13MU3 is a Holocene alkaline basalt from the Sunda Arc, Indonesia; LP7 is a Holocene high μ -like basalt from La Palma, Canary Islands; BG-49 is an Oligocene alkaline basalt from the Bulgarian Rhodopes (Kirchenbaur et al., 2012). Values for the basalts from the Dzheltul'skii massif (Eastern-Siberia, Russia) and Disco Island (Greenland) are from Schulz et al. (2013).

4.4 DISCUSSION

4.4.1 Non-radiogenic effects on $\epsilon^{180}\text{W}$

The measured $\epsilon^{180}\text{W}$ is potentially affected by non-terrestrial compositions of the isotopes that are used for normalisation and instrumental mass bias correction, as well as by secondary neutron capture effects due to exposure to cosmic rays. Although these effects are unlikely to account for the magnitude of the observed ^{180}W heterogeneities (Schulz et al. 2013; Cook et al., 2013), they may affect the calculated half life for ^{184}Os -decay and are therefore further evaluated below.

Most meteorite groups have terrestrial non-radiogenic W compositions (e.g., Qin et al., 2008). The measured $\epsilon^{180}\text{W}$ of meteorites from these groups is therefore unaffected by the normalisation and corrections for instrumental mass bias. However, meteorites from the IVB group, as well as the anomalous IVB iron Chinga, were previously reported to display minor s-process deficits (Qin et al., 2008; Kruijer et al., 2012; Wittig et al., 2013). The effects of these anomalies on the normalised ^{180}W can be estimated from theoretical models for stellar nucleosynthesis. Qin et al. (2008) reported a deficit in $\epsilon^{184}\text{W}$ of -0.08 ± 0.01 for the IVB group, which is based on multiple replicate measurements and is therefore more precise than our ^{184}W data that do not show resolvable anomalies for individual samples. Using this value and the nucleosynthetic model by Arlandini et al. (1999), a downward correction of 0.23 ± 0.03 $\epsilon^{180}\text{W}$ units is required to Weaver Mountains and Cape of Good Hope. Chinga may exhibit a larger s-process deficit, which, however, overlaps in uncertainty with that of the IVB group. Using $\epsilon^{184}\text{W}$ of -0.12 ± 0.06 from our dataset for Chinga, a downward correction of 0.35 ± 0.17 may be applied to $\epsilon^{180}\text{W}$ (Table 4.4).

Table 4.4 Corrections for nucleosynthetic and cosmogenic effects

	Type	$\epsilon^{180}\text{W}$ (s-def. corr.) ^a	$\epsilon^{182}\text{W}$ (s-def. corr.) ^a	$\Delta\epsilon^{182}\text{W}_{\text{CRE}}$ ^b	$\epsilon^{180}\text{W}$ corr. ^c
Bendego	IC	-0.64 ± 1.05	-3.84 ± 0.10	-0.59 ± 0.25	$+0.17 \pm 1.30$
Weaver Mountains	IVB	$+1.04 \pm 0.71$	-3.36 ± 0.09	-0.10 ± 0.15	$+1.18 \pm 0.89$
Cape of Good Hope	IVB	$+3.18 \pm 1.17$	-3.51 ± 0.10	-0.25 ± 0.16	$+3.53 \pm 1.33$
Chinga	IVB-An	$+3.39 \pm 1.22$	-3.22 ± 0.09		$+3.39 \pm 1.22$

^aBased on $\epsilon^{184}\text{W}$ of -0.08 ± 0.01 (Weaver Mountains, Cape of Good Hope (Qin et al., 2008) and -0.12 ± 0.06 (Chinga, this study), and the model for nucleosynthesis by Arlandini et al. (1999). Bendego has a terrestrial non-radiogenic W isotope composition.

^b $\Delta\epsilon^{182}\text{W}_{\text{CRE}} = \epsilon^{182}\text{W}_{\text{meas}} - \epsilon^{182}\text{W}_{\text{pre-exp}}$. Pre-exposure values for $\epsilon^{182}\text{W}$ are taken from Kruijer et al. (2013).

^cCorrected for neutron capture effects and nucleosynthetic effects using the s-deficit corrected value for $\epsilon^{180}\text{W}$ and $\Delta\epsilon^{182}\text{W}_{\text{CRE}}$.

Secondary neutron capture (cosmogenic) effects may have the potential to decrease $\epsilon^{180}\text{W}$ in iron meteorites: Directly by burn-out of ^{180}W , and indirectly by burnout of ^{186}W , where deficits are propagated through the instrumental mass bias correction to $^{186}\text{W}/^{184}\text{W}$. Neutron capture effects are well reported for ^{182}W (e.g., Markowski et al., 2006; Masarik, 1997), which has a similar neutron capture cross section to ^{180}W (Kang et al., 2007). Neutron capture effects on ^{182}W are known to roughly scale with the cosmic ray exposure ages calculated from cosmogenic noble gases, although no simple relation exists. References for the exposure ages for most of our samples are given in Schulz et al. (2013) and are ≤ 100 Myrs for most meteorites. A cosmic ray exposure age of ~ 45 Myr for Negrillos was derived by Leya et al. (2000). At this level cosmogenic effects on $\epsilon^{182}\text{W}$ are generally less than 10 ppm (e.g., Kruijer et al., 2012) and are therefore most likely similarly low for $\epsilon^{180}\text{W}$. Reported cosmic ray exposure ages are larger for three meteorites investigated here, namely 390 ± 50 , 775 ± 70 and 940 ± 90 Myrs for Weaver Mountains, Cape of Good Hope, and Bendego, respectively. At such levels cosmogenic effects on $\epsilon^{182}\text{W}$ could be significant, thus $\epsilon^{180}\text{W}$ may also be affected. The magnitude of cosmogenic effects on $\epsilon^{182}\text{W}$ can be approximated by the difference between the measured $\epsilon^{182}\text{W}$ and the pre-exposure value for the meteorite group that is based on the empirical model for neutron capture effects on W and Pt isotopes by Kruijer et al. (2013), and, for the IVB group, W-Pt-Os isotopes by Wittig et al. (2013). Whereas the consumption by neutron capture reactions of ^{180}W is expected to be similar to ^{182}W , the expected consumption of ^{186}W is a factor ~ 5 lower (Mughabghab, 2003). In order to estimate the effects on $\epsilon^{180}\text{W}$ caused by mass bias normalisation, the latter relation provides an upper limit only, because $\epsilon^{182}\text{W}$ itself is measured relative to $^{186}\text{W}/^{184}\text{W}$. Without detailed

modeling of the neutron capture probabilities it can therefore be calculated that $\epsilon^{180}\text{W}$ is affected by a factor of less than ~ 1.6 times than $\epsilon^{182}\text{W}$. This is in agreement with an estimated factor ~ 1.5 times by Cook et al. (2013).

Unfortunately, no pre-exposure $\epsilon^{182}\text{W}$ has been reported for the IC group, hindering the use of cosmogenic ^{182}W for estimating neutron capture effects on ^{180}W for Bendego. When assuming that the IC irons had a pre-exposure $\epsilon^{182}\text{W}$ value in between those for the IVA and IID groups, which have the lowest and highest reported pre-exposure $\epsilon^{182}\text{W}$, respectively, an upward correction for $\epsilon^{180}\text{W}$ of minimum 0.73 ± 0.07 and maximum 0.87 ± 0.10 ϵ -units would be required. For Weaver Mountains and Cape of Good Hope, meteorites that belong to the IVB group, a downward correction of $\epsilon^{182}\text{W}$ is first applied to correct for an s-process deficit. The maximum corrections for cosmogenic effects on ^{180}W that follow from the pre-exposure value for $\epsilon^{182}\text{W}$ from Kruijer et al. (2013) are -0.14 ± 0.15 and -0.35 ± 0.16 ϵ -units, respectively. Note that the pre-exposure value published by Wittig et al. (2013) overlaps within uncertainty with our s-process deficit corrected values for $\epsilon^{182}\text{W}$, implying that neutron capture effects for Weaver Mountains and Cape of Good Hope may in fact be negligible. For chondrites, neutron capture effects on $\epsilon^{180}\text{W}$ are expected to be negligible for two reasons: (1) Burn-out of W isotopes requires epithermal and higher energies, and therefore predominantly occurs in iron rich target materials such as iron meteorites (e.g., Eberhardt, 1963; Spergel et al. 1986; Kollár et al. 2006); and (2) cosmic ray exposure ages of chondrites are well below the levels at which effects in $\epsilon^{182}\text{W}$ are seen in iron meteorites, i.e., < 50 Myrs (e.g., Leya and Masarik, 2009 and references therein).

When the corrected $\epsilon^{180}\text{W}$ values for Bendego, Weaver Mountains, Cape of Good Hope, and Chinga (summarised in Table 4) are used to recalculate the slope of the combined ^{184}Os - ^{180}W isochron for iron meteorites and chondrites, a slightly shallower slope is obtained ($m = 0.000271 \pm 0.000068$, MSWD = 1.7) than for the uncorrected data (0.000296 ± 0.000061). This slope corresponds to a decay constant $\lambda^{184}\text{Os}(\alpha) = 5.94 \pm 1.47 \times 10^{-14} \text{ a}^{-1}$ that is identical within uncertainty to the slope based on the uncorrected data. We prefer, however, the value for the slope based on the uncorrected data, because the applied corrections increase the uncertainty for individual data due to error propagation. Moreover, these corrections are within the limits of analytical uncertainty and are strongly model-dependent.

4.4.2 Uniform distribution of ^{180}W in the solar nebula at 4.565 Ga

Samples from the same iron meteorite class (i.e. the IIAB and IVB groups) appear to have different $\varepsilon^{180}\text{W}$ anomalies. In this study, we also obtain different isotope abundances of ^{180}W for Cape York and Holland's Store that were previously analysed by Schulz et al., 2013. The observation that ^{180}W appears variable within iron meteorite classes and possibly at the hand specimen scale further weakens the evidence for an origin of the anomalies by nucleosynthetic heterogeneity of ^{180}W in the solar nebula. In situ production by α -decay of ^{184}Os , however, may better explain this variability, because Os concentrations in iron meteorite groups are known to be heterogeneous due to solid metal-liquid metal partitioning, more so than for W (Scott, 1978; Pernicka and Wasson, 1987). Fig. 4.4 shows the measured abundances of ^{180}W in iron meteorites and chondrites corrected for radiogenic ingrowth, i.e., the abundances at the time of parent body formation. These are identical for all samples within analytical uncertainty. It may therefore be concluded that the distribution of non-radiogenic (i.e., p-process-related) ^{180}W between the different meteorite parent bodies is uniform at a level of ~ 1 parts per ten 10^6 and that secondary neutron capture effects appear to be negligible for all measured samples.

4.4.3 Chronological significance of ^{184}Os - ^{180}W systematics in iron meteorites

During core formation on the iron meteorite parent bodies, significant fractionation between Os and W may have occurred during metal-silicate separation (e.g., Righter, 2003 and references therein) as well as during subsequent separation of solid metal from liquid metal during core crystallization (e.g., Chabot et al., 2003 and references therein). Whereas metal-silicate separation can be dated by the short-lived lithophile-siderophile ^{182}Hf - ^{182}W system, core crystallization is well recorded by the ^{187}Re - ^{187}Os system. Indeed, ^{187}Re - ^{187}Os systematics of iron meteorites appear to indicate ages that are slightly younger (< 50 Myrs) than those recorded by the short-lived ^{182}Hf - ^{182}W system (Horan et al., 1998). Most likely, the ^{184}Os - ^{180}W system has recorded a mixture of metal-silicate separation and solid metal-liquid metal separation events. As these processes occurred within 50 Myrs of each other, however, no significant effects on the calculated half life for ^{184}Os -decay are expected.

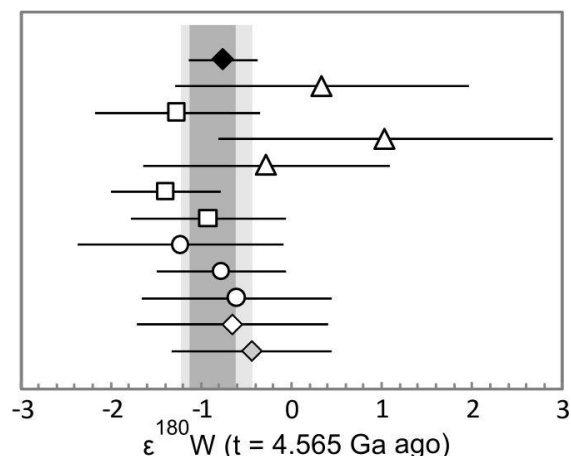


Fig. 4.4 Calculated $\epsilon^{180}\text{W}$ compositions of the iron meteorite and chondrite parent bodies 4.565 Ga ago. $\epsilon^{180}\text{W}$ values are calculated from our preferred value for $\lambda^{184}\text{Os}(\alpha)$, and are relative to the present day average composition of AMES metal. Grey boxes indicate 95% confidence limits of the weighted means for irons and chondrites (light) and for all samples except for the IVA irons (dark). Note that the latter have apparently somewhat higher ^{180}W but plot within error of the weighted mean for the other groups. Key as in Fig. 4.2.

Notably, the IVA iron meteorites La Grange and Gibeon have slightly high $\epsilon^{180}\text{W}$ with respect to the other irons, albeit within uncertainty of the isochron. This may possibly reflect later disturbance of the ^{184}Os - ^{180}W system due to catastrophic disruption of the IVA parent body, as has been suggested to explain the apparently disturbed ^{187}Re - ^{187}Os systematics (e.g., Smoliar et al., 1996) as well as the variable metallographic cooling rates obtained for different IVA irons (Rasmussen, 1995; Haack et al., 1996). If La Grange and Gibeon are excluded from the isochron, a slightly shallower slope ($m = 0.000288 \pm 0.000061$; MSWD = 0.8) is obtained. This slope corresponds to a decay constant $\lambda^{184}\text{Os}(\alpha) = 6.30 \pm 1.35 \times 10^{-14} \text{ a}^{-1}$ that is identical within uncertainty to the calculated value in which the IVA irons are included.

4.4.4 ^{180}W deficit in terrestrial silicates relative to chondrites

During core formation on larger planetary bodies Os behaves as a highly siderophile element, whereas W is only moderately siderophile (e.g., Righter, 2003). Core formation is therefore believed to have resulted in the strong depletion of Os relative to W in the terrestrial primitive mantle ($\text{Os}/\text{W} = 0.3$; Becker et al., 2006; König et al., 2011) compared to chondrite ($\text{Os}/\text{W} = 3.4$, this study). Indeed, the measured deficit of $1.16 \pm 0.69 \epsilon^{180}\text{W}$ -units in terrestrial basalts relative to chondrites therefore confirms a long-term subchondritic Os/W evolution of the Earth's mantle. Importantly, Os and W may additionally be fractionated by partial melting

of silicate reservoirs of the Earth, because during silicate melting, Os behaves compatibly whereas W is one of the most incompatible elements. Fig. 4.5 shows the predicted ^{180}W evolution of the Earth's depleted mantle after core formation and partial melting in comparison to the primitive mantle. The age of the primitive mantle by definition equals that of core formation, whereas radiogenic ^{180}W for average W-depleted mantle ($\text{Os}/\text{W} = 1.1\text{-}1.4$; Salters and Stracke, 2004; König et al., 2011) is modeled here by instantaneous mantle depletion at 3 Ga, when ~65% of the continental crust are thought to have been formed over a relatively narrow age interval (Dhuime et al., 2012). The weighted mean of our terrestrial samples, as well as each terrestrial sample individually, overlaps with the calculated modern value for the depleted mantle reservoir within the limits of uncertainty. With respect to the calculated modern value for the primitive mantle reservoir, the weighted mean of terrestrial samples shows a minor excess in ^{180}W of 0.39 ± 0.34 parts per 10,000, whereas each individual terrestrial sample overlaps with the calculated value within the limits of uncertainty. Our data are therefore consistent with a scenario of rapid terrestrial core formation from a chondritic precursor ~4.5 Ga ago.

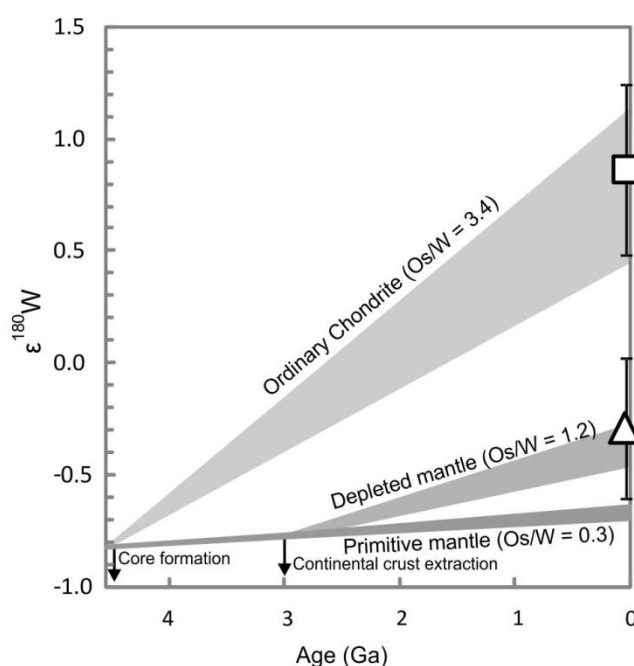


Fig. 4.5 Calculated $\epsilon^{180}\text{W}$ evolution for ordinary chondrites and the Earth's primitive and depleted mantle. Os/W ratios are based on Salters and Stracke (2004) (Os) and König et al. (2011) (W) for the depleted mantle; Becker et al. (2006) (Os) and König et al. (2011) (W) for the primitive mantle; and this work for chondrites. Fields reflect uncertainty on the decay

constant for ^{184}Os and do not include the uncertainty on the initial $\epsilon^{180}\text{W}$. It is assumed that the primitive mantle formed from a chondritic proto-Earth, followed by instantaneous extraction of silicate melt to produce the depleted mantle 3 Ga ago (Dhuime et al., 2012). Square and triangle represent the weighted means for measurements of ordinary chondrites and terrestrial samples, respectively.

4.5 OUTLOOK

4.5.1 Viability of the ^{184}Os - ^{180}W decay system as a geochronometer

The newly discovered ^{184}Os - ^{180}W decay system may be a viable chronometer to record geological processes that fractionate Os from W. At the analytical precision that has been achieved here for $\epsilon^{180}\text{W}$, the time resolution of the geochronometer is still limited. However, the analytical development that is needed to significantly improve this situation is feasible given the advances made in MC-ICPMS throughout the past two decades. Notably, the use of Faraday amplifiers equipped with $10^{13} \Omega$ resistors can improve counting statistics and, most importantly, the signal-to-noise ratios on masses 180 and 178 by a factor 2-3 relative to the $10^{12} \Omega$ resistors employed in the present study. Such amplifiers are currently not commercially available, but have already been tested successfully in TIMS for samples with low concentrations of target elements (Koornneef et al., 2013). Furthermore, it was recently shown that the isotopic composition of W can be measured precisely as WO^{3-} by negative TIMS, with external reproducibilities for $^{182}\text{W}/^{184}\text{W}$ ratios of ~ 4.5 ppm (Touboul and Walker, 2012).

We note that the ^{184}Os - ^{180}W decay system may ultimately provide a tool to study processes active during late accretion. Accretion of a chondritic late veneer that did not equilibrate with the core could have modified the $\epsilon^{180}\text{W}$ inventory of the silicate Earth, directly by contributing radiogenic ^{180}W to the mantle, and indirectly by adding radioactive ^{184}Os (i.e., by increasing Os/W to the present value) (e.g., Chou, 1978; Meisel et al., 1996; Willbold et al., 2011). The magnitude of the combined effect depends on the mass and composition of the late veneer and the time at which the late accreting materials were mixed into the mantle, which are all subject to debate. For example, if late accretion delivered more than $\sim 0.5\%$ of Earth's mass, the $\epsilon^{180}\text{W}$ inventory of the silicate Earth would be dominated by radiogenic ^{180}W that was produced by ^{184}Os -decay on the late accreting bodies. In this case,

the predicted $\epsilon^{180}\text{W}$ in the modern mantle increases in case these materials were efficiently mixed into the mantle at less than < 4.5 Ga. Note that efficient mixing of late accretion material into the mantle may have occurred as late as > 3.8 Ga (Willbold et al., 2011). At such timescales, effects may be significant for a late veneer that was dominated by H chondrite-like material, whereas influx of CI chondrite-like material would have increased $\epsilon^{180}\text{W}$ of the mantle by less than 0.02 units (= 2 ppm) only (Fig. 4.6). Before late accretion, Os/W of the silicate mantle was most likely close to zero because of the high metal-silicate partition coefficients of Os relative to W during core formation. If late accretion delivered less than $\sim 0.5\%$ of Earth's mass, $\epsilon^{180}\text{W}$ in the modern silicate Earth would therefore predominantly reflect the time by which Os/W of the mantle was set to the present value, i.e. the time since terrestrial radiogenic ^{180}W was produced. In contrast to the scenario in which late accretion accounted for a larger fraction of Earth's mass, the latter scenario therefore predicts lower $\epsilon^{180}\text{W}$ in the modern silicate Earth if late accreted material became efficiently mixed into the mantle only at 3.8 Ga rather than at 4.5 Ga.

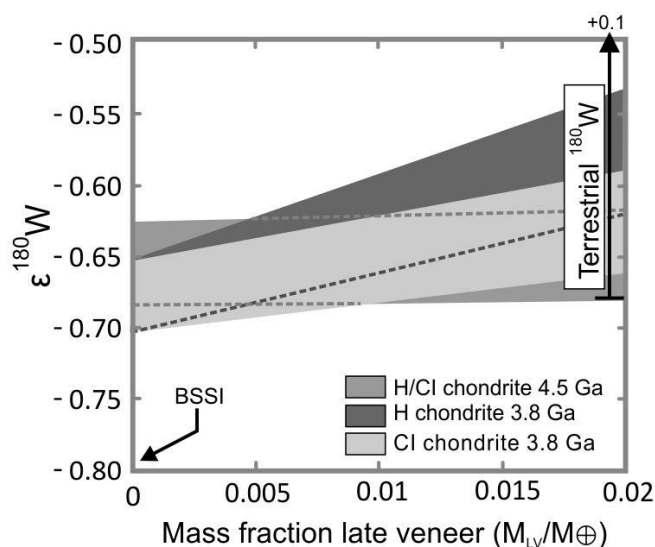


Fig. 4.6. ^{180}W composition of the silicate Earth calculated as a function of mass fraction of the late veneer, shown at fixed times and for given compositions of late accreting materials. Late accretion is modeled as an instantaneous event by which (1) radiogenic ^{180}W is delivered that evolved in a reservoir with chondritic Os/W; (2) the Os/W ratio of the primitive mantle is raised from zero to the present value of 0.3, setting off the ^{184}Os - ^{180}W clock. The Os/W ratio of the mantle before late accretion is assumed to be ~ 0 because of the high metal-silicate partition coefficients of Os relative to W during core formation. Mixing models are based on 12 ppb W in the BSE with ^{180}W identical to the solar system initial; and late accreting

materials with 110 ppb W and 210 ppb W similar to CI (Orgueil; Barrat et al., 2012) and ordinary H chondrites (mean value for this work and the whole-rock data reported in Kleine et al, 2008) respectively, and Os/W of 3.4 (this study). Instantaneous mixing of the late veneer into the mantle is assumed by 3.8 (Willbold et al., 2011) and 4.5 Ga ago. Note that if late accretion accounted for $> 0.5\%$ of Earth's mass, the $\epsilon^{180}\text{W}$ inventory of the silicate Earth is dominated by the delivery of radiogenic ^{180}W by late veneer, whereas at lower mass fractions, the origin of radiogenic ^{180}W in the silicate Earth is predicted to be predominantly terrestrial.

4.6 CONCLUSIONS

We have for the first time shown that ^{184}Os is a radioactive nuclide that α -decays to ^{180}W . This discovery solves the previously debated origin of ^{180}W heterogeneities in early solar system materials, and confirms predictions from nuclear theory. Due to their different Os/W compositions, there is a resolvable offset between $\epsilon^{180}\text{W}$ in chondrites and terrestrial basalts. Hence, the newly discovered ^{184}Os - ^{180}W decay system constitutes a potentially viable tracer and chronometer for geological processes like core formation, silicate differentiation or late accretion processes. Given latest developments in mass spectrometry, the resolving power of the ^{184}Os - ^{180}W system may be dramatically improved in the near future, and its application in earth sciences may become more widespread.

V. References

- Akram, W., Schönbacher, M., Sprung, P. and Vogel, N., 2013. Zirconium-Hafnium Isotope Evidence from Meteorites for the Decoupled Synthesis of Light and Heavy Neutron-rich Nuclei. *The Astrophysical Journal*, 777(2): 169.
- Albarede, F., et al., 2004. Precise and accurate isotopic measurements using multiple-collector ICPMS. *Geochimica et Cosmochimica Acta* 68.12: 2725-2744.
- Albarède, F. et al., 2006. γ -ray irradiation in the early Solar System and the conundrum of the ^{176}Lu decay constant. *Geochimica et cosmochimica acta*, 70(5): 1261-1270.
- Albarède, F. and Beard, B., 2004. Analytical methods for non-traditional isotopes. *Reviews in mineralogy and geochemistry*, 55(1): 113-152.
- Allègre, C.J., 2008. Isotope geology. Cambridge University Press Cambridge.
- Amari, S. et al., 2001. Presolar grains from novae. *The Astrophysical Journal*, 551(2): 1065.
- Amelin, Y., Lee, D.C. and Halliday, A.N., 2000. Early-middle Archaean crustal evolution deduced from Lu-Hf and U-Pb isotopic studies of single zircon grains. *Geochimica et Cosmochimica Acta*, 64(24): 4205-4225.
- Amelin, Y. et al., 2000. Lead isotopic ages of chondrules and calcium-aluminum-rich inclusions. *Science*, 297, 1678-1683.
- Andreasen, R., and Sharma, M., 2007. Mixing and homogenization in the early solar system: clues from Sr, Ba, Nd, and Sm isotopes in meteorites. *The Astrophysical Journal*, 665(1), 874.
- Arlandini, C. et al., 1999. Neutron capture in low-mass asymptotic giant branch stars: cross sections and abundance signatures. *The Astrophysical Journal* 525, 886-900
- Arnould, M., 1976. Possibility of synthesis of proton-rich nuclei in highly evolved stars. II. *Astronomy and Astrophysics*, 46: 117-125.
- Arnould, M. and Goriely, S.p., 2003. The p-process of stellar nucleosynthesis: astrophysics and nuclear physics status. *Physics Reports*, 384(1): 1-84.
- Ávila, J.N. et al., 2012. Tungsten isotopic compositions in stardust SiC grains from the Murchison meteorite: Constraints on the s-process in the Hf-Ta-W-Re-Os region. *The Astrophysical Journal*, 744(1): 49.
- Barrat, J.-A. et al., 2012. Geochemistry of CI chondrites: Major and trace elements, and Cu and Zn isotopes. *Geochimica et Cosmochimica Acta* 83, 79-92.
- Bast, R., et al., 2012. Internal Lu-Hf Isotope Systematics of the Euclites Millbillillie and Piplia Kalan. In *Lunar and Planetary Institute Science Conference Abstracts*, 43: 2542.
- Bast, R., Scherer, E.E., Mezger, K., Fischer-Gödde, M. and Sprung, P., 2013. Internal Lu-Hf Isotope Systematics of the Quenched Angrite D'Orbigny and Two Plutonic Angrites. *Mineralogical Magazine*, 77(5) 665.
- Becker, M., 2013. Kombinierte ^{182}Hf - ^{182}W und ^{176}Lu - ^{176}Hf Untersuchungen an CV-Chondriten und ihren Komponenten. MSc thesis, Universität zu Köln, 85 p.
- Becker, H. et al., 2006. Highly siderophile element composition of the Earth's primitive upper mantle: Constraints from new data on peridotite massifs and xenoliths. *Geochimica et Cosmochimica Acta* 70, 4528-4550.
- Beer, H., and Ward, R. A. (1981). Neutron-capture nucleosynthesis of nature's rarest stable isotope.
- Belli, P. et al., 2013. First search for double- β decay of ^{184}Os and ^{192}Os . *The European Physical Journal A* 49, 1-6.

- Berglund, M. and Wieser, M.E., 2011. Isotopic compositions of the elements 2009 (IUPAC Technical Report). *Pure and Applied Chemistry*, 83(2): 397-410.
- Bizzarro, M., Baker, J.A., Haack, H., Ulfbeck, D. and Rosing, M., 2003. Early history of Earth's crust-mantle system inferred from hafnium isotopes in chondrites. *Nature*, 421(6926): 931-933.
- Bizzarro, M., et al., 2007. Evidence for a late supernova injection of ^{60}Fe into the protoplanetary disk. *Science*, 316(5828), 1178-1181.
- Bizzarro, M., Connelly, J.N., Thrane, K. and Borg, L.E., 2012. Excess hafnium-176 in meteorites and the early Earth zircon record. *Geochemistry, Geophysics, Geosystems*, 13(3).
- Bizzarro, M. and Connelly, J., 2013. *Mineralogical Magazine*, 77(5): 711
- Blichert-Toft, J. and Albarède, F., 1997a. The Lu-Hf isotope geochemistry of chondrites and the evolution of the mantle-crust system. *Earth and Planetary Science Letters*, 148(1): 243-258.
- Blichert-Toft, J., Chauvel, C., and Albarède, F., 1997b. Separation of Hf and Lu for high-precision isotope analysis of rock samples by magnetic sector-multiple collector ICP-MS. *Contributions to Mineralogy and Petrology*, 127(3), 248-260.
- Braun, T., 1975. Extraction chromatography, 2. Elsevier.
- Bouvier, A., Vervoort, J.D. and Patchett, P.J., 2008. The Lu-Hf and Sm-Nd isotopic composition of CHUR: constraints from unequilibrated chondrites and implications for the bulk composition of terrestrial planets. *Earth and Planetary Science Letters*, 273(1): 48-57.
- Bouvier, A., and Boyet, M., 2013. *Mineralogical Magazine*, 77(5): 754
- Brennecka, G.A., Borg, L.E. and Wadhwa, M., 2013. Evidence for supernova injection into the solar nebula and the decoupling of r-process nucleosynthesis. *Proceedings of the National Academy of Sciences*, 110(43): 17241-17246.
- Burbidge, E.M., Burbidge, G.R., Fowler, W.A. and Hoyle, F., 1957. Synthesis of the elements in stars. *Reviews of Modern Physics*, 29: 547-650.
- Burkhardt, C. et al., 2011. Molybdenum isotope anomalies in meteorites: Constraints on solar nebula evolution and origin of the Earth. *Earth and Planetary Science Letters*, 312(3): 390-400.
- Butterworth, J. C., Livens, F. R., and Makinson, P. R., 1995. Development of a method for the determination of low levels of technetium-99. *Science of the total environment*, 173, 293-300.
- Cameron, A. and Truran, J., 1977. The supernova trigger for formation of the solar system. *Icarus*, 30(3): 447-461.
- Caro, G., Bourdon, B., Birck, J. L., and Moorbath, S., 2006. High-precision $^{142}\text{Nd}/^{144}\text{Nd}$ measurements in terrestrial rocks: Constraints on the early differentiation of the Earth's mantle. *Geochimica et Cosmochimica Acta*, 70(1), 164-191.
- Chabot, N. L., Campbell, A. J., Jones, J. H., Humayun, M. and Agee, C. B., 2013. An experimental test of Henry's Law in solid metal-liquid metal systems with implications for iron meteorites. *Meteoritics & Planetary Science* 38, 181-196.
- Chen, J.H., Papanastassiou, D.A. and Wasserburg, G.J., 2010. Ruthenium endemic isotope effects in chondrites and differentiated meteorites. *Geochimica et Cosmochimica Acta*, 74(13): 3851-3862.
- Chou, C. L., 1978. *Lunar and Planetary Science Conference Proceedings* 219-230.
- Chu, N.-C. et al., 2002. Hf isotope ratio analysis using multi-collector inductively coupled plasma mass spectrometry: an evaluation of isobaric interference corrections. *Journal of Analytical Atomic Spectrometry*, 17(12): 1567-1574.
- Clayton, D.D., 1968. Principles of stellar evolution and nucleosynthesis. University of Chicago press.

- Cook, D. L., Kruijer, T. S. and Kleine, T., 2013. ^{180}W Anomalies in Iron Meteorites: Implications for p-Process Heterogeneity. *LPI Contributions* 1719, 1097.
- Creech, J., Baker, J., Handler, M., Schiller, M. and Bizzarro, M., 2013. Platinum stable isotope ratio measurements by double-spike multiple collector ICPMS. *Journal of Analytical Atomic Spectrometry*, 28(6): 853-865.
- Creech, J.B., Baker, J.A., Handler, M.R. and Bizzarro, M., 2014. Platinum stable isotope analysis of geological standard reference materials by double-spike MC-ICPMS. *Chemical Geology*, 363: 293-300.
- Dauphas, N., Davis, A.M., Marty, B. and Reisberg, L., 2004. The cosmic molybdenum-ruthenium isotope correlation. *Earth and Planetary Science Letters*, 226(3): 465-475.
- Dauphas, N., 2005. Multiple sources or late injection of short-lived r-nuclides in the early solar system? *Nuclear Physics A*, 758: 757-760.
- Dhuime, B., Hawkesworth, C. J., Cawood, P. A. and Storey, C. D., 2012. A change in the geodynamics of continental growth 3 billion years ago. *Science* 335, 1334-1336.
- Dickin, A.P., 2005. Radiogenic isotope geology. Cambridge University Press.
- Dimple, D. and de Boer, B., 2010. Extraction chromatography procedures for separating Tc from contaminated nuts and blueberries, *Journal of hungry rodents* 1, 62-63.
- Eberhardt, P. Neutrons in meteorites., 1963. *Earth Science and Meteoritics*. J. Geiss, ED Goldberg, 143-168.
- Elfers B-M., Peters, S.T.M., Wombacher, F., and Muenker, C., 2013. *Mineralogical Magazine*, 77(5) 1034
- Faris, J.P., 1960. Adsorption of Elements from Hydrofluoric Acid by Anion Exchange. *Analytical Chemistry*, 32(4): 520-522.
- Faure, G., 1977. Principles of isotope geology.
- Fisher, D. E., and Schaeffer, O. A., 1960. Cosmogenic nuclear reactions in iron meteorites. *Geochimica et Cosmochimica Acta*, 20(1), 5-14.
- Fischer-Gödde, M., Becker, H. and Wombacher, F., 2010. Rhodium, gold and other highly siderophile element abundances in chondritic meteorites. *Geochimica et Cosmochimica Acta* 74, 356-379.
- Fröhlich, C. et al., 2006. Neutrino-Induced Nucleosynthesis of $A > 64$ Nuclei: The vp Process. *Physical Review Letters*, 96(14): 142502.
- Gangopadhyay, G., 2009. Simple parametrization of an α -decay spectroscopic factor in the $150 \leq A \leq 200$ region. *Journal of Physics G: Nuclear Particle Physics* 36, 095105.
- Goriely, S., Jose, J., Hernanz, M., Rayet, M. and Arnould, M., 2002. He-detonation in sub-Chandrasekhar CO white dwarfs: A new insight into energetics and p-process nucleosynthesis. *arXiv preprint astro-ph/0201199*.
- Goriely, S.p., Garcia Senz, D., Bravo Guil, E. and José Pont, J., 2005. P-process nucleosynthesis in detonating white dwarfs in the light of multidimensional hydrodynamical models., *Astronomy and Astrophysics*, 444: L1-L4.
- Gounelle, M. and Meibom, A., 2008. The origin of short-lived radionuclides and the astrophysical environment of solar system formation. *The Astrophysical Journal*, 680(1): 781.
- Guan, Y., Huss, G.R. and Leshin, L.A., 2007. ^{60}Fe - ^{60}Ni and ^{53}Mn - ^{53}Cr isotopic systems in sulfides from unequilibrated enstatite chondrites. *Geochimica et cosmochimica acta*, 71(16): 4082-4091.
- Haack, H., Scott, E. R. D., Love, S. G., Brearley, A. J. and McCoy, T. J., 1996. Thermal histories of IVA stony-iron and iron meteorites: Evidence for asteroid fragmentation and reaccretion. *Geochimica et Cosmochimica Acta* 60, 3103-3113.

- Hansen, C.J., Kawaler, S.D. and Trimble, V., 2004. Stellar interiors: physical principles, structure, and evolution. Springer.
- Hayakawa, T. et al., 2008. Empirical abundance scaling laws and implications for the gamma process in core-collapse supernovae. *The Astrophysical Journal*, 685(2): 1089.
- Holst, J. C., Paton, C., Bizzarro, M., 2011. Are non-radiogenic W isotope anomalies in iron meteorites analytical artifacts? *LPI Contributions* 1639, 9065.
- Horan, M. F., Smoliar, M. I. and Walker, R. J., 1998. ^{182}W and ^{187}Re - ^{187}Os systematics of iron meteorites: Chronology for melting, differentiation, and crystallization in asteroids. *Geochimica et Cosmochimica Acta* 62, 545-554.
- Hoppe, P. and Zinner, E., 2000. Presolar dust grains from meteorites and their stellar sources. *Journal of Geophysical Research: Space Physics (1978-2012)*, 105(A5): 10371-10385.
- Horwitz, E. P. et al., 1995. Separation and preconcentration of actinides by extraction chromatography using a supported liquid anion exchanger: application to the characterization of high-level nuclear waste solutions. *Analytica Chimica Acta*, 310(1), 63-78.
- Howard, W.M., Meyer, B.S. and Woosley, S.E., 1991. A new site for the astrophysical gamma-process. *The Astrophysical Journal*, 373: L5-L8.
- Hoyle, F., 1946. The synthesis of the elements from hydrogen. *Monthly Notices of the Royal Astronomical Society*, 106: 343.
- Hoyle, F., 1954. On Nuclear Reactions Occuring in Very Hot STARS. I. the Synthesis of Elements from Carbon to Nickel. *The Astrophysical Journal Supplement Series*, 1: 121.
- Jacobsen, S.B., 2005. The birth of the solar system in a molecular cloud: evidence from the isotopic pattern of short-lived nuclides in the early solar system. *Chondrites and the Protoplanetary Disk*, pp. 548.
- Kang, W. G. et al., 2007. Measurement of the thermal neutron capture cross section of ^{180}W . *Physical Review C* 76, 067602.
- Käppeler, F., et al. 2004. Stellar neutron capture on Ta m 180. II. Defining the s-process contribution to nature's rarest isotope. *Physical Review C* 69.5: 055802.
- Kawashima, A., Takahashi, K. and Masuda, A., 1993. Positive thermal ionization mass spectrometry of molybdenum. *International journal of mass spectrometry and ion processes*, 128(1): 115-121.
- Kirchenbaur, M., et al., 2012. Timing of high-pressure metamorphic events in the Bulgarian Rhodopes from Lu-Hf garnet geochronology. *Contributions to Mineralogy and Petrology*, 163.5 897-921.
- Kim, J.I., Lagally, H. and Born, H.J., 1973. Ion exchange in aqueous and in aqueous-organic solvents: Part I. Anion-exchange behaviour of Zr, Nb, Ta and Pa in aqueous HCl-HF and in HCl-HF-organic solvent. *Analytica Chimica Acta*, 64(1): 29-43.
- Kleine, T., Mezger, K., Münker, C., Palme, H. and Bischoff, A., 2004. ^{182}Hf - ^{182}W isotope systematics of chondrites, eucrites, and martian meteorites: Chronology of core formation and early mantle differentiation in Vesta and Mars. *Geochimica et Cosmochimica Acta* 68, 2935-2946.
- Kleine, T., Mezger, K., Palme, H., Scherer, E. and Münker, C., 2005. Early core formation in asteroids and late accretion of chondrite parent bodies: Evidence from ^{182}Hf - ^{182}W in CAIs, metal-rich chondrites, and iron meteorites. *Geochimica et Cosmochimica Acta* 69, 5805-5818.
- Kleine, T. et al., 2008. Hf-W thermochronometry: closure temperature and constraints on the accretion and cooling history of the H chondrite parent body. *Earth and Planetary Science Letters* 270, 106-118.

- Kolesnikov, A. and Svarovsky, 2001. *Science and Technology, KORUS'01. Proceedings of the fifth Russian-Korean International Symposium 1*, 297-298.
- Kollar, D., Michel, R. and Masarik, J., 2006. Monte Carlo simulation of GCR neutron capture production of cosmogenic nuclides in stony meteorites and lunar surface. *Meteoritics and Planetary Science*, 41, 375-389.
- König, S. et al., 2011. The Earth's tungsten budget during mantle melting and crust formation. *Geochimica et Cosmochimica Acta*, 75, 2119-2136.
- Koornneef, J.M., Bouman, C., Schwieters, J.B. and Davies, G.R., 2013a. Use of 10^{12} ohm current amplifiers in Sr and Nd isotope analyses by TIMS for application to sub-nanogram samples. *Journal of analytical atomic mass spectrometry*, 28(5): 749-754.
- Koornneef, J., Bouman, C., Schwieters, J. and Davies, G., 2013b Use of 10^{12} and 10^{13} Ohm Resistors in TIMS Analysis of Sr and Nd Isotopes in Sub-Nanogram Geological and Environmental Samples. *Mineralogical Magazine*. 77(5), 1495.
- Kruijer, T. S. et al., 2012. Hf-W chronometry of core formation in planetesimals inferred from weakly irradiated iron meteorites. *Geochimica et Cosmochimica Acta* 99, 287-304.
- Kruijer, T. S. et al., 2013. Neutron capture on Pt isotopes in iron meteorites and the Hf-W chronology of core formation in planetesimals. *Earth and Planetary Science Letters*. 162, 162-172.
- Lee, D.-C. and Halliday, A.N., 1995. Precise determinations of the isotopic compositions and atomic weights of molybdenum, tellurium, tin and tungsten using ICP magnetic sector multiple collector mass spectrometry. *International journal of mass spectrometry and ion processes*, 146: 35-46.
- Leya, I., 1997. Modellrechnungen zur Beschreibung der Wechselwirkungen galaktischer kosmischer Teilchenstrahlung mit Stein- und Eisenmeteoroiden: Dünntargetbestrahlungen und Dicktargetexperimente, Universität Hannover.
- Leya, I., Wieler, R. and Halliday, A. N., 2000. Cosmic-ray production of tungsten isotopes in lunar samples and meteorites and its implications for Hf-W cosmochemistry. *Earth and Planetary Science Letters*. 175, 1-12.
- Leya, I., Halliday, A. N., and Wieler, R. 2003. The predictable collateral consequences of nucleosynthesis by spallation reactions in the early solar system. *The Astrophysical Journal*, 594(1), 605.
- Leya, I. and Masarik, J., 2009. Cosmogenic nuclides in stony meteorites revisited. *Meteoritics & Planetary Science* 44, 1061-1086.
- Liu, J. and Pearson, D.G., 2014. Rapid, precise and accurate Os isotope ratio measurements of nanogram to sub-nanogram amounts using multiple Faraday collectors and amplifiers equipped with $10^{12}\Omega$ resistors by N-TIMS. *Chemical Geology*, 363: 301-311.
- Lodders, K., 2003. Solar system abundances and condensation temperatures of the elements. *The Astrophysical Journal*, 591(2): 1220.
- Lodders, K. and Amari, S., 2005. Presolar grains from meteorites: Remnants from the early times of the solar system. *Chemie der Erde-Geochemistry*, 65(2): 93-166.
- Ludwig, K. R.. 2008. User's manual for Isoplot 3.00: A geochronological toolkit for Microsoft Excel. *Berkeley Geochronology Central Special Publication 4*, 76 pp .
- Makishima, A. and Nakamura, E., 2010. Precise isotopic determination of Hf and Pb at sub-nano gram levels by MC-ICP-MS employing a newly designed sample cone and a pre-amplifier with a 10^{12} ohm register. *Journal of Analytical Atomic Spectrometry*, 25(11): 1712-1716.
- Makishima, A. and Nakamura, E., 2012. High-resolution MC-ICPMS employing amplifiers with a 10^{12} ohm resistor for bulk sulfur determination in biological and geological samples. *Journal of Analytical Atomic Spectrometry*, 27(5): 891-895.

- Markowski, A. et al., 2006. Correlated helium-3 and tungsten isotopes in iron meteorites: Quantitative cosmogenic corrections and planetesimal formation times. *Earth and Planetary Science Letters*, 250, 104-115.
- Martin, C.I. et al., 2013. REE and Hf distribution among mineral phases in the CV-CK clan: A way to explain present-day Hf isotopic variations in chondrites. *Geochimica et Cosmochimica Acta*, 120: 496-513.
- Masarik, C., 1997. Contribution of neutron-capture reactions to observed tungsten isotopic ratios. *Earth and Planetary Science Letters*, 152, 181-185.
- McCoy, T. J. et al., 2011. Group IVA irons: New constraints on the crystallization and cooling history of an asteroidal core with a complex history. *Geochimica et Cosmochimica Acta*, 75, 6821-6843.
- Medeiros, E. L., Rodrigues, M. M. N., Duarte, S. B. and Tavares, O. A. P., 2006. Systematics of alpha-decay half-life: new evaluations for alpha-emitter nuclides. *Journal of Physics G: Nuclear Particle Physics*, 32, B23.
- Meisel, T., Walker, R. J. and Morgan, J. W., 1996. The osmium isotopic composition of the Earth's primitive upper mantle. *Nature*, 383, 517-520.
- Merrill, P.W., 1952. Spectroscopic Observations of Stars of Class. *The Astrophysical Journal*, 116: 21.
- Meyer, B.S., 2005. Synthesis of short-lived radioactivities in a massive star, *Chondrites and the protoplanetary disk*, pp. 515.
- Morgan, J.W., Walker, R.J., Horan, M.F., Beary, E.S. and Naldrett, A.J., 2002. ^{190}Pt - ^{186}Os and ^{187}Re - ^{187}Os systematics of the Sudbury Igneous Complex, Ontario. *Geochimica et cosmochimica acta*, 66(2): 273-290.
- Mostefaoui, S., Lugmair, G.W. and Hoppe, P., 2005. ^{60}Fe : a heat source for planetary differentiation from a nearby supernova explosion. *The Astrophysical Journal*, 625(1): 271.
- Moynier, F.d.r. et al., 2012. Planetary-scale strontium isotopic heterogeneity and the age of volatile depletion of early solar system materials. *The Astrophysical Journal*, 758(1): 45.
- Mughabghab, S.F., 2003. Thermal neutron capture cross sections resonance integrals and g-factors.
- Murty, S. V. S., and Marti, K., 1987. Nucleogenic noble gas components in the Cape York iron meteorite. *Geochimica et Cosmochimica Acta*, 51(1), 163-172.
- Münker, C., Weyer, S., Scherer, E. and Mezger, K., 2001. Separation of high field strength elements (Nb, Ta, Zr, Hf) and Lu from rock samples for MC-ICPMS measurements. *Geochemistry, Geophysics, Geosystems*, 2(12).
- Pernicka, E. and Wasson, J. T., 1987. Ru, Re, Os, Pt and Au in iron meteorites. *Geochimica et Cosmochimica Acta*, 51, 1717-1726.
- Petaev, M. I. and Jacobsen, S. B., 2004. Differentiation of metal-rich meteoritic parent bodies: I. Measurements of PGEs, Re, Mo, W, and Au in meteoritic Fe-Ni metal. *Meteoritics & Planetary Science*, 39, 1685-1697.
- Németh, Z., Käppeler, F., and Reffo, G., 1992. Origin of Ta-180m and the temperature of the s-process. *The Astrophysical Journal*, 392, 277-283.
- Nevissi, A. E., Silverston, M., Strebin, R. S., and Kaye, J. H., 1994. Radiochemical determination of technetium-99. *Journal of radioanalytical and nuclear chemistry*, 177(1), 91-99.
- Patchett, P.J. and Tatsumoto, M., 1980. Lu-Hf total-rock isochron for the eucrite meteorites. *Nature*, 288(5791): 571-574.
- Patchett, P.J., 1983. Importance of the Lu-Hf isotopic system in studies of planetary chronology and chemical evolution. *Geochimica et Cosmochimica Acta*, 47(1): 81-91.

- Paučová, V., Drábová, V., Strišovská, J., and Balogh, S., 2012. A comparison of extraction chromatography TEVA® resin and MRT AnaLig® Tc-02 methods for ⁹⁹Tc determination. *Journal of Radioanalytical and Nuclear Chemistry*, 293(1), 309-312.
- Peters, S.T.M., Münker, C., Becker, H., Schulz., 2014. Alpha-decay of ¹⁸⁴O_s revealed by radiogenic ¹⁸⁰W in meteorites: Half life determination and viability as geochronometer. *Earth and Planetary Science Letters*, 391, 69-76.
- Pfeifer, M., Münker, C. and Peters, S.T.M., 2013. High-Precision Tantalum Isotope Measurements by MC-ICPMS. *Mineralogical Magazine*, 77(5): 1964.
- Paton, C., Schiller, M. and Bizzarro, M., 2013. Identification of an ⁸⁴Sr-depleted Carrier in Primitive Meteorites and Implications for Thermal Processing in the Solar Protoplanetary Disk. *The Astrophysical Journal Letters*, 763(2): L40.
- Qin, L. et al., 2008. Tungsten nuclear anomalies in planetesimal cores. *The Astrophysical Journal* 674, 1234.
- Qin, L., Carlson, R.W. and Alexander, C.M.D., 2011. Correlated nucleosynthetic isotopic variability in Cr, Sr, Ba, Sm, Nd and Hf in Murchison and QUE 97008. *Geochimica et Cosmochimica Acta*, 75(24): 7806-7828.
- Pruet, J., Hoffman, R.D., Woosley, S.E., Janka, H.T. and Buras, R., 2006. Nucleosynthesis in early supernova winds. II. The role of neutrinos. *The Astrophysical Journal*, 644(2): 1028.
- Rasmussen, K. L., Ulf-Müller, F. and Haack, H., 1995. The thermal evolution of IVA iron meteorites: Evidence from metallographic cooling rates. *Geochimica et Cosmochimica Acta* 59, 3049-3059.
- Righter, K., 2003. Metal-Silicate Partitioning of Siderophile Elements and Core Formation in the Early Earth*. *Annual Reviews in Earth and Planetary Science*, 31, 135-174.
- Ryan, D. E., Holzbecher, J. and Brooks, R. R., 1990. Rhodium and osmium in iron meteorites. *Chemical Geology*, 85, 295-303.
- Rauscher, T. et al., 2013. Constraining the astrophysical origin of the p-nuclei through nuclear physics and meteoritic data. *Reports on Progress in Physics*, 76(6): 066201.
- Rauscher, T., Heger, A., Hoffman, R.D. and Woosley, S.E., 2002. Nucleosynthesis in massive stars with improved nuclear and stellar physics. *The Astrophysical Journal*, 576(1): 323.
- Rayet, M., Arnould, M., Hashimoto, M., Prantzos, N. and Nomoto, K., 1995. The p-process in Type II supernovae. *Astronomy and Astrophysics*, 298: 517.
- Rayet, M., Arnould, M. and Prantzos, N., 1990. The p-process revisited. *Astronomy and Astrophysics*, 227: 271-281.
- Regelous, M., Elliott, T. and Coath, C.D., 2008. Nickel isotope heterogeneity in the early Solar System. *Earth and Planetary Science Letters*, 272(1): 330-338.
- Rehkämper, M. and Halliday, A.N., 1997. Development and application of new ion-dashexchange techniques for the separation of the platinum group and other siderophile elements from geological samples. *Talanta*, 44(4): 663-672.
- Righter, M., Lapen, T.J. and Andreasen, R., 2013. Evidence for Excess Hafnium-176 in Eucrite QUE 97053. *LPI Contributions*, 1719: 2745.
- Russell, S.S., Gounelle, M. and Hutchison, R., 2001. Origin of short-lived radionuclides. *Philosophical Transactions of the Royal Society of London. Series A: Mathematical, Physical and Engineering Sciences*, 359(1787): 1991-2004.
- Salters, V. J. M. and Stracke, A., 2004. Composition of the depleted mantle. *Geochemistry, Geophysics, Geosystems*, 5.
- Schatz, H. et al., 1998. rp-Process nucleosynthesis at extreme temperature and density conditions. *Physics reports*, 294(4): 167-263.

- Scherstén, A., Elliott, T., Hawkesworth, C., Russell, S. and Masarik, J., 2006. Hf-W evidence for rapid differentiation of iron meteorite parent bodies. *Earth and Planetary Science Letters* 241, 530-542.
- Schulz, T., Münker, C., Palme, H. and Mezger, K., 2009. Hf-W chronometry of the IAB iron meteorite parent body. *Earth and Planetary Science Letters*, 280(1): 185-193.
- Schulz, T., Münker, C. and Peters, S., 2013. p-Process ^{180}W anomalies in iron meteorites: Nucleosynthetic versus non-nucleosynthetic origins. *Earth and Planetary Science Letters*, 362: 246-257.
- Scott, E. R. D., 1978. Tungsten in iron meteorites. *Earth and Planetary Science Letters* 39, 363-370.
- Seeger, P.A., Fowler, W.A. and Clayton, D.D., 1965. Nucleosynthesis of Heavy Elements by Neutron Capture. *The Astrophysical Journal Supplement Series*, 11: 121.
- Seki, R., and Kondo, M., 2005. An improved method for technetium determination in environmental samples. *Journal of radioanalytical and nuclear chemistry*, 263(2), 393-398.
- Sharp, Z., 2007. Principles of stable isotope geochemistry. Pearson Education Upper Saddle River, NJ, USA.
- Shirai, N. and Humayun, M., 2011. Mass independent bias in W isotopes in MC-ICP-MS instruments. *Journal of Analytical Atomic Spectrometry*, 26.7, 1414-1420.
- Smoliar, M. I., Walker, R. J. and Morgan, J. W., 1996. Re-Os ages of group IIA, IIIA, IVA, and IVB iron meteorites. *Science* 271, 1099-1102.
- Spergel, M. S., Reedy, R. C., Lazareth, O. W., Levy, P. W. and Slatest, L. A., 1986. Cosmogenic neutron-capture-produced nuclides in stony meteorites. *Journal of Geophysical Research - Sol Ea* 91, 483-494.
- Sperlein, R. F. and Wolke, R. L., 1976. A search for alpha instability in ^{184}Os . *Journal of Inorganic and Nuclear Chemistry*, 38, 27-29.
- Sprung, P., Scherer, E.E., Upadhyay, D., Leya, I. and Mezger, K., 2010. Non-nucleosynthetic heterogeneity in non-radiogenic stable Hf isotopes: Implications for early solar system chronology. *Earth and Planetary Science Letters*, 295(1): 1-11.
- Tachibana, S. and Huss, G.R., 2003. The initial abundance of ^{60}Fe in the solar system. *The Astrophysical Journal Letters*, 588(1): L41.
- Tachibana, S., Huss, G.R., Kita, N.T., Shimoda, G. and Morishita, Y., 2006. ^{60}Fe in chondrites: Debris from a nearby supernova in the early Solar System? *The Astrophysical Journal Letters*, 639(2): L87.
- Tagami, K., and Uchida, S., 2000. Separation of rhenium by an extraction chromatographic resin for determination by inductively coupled plasma-mass spectrometry. *Analytica chimica acta*, 405(1), 227-229.
- Taylor, P.D.P., Valkiers, S., De Bievre, P., Flegel, U. and Kruck, T., 1994. *Proceedings of the Second Alfred O. Nier Symposium on Inorganic Mass Spectrometry, Durango, Colorado, 9-12 May 1994*, pp. 90-94.
- Thirlwall, M.F. and Anczkiewicz, R., 2004. Multidynamic isotope ratio analysis using MC-ICP-MS and the causes of secular drift in Hf, Nd and Pb isotope ratios. *International Journal of Mass Spectrometry*, 235(1): 59-81.
- Thrane, K., Connelly, J.N., Bizzarro, M. and Meyer, B.S., 2010. Origin of excess ^{176}Hf in meteorites. *The Astrophysical Journal*, 717(2): 861.
- Touboul, M. and Walker, R. J., 2012. High precision tungsten isotope measurement by thermal ionization mass spectrometry. *International Journal of Mass Spectrometry*. 309, 109-117.

- Trieloff, M. et al., 2003. Structure and thermal history of the H-chondrite parent asteroid revealed by thermochronometry. *Nature*, 422(6931): 502-506.
- Trinquier, A., Birck, J.-L. and Allègre, C.J., 2007. Widespread ^{54}Cr heterogeneity in the inner solar system. *The Astrophysical Journal*, 655(2): 1179.
- Trinquier, A. et al., 2009. Origin of nucleosynthetic isotope heterogeneity in the solar protoplanetary disk. *Science*, 324(5925): 374-376.
- Uchida, S., and Tagami, K., 1997. Separation and concentration of technetium using a Tc-selective extraction chromatographic resin. *Journal of radioanalytical and nuclear chemistry*, 221(1), 35-39.
- Völkening, J., Köppe, M. and Heumann, K.G., 1991. Tungsten isotope ratio determinations by negative thermal ionization mass spectrometry. *International Journal of Mass Spectrometry and Ion Processes*, 107(2): 361-368.
- Völkening, J., Walczyk, T. and G Heumann, K., 1991. Osmium isotope ratio determinations by negative thermal ionization mass spectrometry. *International Journal of Mass Spectrometry and Ion Processes*, 105(2): 147-159.
- Vanhaecke, F., Balcaen, L. and Malinovsky, D., 2009. Use of single-collector and multi-collector ICP-mass spectrometry for isotopic analysis. *Journal of Analytical Atomic Spectrometry*, 24(7): 863-886.
- Vin, Y.Y. and Khopkar, S.M., 1991. Separation of niobium and tantalum by extraction chromatography with bis (2-ethylhexyl) phosphoric acid. *Talanta*, 38(9): 971-975.
- Voshage, H., and Feldmann, H. 1979. Investigations on cosmic-ray-produced nuclides in iron meteorites, 3. Exposure ages, meteoroid sizes and sample depths determined by mass spectrometric analyses of potassium and rare gases. *Earth and Planetary Science Letters*, 45(2), 293-308.
- Walker, R.J., 2012. Evidence for homogeneous distribution of osmium in the protosolar nebula. *Earth and Planetary Science Letters*, 351: 36-44.
- Wallerstein, G. et al., 1997. Synthesis of the elements in stars: forty years of progress. *Reviews of Modern Physics*, 69(4): 995.
- Wasson, J. T. and Kallemeyn, G. W., 1988. Compositions of chondrites. *Philosophical Transactions of the Royal Society* 325, 535-544.
- Weyer, S., Münker, C., Rehkämper, M. and Mezger, K., 2002. Determination of ultra-low Nb, Ta, Zr and Hf concentrations and the chondritic Zr/Hf and Nb/Ta ratios by isotope dilution analyses with multiple collector ICP-MS. *Chemical Geology*, 187(3): 295-313.
- White, J.R. and Cameron, A.E., 1948. The natural abundance of isotopes of stable elements. *Physical Review*, 74: 991-1000.
- White, F.A., Collins, T.L. and Rourke, F.M., 1956. Search for possible naturally occurring isotopes of low abundance. *Physical Review*, 101(6): 1786.
- Wieser, M.E. and Schwieters, J.B., 2005. The development of multiple collector mass spectrometry for isotope ratio measurements. *International Journal of Mass Spectrometry*, 242(2): 97-115.
- Willbold, M., Elliott, T. and Moorbath, S., 2011. The tungsten isotopic composition of the Earth's mantle before the terminal bombardment. *Nature* 477, 195-198.
- Wisshak, K., et al., 2001. Neutron Capture on $^{180}\text{Ta}^m$: Clue for an s-Process Origin of Nature's Rarest Isotope. *Physical review letters* 87.25: 251102.
- Wisshak, K. et al., 2006. Fast neutron capture on the Hf isotopes: Cross sections, isomer production, and stellar aspects. *Physical Review C*, 73(4): 045807.
- Wittig, N., Humayun, M., Brandon, A. D., Huang, S. and Leya, I., 2013. Coupled W-Os-Pt isotope systematics in IVB iron meteorites: In situ neutron dosimetry for W isotope chronology. *Earth and Planetary Science Letters* 162, 152-161.

- Wolff Briche, C.S.J., Held, A., Berglund, M., De Bièvre, P. and Taylor, P.D.P., 2002. Measurement of the isotopic composition and atomic weight of an isotopic reference material of platinum, IRMM-010. *Analytica Chimica Acta*, 460(1): 41-47.
- Woosley, S.E. et al., 2004. Models for type I x-ray bursts with improved nuclear physics. *The Astrophysical Journal Supplement Series*, 151(1): 75.
- Woosley, S.E. and Howard, W.M., 1978. The p-process in supernovae. *The Astrophysical Journal Supplement Series*, 36: 285-304.
- Yin, Q., Jacobsen, S.B. and Yamashita, K., 2002. Diverse supernova sources of pre-solar material inferred from molybdenum isotopes in meteorites. *Nature*, 415(6874): 881-883.
- Zadnik, M. G., S. Specht, and F. Begemann., 1989. Revised isotopic composition of terrestrial mercury. *International Journal of Mass Spectrometry and Ion Processes* 89.1: 103-110.
- Zinner, E., 1998. Stellar nucleosynthesis and the isotopic composition of presolar grains from primitive meteorites. *Annual Review of Earth and Planetary Sciences*, 26(1): 147-188.
- Zinner, E.K., 2003. Presolar grains. *Treatise on Geochemistry*, 1: 17-39.

VI. Acknowledgements

If it were not for the scientific and moral support of certain people, this thesis may have not have existed in its current form.

Let me start by thanking my advisor and mentor Carsten Munker for believing in my capabilities as a scientist. Carsten, you once mentioned that at the end of a successful PhD project the topic is better understood by the candidate than by the candidate's advisor. I hope that you agree that we have reached this status quo today; and we share the credits for this. Thanks for the countless fruitful discussions, brainstorming and ideas. Working with you has been a great pleasure and so has been getting to know you as a person. I am looking forward to continue chasing the big questions together!

Erik Scherer is thanked for reviewing this thesis as an external referee. Erik, I know that you have many interesting projects running, and thanks for taking time off from those!

Strong appreciation furthermore goes out to those that have contributed scientifically to this thesis, particularly Prof. Harry Becker (Freie Universität Berlin) and Dr. Toni Schulz (Universität Wien). Bo-Magnus Elfers is greatly acknowledged for helping with tests on the TEVA resin. Korinna Wulfinghoff is thanked for linguistic assistance with the Kurzzusammenfassung. Special thanks go out to Frank Wombacher for perceptive advice on mass spectrometry, valuable scientific discussions, as well as for a series of unforgettable memories from Goldschmidt conferences. Frank, you taught me the meaning of careful analyses and the significance of high-quality data and I hope that our paths will continue to cross in future.

I am uttermost grateful to the Köln and Bonn geosciences communities for setting a scientifically high-quality and socially supportive environment to work. I particularly would like to thank those who regularly participated in the late night cooking sessions at the Poppelsdorfer Schloss, among whom Christoph Lenting (for homemade pizza and good music), Alessandro Bragagni (for the best Caneloni outside Italy), Claudia Funk (for snow ball fights), Alex Heuser, Johanna Sommer, and many others. These nights kept me going in good and bad times and I appreciate how unique they are to the Köln-Bonn institutes. I especially would like to thank Elis Hoffmann for scientific input and friendship; Raúl Fonseca for beating me at squash; Bo Elfers and Markus Pfeifer for scientific discussions, fruitful and

relaxed times in the lab; and my long-term office mates Jude Coggon and Jo Hellowell for being not just sources of procrastination, but also great friends.

I am furthermore indebted to many of those who reminded me that a world exists outside the field of isotope geochemistry, keeping my mind sharp and helping me to think out of the box. Thomas Kruijer is thanked for being great company during conferences and for being able to raise our friendship above work; Quinten van der Meer for beers and aquavit; Dennis Voeten for inspirational discussions on the astonishing combination of astronomy, dinosaurs and heavy metal; Harmen van den Berg and Jop Klaver for hard times at the Barbara fests in Köln; Florian Fuchs for philosophical evenings at the Superbude/Alte Liebe, helping me through rough times. Warm thanks go out to my friends from the Bonn university choir Collegium Musicum for continuous inspiration and helping me to integrate in Germany. Danielle Wills, thank you for the inspirational discussions and for convincing me that the universe yields more than what we can probe empirically. Anouk van den Broeck, today I am also celebrating for you - I know that you would have been here.

If it were not for the warm support of my family, I would not have been where I am today. Pa, ma, jullie vele bezoeken aan Bonn, liefde en vertrouwen in mij, alsmede in mijn werk, motiveren en inspireren tot op heden. Jullie enthousiasme voor de natuur heeft me van kinds af aan aangegrepen en me in de richting van de natuurwetenschappen gedreven. Pa, onze eerste excursie naar de Hunsrück met GEA-kring West-Brabant heeft de hoeksteen gelegd van mijn enthousiasme voor de geologie. Heel wat stenen verder strijk ik nu neer in Niedersachsen, maar nog altijd door datzelfde enthousiasme gedreven. En Ma, ik zou niet weten hoe ik bijna tien jaar studeren zonder jouw moederlijke warmte en goede zorgen had kunnen volbrengen. Remco, bedankt voor innovatieve brainstorming sessies, inspiratie en gezelligheid (hadden we trouwens niet ergens een krat bier op verwed?). Je bezoek aan Bonn kom ik snel in Johannesburg retourneren! Erwin, bedankt voor je broederlijke vriendschap, oprechte interesse en gezelligheid!

Liebe Korinna, jetzt ziehen wir zusammen in der Zukunft, und ich kann nicht warten das Abenteuer des Lebens zusammen mit dir mit beide Hände fest zu nehmen. Danke für deine liebevolle Unterstützung während den letzten Monaten, für dein Vertrauen in einen Zukunft nach dieser Arbeit, und für die Inspiration die du mich gebracht hast. Du bist meine Muse.

VII. Erklärung

Ich versichere, dass ich die von mir vorgelegte Dissertation selbständig angefertigt, die benutzten Quellen und Hilfsmittel vollständig angegeben und die Stellen der Arbeit – einschließlich Tabellen, Karten und Abbildungen –, die anderen Werken im Wortlaut oder dem Sinn nach entnommen sind, in jedem Einzelfall als Entlehnung kenntlich gemacht habe; dass diese Dissertation noch keiner anderen Fakultät oder Universität zur Prüfung vorgelegen hat; dass sie – abgesehen von unten angegebenen Teilpublikationen – noch nicht veröffentlicht worden ist, sowie, dass ich eine solche Veröffentlichung vor Abschluss des Promotionsverfahrens nicht vornehmen werde. Die Bestimmungen der Promotionsordnung sind mir bekannt. Die von mir vorgelegte Dissertation ist von Prof. Dr. Carsten Münker betreut worden.

Nachfolgend genannte Teilpublikationen liegen vor:

1. Peters, S.T.M. Münker, C. Becker, H. Schulz, T. Alpha-decay of ^{184}Os revealed by radiogenic ^{180}W in meteorites: Half life determination and viability as geochronometer (2014). *Earth and Planetary Science Letters* **391**, 69-76

VIII. Lebenslauf (Februar 2014)

Name: **Stefan Theodorus Maria Peters**
Geburtsdatum: **12.01.1986**
Geburtsort: **Teteringen, die Niederlande**
Eltern: **Jacobus Johannes Simon Maria Peters**
Mariëtta Wilhelmina Francisca Peters-Dullaert
Staatsangehörigkeit: **Niederländisch**
Familienstand: **Ledig**

Schullaufbahn

1992-1998: **Kbs Helder Camara, Teteringen, die Niederlande**
1998- 2004: **Sekundarschule: Stedelijk Gymnasium Breda, die Niederlande**
(Deutsches Klassisches Gymnasium Äquivalent)

- Wahlfächer: Chemie, Physik, Mathe, Biologie, Musik, Latein

Studium

2004-2008: **Bachelor of Earth Sciences, Vrije Universiteit, die Niederlande**

- Wahlrichtung: Geologie
- Geowissenschaften Abschluss (BSc)

2008-2010: **Master of Earth Sciences, Vrije Universiteit Amsterdam, die Niederlande**

- Wahlrichtung: Geologie
- Geowissenschaften Abschluss (MSc)

Promotionsstudium:

Oktober 2010: **Beginn der Dissertation am Institut für Mineralogie und Geologie, Universität zu Köln**

- Unter der Betreuung von Prof. Dr. Carsten Münker

